5-2016

Evaluation of the Effects of Radiation on the Positioning of Histones and Other Proteins

Ashley Elizabeth Foster

University of Nebraska-Lincoln, ashleyfoster1219@gmail.com

EVALUATION OF THE EFFECTS OF RADIATION ON THE POSITIONING

OF HISTONES AND OTHER PROTEINS

By

Ashley E. Foster

A THESIS

Presented to the Faculty of

The Graduate College at the University of Nebraska

In Partial Fulfillment of Requirements

For the Degree of Master of Applied Science

Major: Applied Science

Under the Supervision of Professors Ashley M. Hall and Fred P. Baxendale

Lincoln, Nebraska

May, 2016

EVALUATION OF THE EFFECTS OF RADIATION ON THE POSITIONING OF HISTONES AND OTHER PROTEINS

Ashley Elizabeth Foster, M.A.S.

University of Nebraska, 2016

Advisors: Ashley M. Hall and Fred P. Baxendale

Nucleosomes and the secondary structure of DNA play an important role in many cellular processes that are contingent on DNA accessibility, such as replication, transcriptional regulation, and DNA repair. Recently, there is also growing evidence that the association of histones and DNA to form a nucleosome offers protection from DNA degradation. Specifically, that the inherent structural properties of DNA organization can help protect DNA from exogenous damage such as radiation. In this study, we sought to evaluate the effects of radiation on the positioning of histones and other proteins.

In this experiment, we optimized established protein protocols in *Saccharomyces cerevisiae.* Briefly, yeast cells were exposed to radiation, isolated, and then enzymatically treated with nucleases that digest regions of DNA that aren't bound to a protein. Two enzymatic digestions were performed to determine the positioning of histone-bound DNA as nucleosomes and likewise, the positioning of all protein-bound DNA, histones and non-histones alike. The DNA was purified and then quantitative real-time PCR with multiple primer sets was used to analyze a particular region of DNA. By comparing enzymatic digestion amplicon recovery, we were able to determine the relative protection value for each ~100 bp region of DNA and evaluate whether it was protected from digestion or not.

We evaluated the effects of two, single doses of radiation on the positioning of proteins in yeast cells. This system was subsequently applied to evaluate eight doses of a higher amount of radiation. Four loci were evaluated and we found that the pattern of nucleosome positioning and other proteins was conserved regardless of radiation exposure. Lastly, we applied the system to evaluate three forensically important Short Tandem Repeat (STR) loci in human white blood cells. We also found that the pattern of positioning was conserved. Our work may suggest that nucleosomes and other proteins play an important role in protecting DNA, illustrated by the conservation of positioning regardless of radiation exposure. This work advocates for the importance of the intrinsic structural properties of DNA and the use of such information to aid in the selection of regions of DNA that are more likely to be protected in situations of degradation.

ACKNOWLEDGEMENTS

I would like to first thank my co-advisors Drs. Ashley Hall and Fred Baxendale. I would not have been able to get to this point in my life without their constant support. I worked under the direction of Dr. Hall in her forensic science research lab for just over two years. I had the opportunity to be involved with a few different research projects in addition to the work I completed for my thesis research. Dr. Hall continuously challenged me to grow as a scientist and helped me to develop a range of laboratory skills. I am forever grateful for all that I have learned while I worked under her direction and that I was able to work with her on projects that will make an impact on the forensic science community.

In addition to Dr. Hall, Dr. Baxendale also served as my co-advisor throughout my graduate program. I would like to thank Dr. Baxendale for always supporting me through my research and academic endeavors. He always made time to help me with whatever I asked and was always willing to edit my work whether it was my thesis, a seminar, paper, poster, or application.

I would also like to thank my third committee member, Dr. Sydney Everhart. Dr. Everhart was very accommodating and provided great insight into my research. She helped me formulate additional questions in regards to my research approaches and gave valuable advice in regards to data interpretation and presentation. Furthermore, although not currently a committee member, Dr. Nick Miller served as a committee member for the majority of my graduate career and was instrumental in assistance with many components of my research, especially data analysis and presentation.

I am also very grateful for the Department of Entomology at UNL for providing me with a home on campus and constant support during my time here. I enjoyed being a part of this department and getting to know the faculty, staff, and students through various departmental activities and outreach events. I am also thankful for the opportunity to be involved with and assist in teaching courses in the Forensic Science Degree Program here at UNL.

Additionally, I would like to thank my family, especially my parents, Ian and Cecilia Foster, and my sister, Claire Foster, for their continuous support throughout my entire educational career. It has been quite the adventure and even though they were hundreds of miles away, they were always willing to lend a helping hand. Lastly, my boyfriend, Mike Korsakas, was the best support system I could have asked for. He was there through overnight experiments and late nights working, writing, and studying. I don't think I could have gotten through everything without him.

TABLE OF CONTENTS

CHAPTER 3: EVALUATION OF THE EFFECTS OF MULTIPLE DOSES OF

IRRADIATION ON *SACCHAROMYCES CEREVISIAE*

LIST OF TABLES

LIST OF FIGURES

ACRONYMS

A- adenine

ASF1- anti-silencing factor 1

AP site- apurinic/apyrimidinic site

BER- base excision repair

BME- β-mercaptoethanol

bp- base pairs

BSA- bovine serum albumin

CAF1- chromatin assembly factor 1

CODIS- combined DNA index system

CpG- cytosine-phosphate-guanine

Cq- quantification cycle

C- cytosine

DNA- deoxyribonucleic acid

G- guanine

HAT- histone acetyltransferase

HDR- homology-directed repair

HP- heterochromatin binding protein

LMDS- local multiple damaged sites

MMEJ- microhomology-mediated end joining

MMR- mismatch repair

NER- nucleotide excision repair

NHEJ- nonhomologous end-joining

NTC- no template control

PCR- polymerase chain reaction

qPCR- quantitative real-time polymerase chain reaction

RCAF- replication-coupling assembly factor

RFLP- restriction fragment length polymorphism

RFU- relative fluorescent unit

RNA- ribonucleic acid

ROS- reactive oxygen species

RPM- revolutions per minute

SNP- single nucleotide polymorphism

SQ- starting quantity

SSBR- single strand break repair

STR- short tandem repeat

SWI/SNF- Switch/Sucrose Non-Fermentable

T- thymine

TAE- Tris-acetate-EDTA

TBE- Tris-borate-EDTA

TLS- translesion synthesis

UV- ultraviolet

YPD- yeast extract peptone dextrose

CHAPTER 1:

LITERATURE REVIEW

Introduction

The goal of this project was to investigate how exposure to radiation affects the positioning of histones and other proteins. This is a small component of the comprehensive investigation into the relationship between DNA damage and DNA structure. The mechanisms of DNA damage and repair have been thoroughly studied and evaluated, but there is still a lack of a comprehensive understanding of the genomic environment and how it may relate to the incidence of DNA damage. In recent years, scientists have started to evaluate the intrinsic structural properties of DNA that can help protect from damage (1). In order to assist in this understanding, this project sought to evaluate how exposure to radiation affected the positioning of histones and other non-histone proteins. The histones and non-histone proteins make specific contacts with the DNA sequence and constitute the genomic environment (2). The interactions between DNA and proteins are known to have an important role in controlling and regulating many cellular and genetic processes (3). Furthermore, the protective capabilities of proteins have been indicated and are beginning to be elucidated further to aid in the understanding of DNA damage at the molecular level (4). If it is found that the positioning of histones and other proteins is conserved after radiation exposure, this might further support their role in protecting particular regions of DNA from damage.

An investigation into the relationship between DNA damage and structure will be useful for many applications in the fields of biology, genetics, evolution, medicine, and most relevant to this study, forensic science. Forensic scientists are constantly working towards combatting downstream issues associated with the incidence of DNA damage. This work will provide an insight to the effect that radiation may have on histones and

non-histone proteins. The results of these experiments will allow us to evaluate the regions containing these elements and to determine not only the potential locations of nucleosomes and other proteins, but whether or not such positioning is conserved after exposure to radiation. This may aid in the overall understanding of the distribution of the sites of damage and lead to additional experiments that can determine the sequence association of sites of damage. Forensic scientists will find this information useful as they continue to evaluate and expand regions of DNA that can be reliably analyzed due to their protection in degraded or compromised samples.

It is important to begin with an overview of DNA at the molecular level, mainly focusing on its interactions with proteins to form chromatin. The positioning and role of nucleosomes will be discussed. The protective role of chromatin will lead into a discussion of the different types and sources of DNA damage that can occur. Organisms have repair systems in place that respond to insults of damage after they have occurred, but in some situations, damage will go unrepaired. *Saccharomyces cerevisiae* will be evaluated as model organism and how its developed genomic analysis techniques can then be applied to study systems in humans. The human genome will be discussed, with a focus on the Short Tandem Repeat (STR) loci and their importance in forensic science. The intent is to provide a comprehensive review of the important systems and components evaluated in this study.

Characteristics and Structure of DNA

The primary structure of DNA is comprised of units of base pairs, in which the four DNA bases, adenine (A), guanine (G), cytosine (C), and thymine (T), systematically pair together. The purines are A and G, which are composed of two-ring structures and

the pyrimidines are C and T, which are one-ring structures (Figure 1). Specific base

pairing according to the chemical structure of each base occurs through hydrogen

bonding between A and T and between G and C. There are three hydrogen bonds

between G and C and two hydrogen bonds between A and T (Figure 2). These

interactions, A-T and G-C, are classified as the Watson-Crick base pairs (5). Moreover,

each of these bases will be associated with a sugar group and a phosphate group (PO_4) to

form a nucleotide, as seen in Figure 1. The sugar group associated with the DNA bases is

deoxyribose (2-deoxyribose), a five-carbon sugar. Deoxyribose differs from ribose due to

the replacement of a hydroxyl group by a hydrogen atom (6).
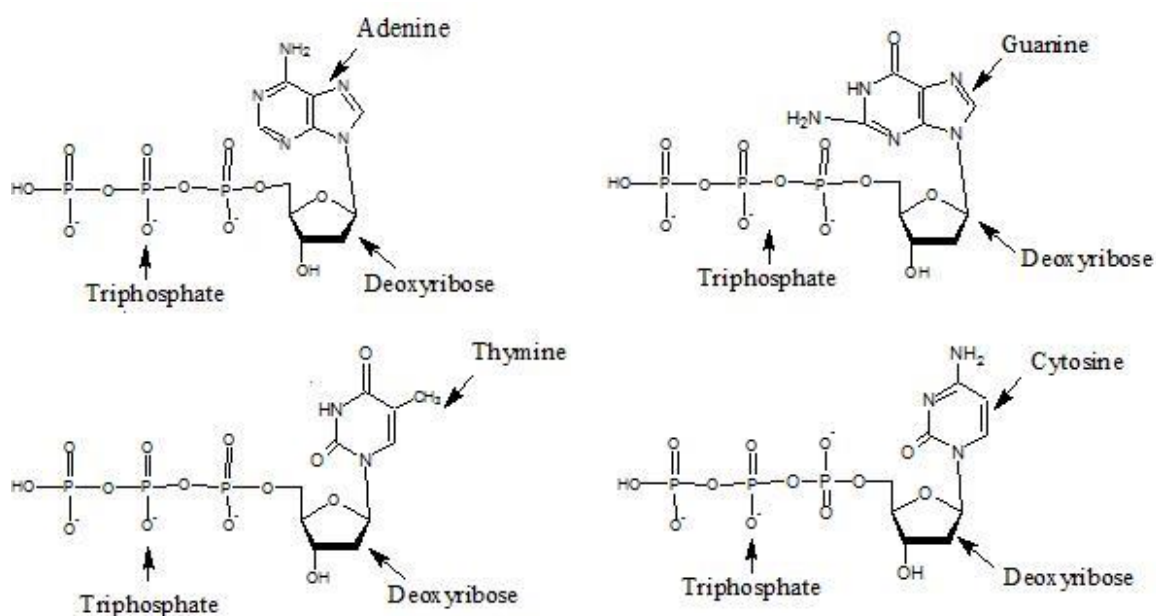
Figure 1. Deoxyribonucleoside Triphosphates (dNTPs) of DNA.

These structures were generated using ACD/ChemSketch. They are modeled after those in *Principles of Biochemistry* (Lehninger) (7). This depicts the nucleotide, which is comprised of three phosphate groups, deoxyribose sugar group, and one of four bases. The four bases of DNA are: adenine (A), guanine (G), thymine (T), and cytosine (C).
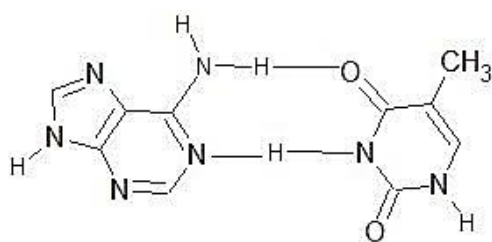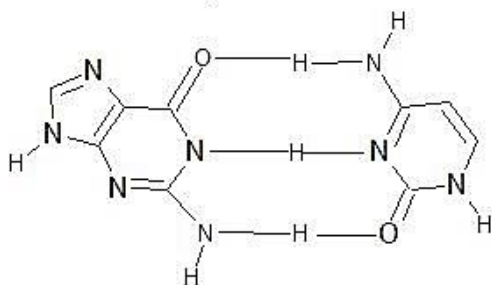
Figure 2. The Watson-Crick Base Pairs.

These structures were generated using ACD/ChemSketch. They are modeled after those in *Principles of Biochemistry* (Lehninger) (7). This shows two hydrogen bonds between A and T and alternatively, three hydrogen bonds between G and C.

Multiple nucleotides are covalently linked together to form a single strand of DNA. Moreover, two strands of DNA associate with one another to form the DNA double helix, thus making DNA double-stranded. The double helical structure of DNA was first proposed by Watson and Crick in 1953 (8). Their publication was also instrumental in proposing that the two strands of the double helix must separate in order for DNA to replicate (8). The first important feature of the DNA double helix is the backbone, which is comprised of the covalent linkage of the sugar group of one nucleotide and the phosphate group of the adjacent nucleotide in the same strand. The association motif is then repeated throughout the backbone. This backbone is present in each of the two individual strands of DNA, ensuring the stability of both the major and

minor grooves of the helix (9). The essential feature that creates the double helix

association of the two strands of DNA is the hydrogen bonding that occurs between the

bases of the two different strands (2). As previously described and visualized in Figure 2,

the base pairing is according to Watson-Crick base pairs; A-T and G-C. The orientation

of the double helix is anti-parallel, meaning that the two strands run in opposite

directions; the 5' end of strand one will associate with the 3' end of the second strand and

vice versa. The 5' end of DNA will conclude with a phosphate group and the 3' end of

the strand is terminated with a hydroxyl group (5). The basic characteristics of the

double-stranded nature of DNA can be visualized in Figure 3.
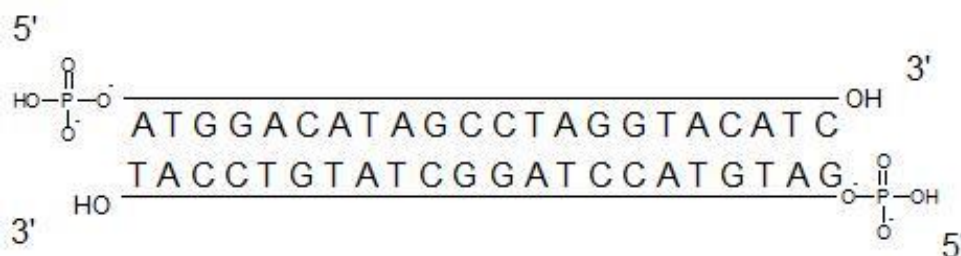
Figure 3. Basic Features of the DNA Double Helix.

This basic representation was produced in ACD/ChemSketch and highlights some of the
important features of the DNA double helix. There are two strands of DNA that run anti-
parallel; one strand runs 5'-3' and the other strand runs 3'-5'. The 5' end terminates with
a phosphate group whereas the 3' end has a terminal hydroxyl group. The sugar and
phosphate groups (shown as a solid line) make up the backbone of the ladder whereas the
Watson-Crick base pairs are the rungs of the ladder and permit the association of the two
strands. The helical orientation of DNA is not depicted in this figure.

The majority of DNA double helices are in the right-handed orientation, but there is also an exception to this orientation. B-DNA is the most common conformation of the double helix in living cells and is right-handed, with 10.5 bases per helical turn. A-DNA, like B-DNA, is also right-handed, but instead has 11 base pairs per helical turn. The difference in the number of base pairs per helical turn in A-DNA makes this conformation shorter and wider than B-DNA. A-DNA typically exists in environments and solutions with very little water. Contrary to both B-DNA and A-DNA, Z-DNA is in the left-handed helical conformation and possesses 12 base pairs per helical turn (7). Similar to A-DNA, Z-DNA is also rare and only occurs in response to certain types of biological activity. The function of Z-DNA is still somewhat unclear, but scientists believe that it may play a role in regulating gene expression and genetic recombination (10).

Beyond the nucleic acid structure, the higher order levels of organization of DNA provide insight to external interactions that DNA maintains. DNA interacts with certain proteins, called histones, which will enable the DNA to be compacted (11). An important feature of this interaction is that histones are positively charged because they contain arginine and lysine residues, which are basic amino acids. On the contrary, DNA carries a negative charge from the phosphate groups present in its backbone (12). The opposite charges cause the DNA and histones to be attracted to one another and permits their close association. Beyond the attraction of opposing charges, the association of histones and DNA is also maintained by hydrogen bonding between the histones and DNA backbone, nonpolar interactions between the histones and the deoxyribose sugars, salt bridges between the histones and phosphate groups of DNA, and lastly, non-specific insertion of

the histone tails into the minor grooves of DNA (13, 14). The interaction results in a

DNA-protein complex known as chromatin. The majority of chromatin is comprised of

equal mass proportions of DNA and proteins, but chromatin also contains very small

amounts of RNA (7). Furthermore, the interaction of eight histone proteins, H2A, H2B,

H3, and H4 (two copies of each) forms a histone octamer. Prior to formation of the

octamer, the histones associate as dimers with a distinct histone fold domain. The domain

of three alpha helices connected by two loops associates two histones in a head-tail

orientation (15). This histone octamer is then wrapped up approximately 1.65 times by

147 base pairs (bp) of DNA and is known as a nucleosome (16). The linker histone H1

will bind at the entry and exit sites of the histone core and DNA interaction and

essentially lock the DNA in place (17). Nucleosomes are the fundamental organizational

units of chromatin and are joined together by linker DNA that is not contained within the

nucleosomes, but rather links adjacent nucleosomes in what is often called the "beads on

a string" model, as seen in Figure 4 (18). About 75-90% of DNA is wrapped in

nucleosomes and any two nucleosomes are separated by approximately 20-55 bp of linker

DNA (12, 19).
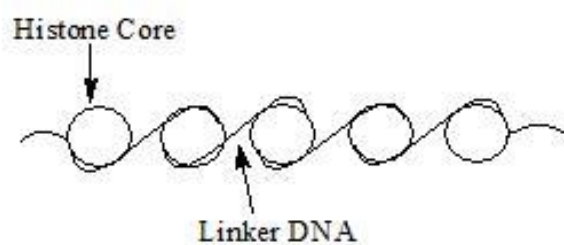
Figure 4. Nucleosomes.

This basic representation was produced with ACD/ChemSketch and shows the "beads on
a string model". The histone core of the nucleosome is represented as a circle and the
DNA is visualized as wrapping around the histone core. The linker DNA is not wrapped
around the histone, but rather connects the nucleosomes.

Nucleosome Positioning and Influence Factors

It is known that the sequence of nucleotides in a particular region of DNA plays a major role in determining the positioning of nucleosomes (20). The sequence preferences for histone-DNA interactions can be categorized as those that promote nucleosome positioning and alternatively, those that disfavor the association between DNA and histones to form a nucleosome (21). What is interesting about the DNA sequence preferences of nucleosomes is that it is not necessarily dictated by the specific interactions between particular functional groups of the histone protein and bases of the DNA. Contrary to the majority of other DNA-binding proteins, there are few base-specific interactions between histones and DNA (22). The sequence preference of nucleosomes is a result of the ability of a particular DNA sequence to bend in order to interact with the histones. Certain sequences of DNA confer accommodation to the sharp DNA bending that is due to association as a nucleosome (23). The sharp bending of DNA forces the DNA to deform and there are particular dinucleotides and other motifs that permit such deformation. Examples of these motifs include GG/CC, AA/TT/AT, and regions with a low deformation energy (24). The particular location of the dinucleotides in the DNA is then a major determinant of where nucleosomes will be positioned (25).

Just as particular sequence motifs favor the formation of nucleosomes, there are also sequence motifs that disfavor nucleosomes and thus are not usually found within a nucleosome. The sequences that permit sharp DNA bending will promote nucleosomes, so it is logical that sequences that are stiff will oppose the formation of nucleosomes due to their lack of flexibility and resistance to structural distortion (26). Sequences such as poly (dA:dT) elements are known to exclude nucleosome formation and thus serve as negative determinants. By rejecting the association with histones, these regions of DNA

influence positioning by forcing the nucleosomes to be positioned elsewhere (27). Still, the negative preference motifs are not fully understood and scientists are working towards characterizing the molecular basis of this phenomenon and distinguishing additional DNA motifs that might inflict negative preference (21).

In addition to DNA sequence preferences, there are other factors that have an influence on the positioning of nucleosomes. Such factors include DNA methylation, histone variants, post-translational modifications, higher order chromatin structure, and other non-histone proteins, including transcription factors, chromatin remodelers, and other DNA-binding proteins (21). Similar to the reasoning behind sequence preference, DNA methylation also affects nucleosome positioning due to the resulting flexibility of DNA post-methylation. When DNA is methylated, a methyl group is added to cytosine at the site of a CpG (cytosine-phosphate-guanine), which will generate a steric bulk in DNA and an overall decrease in flexibility (28). Thus, CpG methylation decreases the affinity for nucleosomes due to a decrease in DNA bendability (29).

Histone variants and post-translational modifications also play a crucial role in the positioning of nucleosomes (30). The normal histones, H2A, H2B, H3, and H4, which are found in the nucleosome core, and the H1 linker histones are not the only histones that exist. There are histone variants with distinct properties that will alter how the histones interact with DNA and subsequently, the positioning of nucleosomes (31). Histone variants are known to have both functional and structural roles within chromatin. Histone variants can be due to a few amino acid changes such as the variants H2A.1 and H2A.2 or alternatively, larger portions of the amino acid sequence can be changed to generate variants such as H2A.X and H2A.Z (32). An example of the functional role that histone

variants play can be illustrated by H2A.X. H2A.X is very important to DNA damage and repair. When there is an incidence of a double strand break in DNA, usually after exposure to radiation, H2A.X will be phosphorylated and mark the region undergoing repair (33). In some situations, the histone variant or modified histone can actually permit association with other DNA-binding proteins, further disfavoring nucleosome positioning (21). An example would be the association of H2A.Z with the heterochromatin binding protein (HP). This interaction gives this histone variant an important role in transcription due to reduced nucleosome stability (34).

Post-translational modifications can also alter histones and interactions with DNA, just as histone variants do (35). Post-translational modifications include acetylation, citrullination, methylation, phosphorylation, glycosylation, SUMOylation, ubiquitination, and poly-ADP-ribosylation (30). These modifications are usually carried out by specific enzymes that act on the N-terminal tail domains of the histone or in some cases, the core domain of the histone (14). The modifications can alter the chromatin structure through electrostatic mechanisms. For example, acetylation will neutralize the positive charge of the histone tail, which subsequently weakens its association with the negatively charged phosphate groups of DNA (36, 37). It is important to recognize that the post-translational modifications are not mutually exclusive and there will be regulation of the different modifications. The modifications have the potential to directly alter the histone or alternatively, a modification may create docking sites for other non-histone proteins (37). Different domains will recognize the result of the post-translational modification, such as the recognition of methylated residues by chromodomain (38).

The relationship between the positioning of nucleosomes and other DNA-binding proteins is competitive in nature, as the DNA-binding proteins can't bind to regions of DNA where nucleosomes are positioned. The sharp bending of nucleosomal DNA is not a preferential conformation for the DNA-binding proteins, so they will bind DNA that is not encompassed within a nucleosome (39). This relationship is exhibited by the lack of nucleosomes in regions such as promoters and sites where transcription factors bind (40). This competition will have an influence on the positioning of nucleosomes based on the function of a region of DNA. There are also ATP-dependent remodeling complexes such as SWI/SNF (Switch/Sucrose Non-Fermentable) that will directly impact the positioning due to their ability to slide or displace nucleosomes (41, 42).

Chromatin is condensed beyond the association of DNA with histones to form a higher order of chromatin structure in the form of a 30 nm fiber. The 30 nm fiber is subsequently looped, compressed, and coiled to compact the DNA even further (7). The succession of the levels of organization will culminate in the 10,000 fold compaction of chromatin. This higher-order structure is controlled by the enzymatic modifications to histones as discussed earlier in this section. The post-translational modifications can affect the net charge, shape, and other properties of histones, altering their association with DNA (35). Higher order chromatin structure creates additional interactions between nucleosomes due to their geometric proximity. The structure of chromatin produces attractive and repulsive interactions between nucleosomes, thus influencing positioning. There is some evidence that nucleosomes may alter their conformation to adapt to higher order structure constraints, but this relationship requires additional investigation to be fully understood (43, 44). There are also architectural, non-histone proteins involved in

the maintenance of DNA structure. Examples of important proteins are the replication-coupling assembly factor (RCAF), chromatin assembly factor 1 (CAF1), and anti-silencing factor 1 (ASF1) (45). The maintenance and regulation of the structure of DNA dictates essential genetic functions in the cell (3).

Lastly, it is important to note that nucleosome positioning can be either dynamic or static. A portion of nucleosomes can change their positioning along the DNA sequence. This shift in positioning is usually a result of different biological conditions, changing of stages in the cell-cycle, or variance in the type of cell. The nucleosomes are moved in a sliding mechanism by remodeling complexes that allows them to be repositioned. The sliding of nucleosomes to an alternate region of DNA that can then leave certain sites of DNA exposed (46). Alternatively, there are some nucleosomes that are static and their positioning remains unchanged (47).

The Role of Nucleosomes

The positioning of nucleosomes and their structural role is directly correlated with the functional role that they play in the cell. Nucleosomes have important functional roles in regards to DNA damage and repair, transcription, and functions associated with chromatin compaction, such as cell division and apoptosis (37). Likewise, the role that nucleosomes play in effective genome packaging must be balanced and coordinated with DNA accessibility (48). The positioning of nucleosomes can dictate where other proteins bind due to competition for a particular region of DNA. For example, if a sequence of DNA is already tightly bound by a nucleosome, a transcription factor will not be able to access it (21). Identifying the positions of nucleosomes is important because nucleosomes determine the accessibility of the underlying DNA sequences and additionally, whether or not modifications and nucleosome repositioning are necessary to make DNA

accessible. Some examples of essential molecular processes that are contingent upon nucleosome positioning and DNA accessibility include RNA polymerase activity, transcription factor binding kinetics, DNA replication, centromere structure, and gene splicing (49). Subsequently, nucleosomes will affect gene expression, development, and aging (50).

A promoter is a region of DNA that serves as the binding site for RNA polymerase (51). With the assistance of additional transcription factors, the binding of RNA polymerase will initiate transcription, in which a region of DNA is transcribed into RNA. Due to the crucial role that promoters play in the initiation of transcription, the nucleosome positioning must be correlated with the needs of the cell. Constitutive genes that are expressed at all times must therefore have what is known as an 'open' promoter. This means that the promoter region will be depleted of nucleosomes to allow the transcription factors and RNA polymerase to bind without conflict (48). Regulated genes differ from constitutive genes in that they are not continuously expressed and are subject to regulation. Thus, the promoters of regulated genes will also vary to accommodate such regulation. These promoters are classified as 'covered' because the nucleosome occupation and positioning can vary depending on the state of the gene. When a gene is repressed, nucleosomes can be positioned in sites that transcription activators would normally bind to because transcription is not active and it is not necessary for the activators to bind. However, when the gene is being expressed, there is competition for these sites between nucleosomes and transcription factors. In this scenario, other genomic elements will ultimately control what is bound, thereby regulating gene expression (42, 48). These different scenarios demonstrate the variable positioning of nucleosomes.

The investigations into the nature of nucleosomes and the structure of DNA have conveyed that nucleosomes are a key factor in determining DNA accessibility (52). Thus, it is logical for nucleosomes to also play a role in protecting DNA from a damaging agent, such as radiation. Sites of damage must then occur at regions of DNA that are exposed, due to their lack of an association as nucleosomes and a lack of a strong, higher-level structure (53). DNA compaction has been shown to play a key role in protecting genomic DNA from radiation damage, such as double-strand breaks that result from γ-rays (54). A previous experiment by Ljungman et al. (55) investigated this theory further by removing both intracellular compounds and DNA-bound proteins from cultured human cells and then exposing the cells to gamma radiation. They found that when the DNA-bound proteins were removed, the amount of DNA damage, in the form of strand breaks, was increased. This experiment suggested the intrinsic protective role that proteins and the genomic environment play in protecting bound DNA from damaging agents, such as radiation (55). Although the results of this experiment are important to understanding the protective role of DNA-bound proteins, we hope to investigate this role further by analyzing whether radiation affects the positioning of the proteins. This expands on solely evaluating the presence of proteins and goes into evaluating the positioning of proteins and whether or not their positioning may be altered as a result of exposure to radiation.

Elmroth and Stenerlow were able to show that chromatin organization in mammalian cells had an influence over the incidence of double strand breaks (4). They arrived at this conclusion by subjecting hamster cells to gamma irradiation at different growth stages. The cells in the different growth states, early and late S phase, had

different chromatin organization and they found that the yield of double strand breaks was increased in late S phase. Thus, when the secondary structure was not as strong, the DNA was more susceptible to the incidence of strand breaks. Such a result again demonstrates the role DNA/histone interactions and the genomic environment play in controlling insults of damage such as double strand breaks (4). The secondary structure of DNA and interactions with proteins help diminish the negative effects of radiation, however the question on whether or not radiation alters the positioning of the proteins still remains. By investigating this question, we will gain a more comprehensive understanding of the protective role that proteins play.

Additional Non-Histone Proteins

As previously mentioned, the regions of DNA that are not bound to histones as nucleosomes are classified as linker DNA. Linker DNA is sometimes called naked DNA due to its lack of association with nucleosomes. Rather, it is accessible to other modifications and interactions with other non-histone proteins (56). These interactions with non-histone proteins may also play a role in maintaining DNA structure, similar to histones, or, alternatively, they may also regulate expression of specific genes (57). These specific proteins have distinct DNA-binding domains that permit the close interactions between the functional groups of the protein and bases of DNA. The common structural features of these DNA-binding domains include helix-turn-helix, zinc finger, and homeodomain (58). Other types of proteins include, but are not limited to repair proteins, chromatin remodeling proteins, structural proteins, enzymes, and transcription factors (7). The regulation of specific genes is controlled by transcription machinery that is required for transcription to be active and thus for a gene to be expressed. The proteins involved in

gene regulation can bind to the region of DNA that is contained within the promoter or they can bind to a region that is near the promoter. The types of DNA-binding proteins that regulate transcription are basal transcription factors, specificity factors, repressors, co-activators, activators, and chromatin modification and remodeling proteins. Basal transcription factors are the transcription factors required at every promoter that will bind RNA polymerase. Specificity factors ensure the interaction between RNA polymerase and a promoter or group of promoters is unique. Repressors and activators also work to control the interaction between RNA polymerase and the promoter. Repressors are involved in negative regulation and a bound repressor will inhibit transcription. On the contrary, activators are positive regulators and when they are bound to DNA, they will facilitate transcription. Co-activators are intermediates between the activators and the RNA polymerase complex, an example being a mediator (7).

Chromatin modification and remodeling proteins are capable of altering chromatin through structural changes that will permit transcription. These DNA-binding proteins are involved in the post-translational modifications of histones and chromatin. For example, the proteins are sometimes enzymes, such as histone acetyltransferases (HATs), which can affect the interaction between histones and DNA. HATs work by transferring an acetyl group from acetyl CoA to the lysine residues of the histone protein. The resulting acetylated histones have a weaker affinity for DNA and are known to increase gene expression (36). This allows the previously inaccessible DNA to be accessible to appropriate transcription machinery because if the DNA is not associated with histones, other proteins will be able to interact with DNA. Although the mechanisms of the proteins are different, they all have the potential to associate with DNA and

subsequently play a role in regulating gene expression (7, 57, 59). DNA-binding proteins can also have an impact on maintaining higher-order structure that allows chromatin to be further compacted and eventually packaged into chromosomes. High-mobility group proteins 1 and high mobility group 2 proteins do not bind to a particular DNA sequence, but rather a particular DNA structure. Their high affinity for bent DNA and thus facilitate the bending of packaged nucleosomes into higher-order structures (60).

DNA Damage

The previously described structure of DNA is maintained under stable cellular conditions. However, there are endogenous and exogenous agents that create unstable conditions, cause damage to DNA, and negatively affect its integrity (61). Endogenous sources of damage are those associated with processes that are maintained within a cell and exogenous sources are external and act from outside of the cell (62). Different causative agents will affect the DNA in different ways and result in variable insults. There are a variety of lesions found in the primary structure of DNA that can be indicative of damage. Such lesions can take the form of single or double strand breaks, oxidation products, UV-induced photoproducts, crosslinks in DNA or protein, covalent adducts, and other base modifications (63). Certain types of damage can be repaired by the cell due to existing repair pathways that recognize, signal, and repair the damage, but in some cases, damage will go unrepaired (64). It is important to be aware of the different sources of damage and how they affect the structure of DNA because unrepaired damage is problematic to the cell. Damage to DNA can be detrimental to cell survival and also has the potential to hinder processes such as replication and transcription (65). Alternatively, from a forensic science standpoint, lesions in the DNA resulting from

damage make it difficult to successfully carry out analysis techniques. The primary

forensic analysis performed is amplification by the polymerase chain reaction (PCR), but

this technique may be unsuccessful if the lesions are inhibitory to the reaction carried out

by the enzyme DNA polymerase (66).

Endogenous damage may be due to spontaneous deamination, depurination,

depyrimidination, and other metabolic reactions (67). These reactions can result in the

production of both water and highly reactive oxygen species (ROS). Examples of ROS

are hydrogen peroxide (H_2O_2), superoxide (O_2^-), and the hydroxyl free radical (OH) (68).

The presence of ROS becomes problematic when these species are present at a very high

level and have deleterious effects on the integrity of DNA. If the level of ROS is severely

increased, the cell can't readily eliminate these species through detoxification. The

presence of large quantities of these species will then inflict oxidative damage to the

DNA (69). Oxidative damage primarily leads to the production of oxidized purines and

pyrimidines. These lesions create issues for the cell due to the fact that they are primarily

mutagenic. The formation of 8-oxo-guanine is the most common resulting insult due to

the presence of ROS, more specifically, the presence of the hydroxyl radical (70). The

structure of 8-oxo-guanine can be visualized in Figure 5. 8-oxo-guanine disrupts normal

Watson-Crick base-pairing due to its interaction with adenine rather than cytosine.
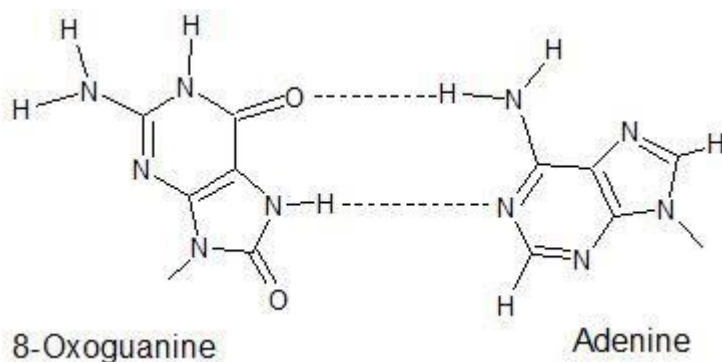
Figure 5. 8-oxo-guanine

This structure was generated using ACD/ChemSketch. 8-oxo-guanine is the lesion associated with oxidative damage. This lesion is mis-coding because it will cause the base to pair with adenine, rather than the normal pairing between guanine and cytosine.

Exogenous damaging agents include irradiation, heat, humidity, and genotoxins, and all have the potential to damage the structural integrity of DNA (71). Sources of radiation that have been found to cause damage to DNA include UV rays, x-rays, and gamma rays (72). The high level of energy contained within these sources is what causes the damage to DNA, but the mechanism and resulting insult will vary. Longer wavelengths (> 500 nm) are correlated with a lower frequency and a lower amount of energy, whereas the shorter wavelengths (10^{-7}-10^{-13} m), such as x-rays and gamma rays, have very high frequencies and thus a high energy level (73). Around the middle of the electromagnetic spectrum is the ultraviolet (UV) portion, which contains UVA (320-400 nm), UVB (290-320 nm), and UVC (100-290 nm). Because UVC is at the shortest wavelength of this group, it has the most energy and the greatest potential to cause DNA damage of the three types of UV light (74). However, UVC from the sun doesn't reach the earth, so it is not problematic for environmental samples, but rather has an important

role in experimental and laboratory systems that seek to investigate UV damage (75). The longer wavelength and less energetic UVA and UVB rays from the sun reach the earth and have the potential to damage DNA. The damage resulting from UVA and UVB rays is encountered in real-world or environmental samples, and is more relevant from a forensic science viewpoint due to the collection of samples from crime scenes (75).

UV radiation primarily causes the formation of covalent bonds between adjacent pyrimidines, and the result can be either cyclobutane pyrimidine dimers (CPDs) or 6-4[pyrimidine-2'-one] pyrimidines (6-4 photoproducts, (6-4) PPs). Studies have shown that CPDs are more common than (6-4) PPs in a ratio of roughly 2-1 for UVC-induced photoproducts (76, 77). Exposure to UV light can also cause base modifications, oxidative lesions, and strand breaks in addition to the photoproducts. Oxidative lesions were discussed in more detail in the previous paragraph, but in this situation, the presence of ROS is a direct result of the transfer of energy from light to oxygen. The resulting oxidative products are primarily mutagenic (78, 79).

Strand breaks present an interesting case of damage because although there is the potential for both single and double strand breaks to occur from exposure to radiation, the occurrence of single strand breaks is much more common. A strand break can be due to the addition of a proton to a base or removal of a hydrogen from the deoxyribose sugar. When base protonation occurs, the N-glycosyl bond is subsequently cleaved and, through a β-elimination reaction, there is a conversion to a single strand break (80). Removal of hydrogen from the deoxyribose sugar by hydroxyl radicals is not as common and only about 1/5 of the hydroxyl radicals that interact with DNA will actually attack the deoxyribose sugar (80). In some situations, what appears to be a double strand break may

actually be a region of clustered damage known as local multiple damaged sites (LMDS) (65). Also, when multiple single strand breaks occur in close proximity, within a range of 10-20 bases, this may appear as a double strand break when visualized using electrophoretic analysis methods (81). Likewise, x-rays and gamma-rays can also induce the formation of strand breaks in DNA due to their characteristically high energy potential (82). Another source of exogenous damage is harsh chemicals, such as anti-tumor agents, that also have the potential to induce strand breaks (83). Strand breaks are problematic insults to the structure of DNA because they will cause a break in the sugar-phosphate backbone of DNA, a very important feature to maintain the stability and integrity of DNA (63).

The cell maintains repair pathways in order to recognize, signal, and repair sites of damage in order for normal processes to continue. After the publication of the human genome sequence, it was revealed there are at least 130 genes that code for products involved in DNA repair. It is believed that more genes will be identified through future research endeavors (84). The cell closely regulates these genes and thus controls the function of its repair pathways. Repair pathways include the Base Excision Repair (BER), Nucleotide Excision Repair (NER), the Single Strand Break Repair (SSBR), Mismatch Repair (MMR), Direct Repair, Translesion Synthesis (TLS), Non-Homologous End-Joining (NHEJ), and Homologous Recombination or Homology-Directed Repair (HDR) (74, 85-87). These pathways vary in the type of lesion they repair and additionally, in the mechanisms in which they are able to recognize, remove, and repair damage. However, all of the repair pathways characteristically involve the recruitment of specific enzymes that are capable of such functions. For example, BER is capable of

removing a damaged base from DNA, which are problematic because base mispairing can lead to mutations and strand breaks (88). The first step in BER involves a specific glycosylase, which is an enzyme that recognizes a damaged base. This enzyme will nick the DNA to generate an apurinic or apyrimidinic (AP) site, which lacks a base. The AP site is then recognized by a second enzyme known as AP endonuclease. The AP endonuclease will cleave the phosphodiester backbone of the DNA, which will generate a single strand break where the damaged base once existed (86). After a single strand break is created, the gap is filled, and lastly, the nick is sealed to restore DNA to its functional state (69). The last steps of restoration require the enzymes DNA polymerase and DNA ligase. Using the BER as an example, the systematic approach of DNA repair is illustrated. The existing repair pathways work in conjunction to ensure that DNA is repaired and restored. Repairing DNA is crucial due to the nature of DNA and the genetic information that is encoded within. If DNA damage is not detected and repair is not signaled for, this will lead to a mutation. Although not every mutation is harmful to the cell, some mutations can lead to cancer (89, 90). Even so, not all damage will be repaired and therefore it is important to continue to study the effects of damage on DNA and the cell.

Saccharomyces cerevisiae Genome

Saccharomyces cerevisiae (*S. cerevisiae)* is classified as a model organism and is utilized as a test subject for many researchers, including geneticists, molecular biologists, and a variety of other research scientists (91). *S. cerevisiae* is a great model organism and research subject because it is easy to maintain a culture-line in the laboratory, it is a feasible host in which to induce genetic manipulations, and its genome is fully

sequenced. *S. cerevisiae* was first studied by geneticists in the mid-1900s and its' system

of gene controls was investigated by Lindegren et al. (92) and genetic and physical maps

were published in 1949 (92). In 1996, *S. cerevisiae* became the first eukaryote to have its

genome completely sequenced and published. The release of its genome was due to a

collaborative effort of hundreds of scientists from all around the world, including the

United States, Canada, England, France, Germany, Belgium, Switzerland, and Japan. The

original sequencing project involved multiple different sequencing methodologies and

multiple updated versions of each chromosome. The genome contains 12,068 kilobases,

with 5,885 potential protein-encoding genes, 140 ribosomal RNA genes, 40 small nuclear

RNA genes, and 275 transfer RNA genes. The entire genome is organized into 16

chromosomes (93). The strain of *S. cerevisiae* that was sequenced and the sequence

deposited is S288C, which is a derivative of a strain EM93 that was first isolated in 1938

(94). S288C is a strain of *S. cerevisiae* that is widely used for many laboratory

experiments due to its minimal nutrient requirements (94). This particular strain can then

be used for comparison studies in which other yeast sequences can be mapped against a

single, consensus sequence (91). The genome of *S. cerevisiae* has been extensively

maintained and annotated and such information is available in an online database,

Saccharomyces Genome Database (www.yeastgenome.org). This database is an

excellent, up-to-date resource of information, and lends itself as a tool for collaboration

between researchers. While a few updates were made to the genome from 2006-2010, the

majority of these updates were minor, including 29 sequence changes and 116 annotation

updates. More recently, the *S. cerevisiae* reference sequence has been updated with the

introduction of "S288C 2010" by Engel et al. (91). This updated sequence differs from

the original sequence determination because it was determined from a single colony, in a single laboratory, but the strains that were used in both the original and updated sequence projects were indistinguishable. This maintenance of the yeast genome has made it possible for researchers to study sequence variations, evolution, and the molecular biology of this organism. It has become desirable to design experiments in yeast that seek to evaluate various aspects of the genome and genetic functions. An important criterion that makes yeast a valid model organism is the amount of homologies present between yeast and other mammals. Such homologies include genes, then the proteins, and protein families that they encode (95). Yeast also provides a system in which genetic manipulation and investigation is cheap, easy, and feasible to complete. This is an experimental alternative to performing optimization and initial experiments in humans or other mammals, which can present complicated and expensive experiments (96). This is especially useful in terms of using the yeast as a model system to study human diseases and potentially associated genes (97).

The Human Genome

The importance and success of the yeast model system is highlighted in its genetic application to understanding eukaryotic biology, especially in humans (*Homo sapiens)*. *Saccharomyces cerevisiae* became the first eukaryotic genome to be fully sequenced and seven years later, in 2003, it was announced that the Human Genome Project had been successfully completed. The planning for the project began in 1984 and work began on the project in 1990 (84). The first version of the human genome generated by the collaborators of the Human Genome Project and was published in *Nature* in 2001 (84). Simultaneously in 2001, Celera Genomics, a private company competing with the Human

Genome Project, also published a version of the human genome sequence in *Science* (98).

Upon comparison, it was found that the two sequences published exhibited the same

features.

The human genome contains about 2.9 billion base pairs and these base pairs are

contained within 24 different chromosomes, 22 autosomes and 2 sex chromosomes, X

and Y. Each human cell will contain 23 pairs of chromosomes, females will have 22 pairs

of autosomes and then 2 copies of the X chromosome as the 23rd pair, while males will

have 22 pairs of autosomes, 1 copy of the X chromosome, and 1 copy of the Y

chromosome (99). Furthermore, the genome sequence revealed 26,588 protein-encoding

transcripts. Interestingly, only about 1% of the human genome is made up of exons, 24%

is composed of introns, and 75% of the genome, the largest portion, is intergenic DNA.

This finding is interesting because exons are the coding regions of DNA, whereas introns

and intergenic regions either don't get translated (introns) or fail to get transcribed

(intergenic) (98). The human genome reference sequence is a very useful tool because

~99.9% of the human genome is identical across all individuals, which makes it

applicable to various investigative endeavors (100). On the contrary, this extreme

consensus and similarity of the human genome is potentially problematic for forensic

scientists and those who seek to differentiate individuals on the basis of DNA. Therefore,

forensic scientists have worked to identify regions of DNA that can be analyzed in order

to identify and distinguish individuals (101). The analysis of variations in DNA

sequences between individuals began with Restriction Fragment Length Polymorphism,

known as RFLP. Briefly, the technique of RFLP involves the use of specific restriction

enzymes to digest the DNA, resulting in DNA fragments. The fragments are then

analyzed using native gel electrophoresis, denatured, and transferred to a nylon membrane (Southern blotting). Specific, radioactive-labelled probes are then used to detect complimentary DNA fragments and an x-ray image allows the patterns of DNA to be compared among individuals (102, 103).

Short Tandem Repeat (STR) Loci

In their quest to identify regions of DNA that can be differentiated and used to profile individuals, forensic scientists targeted and began to utilize the analysis of microsatellite polymorphisms and Short Tandem Repeat (STR) loci (104). Forensic STR loci are found within the noncoding regions of DNA, meaning that they do not code for proteins. In some cases, STRs can be found in intergenic regions of DNA and they will not be transcribed into ribonucleic acid (RNA). Additionally, STRs can be located within introns, which are regions that are transcribed, but aren't translated into proteins (105). STRs can easily be bound as nucleosomes because it is not necessary for them to be readily accessible to other cellular components. Thus, they may also have an important role in determining the structure of DNA in terms of higher level folding and association with histones as nucleosomes (106).

STRs are combinations of 2-6 bases that make up what is known as a repeat unit. For example, a repeat unit may be "TATC" or "AATG". An array of the same repeat unit put together is what makes up the STR and they are typically anywhere from 100 to 500 base pairs in length (107). The important feature of STR loci is that they are polymorphic among individuals and will vary based on the number of a particular repeat unit within the STR. For example, the STR D13S317 is comprised of an array of the repeat unit TATC. One individual may have seven repeat units for this STR whereas a

second individual may have nine repeat units. This example of the length variance of

STRS can be visualized in Figure 6.
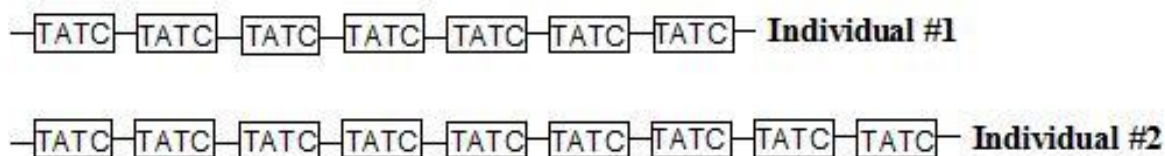
Figure 6. Length Variation in STRs

These structures were generated using ACD/ChemSketch and show the repeat unit of the STR D13S317, 'TATC'. Individual #1 has 7 repeat units and Individual #2 has 9 repeat units. Each individual will have two alleles for each STR; one allele is inherited from each parent.

STRs play an important role in forensic science because they allow a DNA profile

to be generated based on their amplification. A multiplex polymerase chain reaction

(PCR) is designed to simultaneously amplify multiple STRs using fluorescently-labeled

primers (108, 109). The primers are designed to amplify the targeted regions of DNA

containing the STR. The post-PCR, DNA product is then analyzed by capillary

electrophoresis on a genetic analyzer. Capillary electrophoresis separates the amplified

DNA based on the size of the fragments. Additionally, the primers are tagged with

different fluorescent dyes so that they are distinguishable by color as well as amplicon

size (110). The result of this analysis is translated by a computer algorithm to an

electropherogram, which is a software-generated plot of relative fluorescent units (RFU)

versus base pairs (bp) (111). The peaks on the electropherogram can be genotyped in

order to determine which alleles an individual possesses at each locus. The alleles are

determined based on the allelic ladder that correlates the size of a resulting fragment with an allele for each locus (112).

After a generated STR profile is genotyped for each locus, allele frequencies at each locus can be used to calculate the genotype frequency. Because the loci analyzed are independently segregating, the product rule can be used to statistically evaluate a profile (113). This statistical analysis is based on the expected allele frequency in a population, which is derived from the proportion of alleles at a locus that is a particular allele; how often that particular allele occurs in the population. Allele frequencies are maintained for different sub-populations and are readily available, as supplied by the Combined DNA Index System (CODIS). The expected genotype frequency can then be calculated using the Hardy-Weinberg Equation and the formula used is contingent on whether the individual is homozygous or heterozygous at a particular locus. If the person is homozygous, he/she will have two copies of the same allele, if he/she is heterozygous, he/she will have two different alleles. Another consideration for individuals that are homozygous is the theta correction. The theta correction is used to account for population substructure and inbreeding or nonrandom mating, which cause deviations from Hardy-Weinberg equilibrium. In reality, there will be more homozygotes observed in a population than are expected under Hardy-Weinberg equilibrium. Without employing the theta correction for this deviation, the strength of evidence would be overestimated. The value of theta is determined based on the size of the population, but a value of 0.01 is acceptable for the general population of the United States (114, 115).

The allele frequencies determine the genotype frequency at each locus and the independent, genotype frequencies can be multiplied together according to the product

rule. The end result is an expected genotype frequency for the entire, multiple locus profile and the estimates are normally that the probability for a randomly selected unrelated person in the population to have the exact, same multi-locus genotype is around one in a trillion (116). This makes it very unlikely that finding two identical profiles would be a random occurrence, especially given the world population of approximately 7.3 billion people (117).

However, it is not possible to state that the source of DNA for two identical profiles is the same with 100% certainty. There is always the possibility that a coincidental match can occur between two different people that share the same profile. In 1994, the DNA Identification Act standardized procedures for DNA analysis and the FBI received the authority to administer a database that would contain DNA profiles. In 1998, the Combined DNA Index System (CODIS) was launched. CODIS set the standard for the thirteen STR loci that have to be genotyped in order to generate a DNA profile (118). Results of at least ten loci are required in order to submit a DNA profile to CODIS, but all thirteen core loci must be attempted (118). Recently, analysis of offender databases have revealed that different individuals share the same DNA profile and thus duplicate profiles from non-related individuals exist in the CODIS database (119). It is also not unexpected for partial profiles, that contain fewer loci, to be an identical match between individuals (120). This possibility speaks to the limitations of DNA profiling that need to be taken into consideration when interpreting results. Although DNA evidence has its limitations, a DNA profile match can still be very strong evidentiary material when used in conjunction with other evidence and has the potential to support or corroborate other details of a case.

Forensic Science Application and Project Significance

Understanding the effects of damage on DNA is very important in the realm of forensic science. Collected DNA evidence is often times some of the most important evidentiary material analyzed in a case because it has the potential to make associations between the victim, perpetrator, and crime scene. In some cases, DNA has also been a crucial link between more than one case or offense due to the establishment of DNA databases (118, 121). Due to analysis and comparison techniques, such evidence can exonerate an innocent individual or convict the guilty. Although the power of DNA is unmatchable, sometimes the analysis of DNA is difficult. There are many types of damage that can occur due to the number of exogenous agents that are present in the environment. In many cases, body fluids deposited and developed into physiological stains at crime scenes will be damaged by a combination of multiple agents including harsh weather conditions, precipitation, radiation, heat, humidity, and microbial growth (77). The DNA damage can manifest itself as different types of insults as discussed earlier in this literature review. Although much is understood about what causes DNA damage, the types of DNA damage, and the repair mechanisms, an area that is not as well-studied, is the structure of DNA and its role in the incidence of damage. This involves investigating the genomic characteristics and intrinsic properties of DNA that either promote damage or more importantly, protect a region of DNA from damage. It has been documented that DNA enveloped in the protein-rich chromatin state of the nuclear environment is more protected from radiation damage (54). By investigating the effect of radiation on the positioning of histones and other proteins, we will begin to work towards elucidating the protective role further.

This information could be extremely beneficial to forensic scientists as they continue to battle with the negative, downstream effects of DNA damage. If we are able to identify characteristics and subsequently regions of DNA that are better protected, forensic scientists could ultimately utilize this information when selecting regions of DNA to analyze in the future. For example, it appears that the future of forensic DNA analysis is moving towards large-scale analyses such as single nucleotide polymorphisms (SNPs) and whole-genome sequence data (122). A comprehensive understanding of damage at the molecular level could guide the selection of regions of the human genome that may be reliable to analyze based on their likelihood to be protected (1). Thus, even if samples are collected from a crime scene and are likely to possess insults of damage, there is a good chance that successful analysis may still be possible.

Research Objectives

The goal of this research project is to investigate the effects of radiation exposure on the positioning of histones and other proteins. This study will allow for a better understanding of the relationship between radiation and DNA structure. By maintaining proper control samples, we can compare the samples exposed to radiation back to the control sample, not exposed to radiation, and determine if there are similarities or differences that may be related to radiation exposure. A conservation of positioning of histones and other proteins may further suggest the protective role that these features of DNA play.

Specifically, the objectives of this research were to:

1. Optimize protocols for mapping the positioning of histones and other proteins in *Saccharomyces cerevisiae* and evaluate the effects of two, single doses of irradiation.

2. Evaluate the effects of increased radiation dosage as well as increased number of doses of radiation on *Saccharomyces cerevisiae*.

3. Apply the techniques of nucleosome and protein mapping that were optimized in *Saccharomyces cerevisiae* to investigate three forensically important Short Tandem Repeat (STR) loci in human white blood cells.

CHAPTER 2:

OPTIMIZATION OF NUCLEOSOME AND PROTEIN MAPPING

Introduction

Nucleosome mapping is a technique that allows the positions of nucleosomes within the genome to be determined (123). This technique requires linking proteins and DNA together, which will protect bound DNA from enzymatic digestion and allow these regions of DNA to be analyzed. A few different experimental approaches have been designed to map out the locations of nucleosomes and they all involve certain preparatory steps that are essential to the success of the mapping procedure. The techniques usually vary in the method used to analyze and determine the positioning. An initial formaldehyde treatment will cross-link the proteins to DNA and then glycine can be used to quench this reaction (124). In some cases, such as with *Saccharomyces cerevisiae,* the cell wall must be digested, usually with an enzymatic digestion such as zymolase, to generate a spheroplast, rendering the nuclear DNA accessible. After the cells have been properly prepared, they are digested with an enzyme known as micrococcal nuclease (MNase). MNase is an endo-exonuclease that results in preferential cleavage at nucleosome linker regions, thus generating nucleosomal DNA (125). DNA that is protected by a nucleosome will not be digested by this enzyme, but the regions that lack protection will be digested by the enzyme and thus not present in the purified DNA. After digestion, DNA is purified using a phenol-chloroform extraction and is analyzed on a native agarose gel. The success of the MNase digestion can be evaluated based on the fragments observed. The goal is to obtain mono-nucleosomal DNA, which will be a fragment around ~147 bp. However, there will also be di-nucleosomal, and tri-nucleosomal DNA which will larger in size, but each with a length that is a multiple of the mononucleosomal DNA. The mononucleosomal DNA can then be extracted from the gel and subsequently analyzed.

Additionally, DNA can be digested with the enzyme deoxyribonuclease (DNase) that will digest regions of the DNA that are not protected by proteins (126). The DNase digestion can provide insight into the potential locations of other non-histone proteins in addition to the locations of histones (127). Analysis of the DNA by performing quantitative real-time PCR (qPCR) with tiling primers covering a region of DNA allows the position of nucleosomes and other DNA-binding proteins to be determined. The positioning of proteins is based on the fact that only specific regions of DNA that are protected by their association with proteins will be amplified; if a region of DNA is not bound by a protein, it will be digested, and not amplified in the qPCR analysis (16, 125).

In the first experiment, we sought to not only optimize the procedures and protocols involved in this study, but additionally to provide insight to the positioning of nucleosomes and other proteins in samples exposed to two different doses of irradiation. Cultures that were exposed to irradiation were compared to a no exposure control sample. This allowed us to evaluate if radiation affects the positioning of histones and other proteins at four loci in *Saccharomyces cerevisiae*.

Materials and Methods

Preparation and Maintenance of Culture

The first step of this experiment involved preparing and maintaining a culture line

of *Saccharomyces cerevisiae (S. cerevisiae)*. A stock culture of parental strain S288C was

purchased from GE Healthcare Dharmacon Inc. (Lafayette, CO). The genotype of this

strain of yeast is *MATα SUC2 gal2 mal2 mel flo1 flo8-1 hap1 ho bio1 bio6* (91). To

prepare the YPD (yeast peptone dextrose) media, 50 grams of YPD complete medium

(Amresco, Solon, OH) were combined with 1 L of nanopure water with stirring using a

magnetic stir bar on a stir plate. The solution was then autoclaved for 15 minutes on the

liquid setting and subsequently allowed to cool to approximately 50 °C. The solution was

then divided into two, equal, 500 mL portions. One 500 mL portion was kept as-is, stored

at 4 °C, and later used as YPD broth for liquid cultures. To the second 500 mL portion,

0.5 grams of sodium hydroxide (NaOH) and 10 grams of agarose were added, with

continuous stirring using a magnetic stir bar on a stir plate. The solution was then

autoclaved for 15 minutes on the liquid setting. The solution was allowed to cool to 50 °C

and then poured into ~25, standard 90 x 16 mm sterile, plastic petri dishes in 20 mL

portions. After the plates solidified at room temperature, they were sealed with Parafilm

laboratory film and stored at 4 °C (128).

For optimal culture growth, the initial frozen culture was streaked on multiple

YPD plates. The plates were incubated for 2-3 days at 30 °C. After colony growth, a

single colony was isolated from the plate using a sterile loop, and then inoculated in YPD

broth (Figure 7). Liquid culture was grown in a culture flask in an incubator at 30 °C,

with shaking at 250 RPM. To obtain a culture that had cells in the growth phase, a liquid

culture was incubated for 12-15 hours based on the results of the experimentally

determined culture growth curve (Figure 8). This required measuring the absorbance of

the culture on the GENESYS 10S Vis Spectrophotometer (Thermo Fisher Scientific,

Waltham, MA) at 600 nm. Additionally, to ensure that the cells were in the growth phase,

they were visualized under the microscope (Figure 9). The growth phase can be

visualized in the form of budding yeast cells that are in the process of division. The

culture maintenance methods were used throughout the length of this study in order to

keep a continuous stock of yeast culture. All plates were properly stored at 4 °C after

initial incubation and glycerol stocks of the yeast culture were kept at -80 °C (128).

Irradiation Exposure

In a series of preliminary experiments, we surveyed a range of doses of irradiation

in order to determine the doses to use in the experiment discussed in this chapter. Briefly,

samples of yeast were exposed to 0, 50, 100, 150, 200, 250, 300, 350, 400, 450, and 500

Gray of irradiation in the RS-2000 X-Ray Irradiator (Rad Source Technologies, Suwanee,

GA). After exposure, the cultures were streaked on YPD plates and the remaining portion

of each culture was flash frozen in liquid nitrogen and stored at -80 °C. DNA was

extracted from each sample and analyzed using native gel electrophoresis. We saw that

the cultures were still viable after exposure to 50 and 150 Gray of irradiation based on

their growth on YPD plates, but these samples indicated DNA damage by the

fragmentation visualized using gel electrophoresis. We decided to examine two doses of

irradiation in order to see if any differences were exhibited between them.

Using the previously discussed yeast growing protocols, six, separate, 250-mL

liquid YPD broth cultures were prepared in 500 mL culture flasks. Six cultures were

prepared in order to perform experiments at three different radiation exposures and for two different enzymatic digestions at each exposure. The cultures were then divided into 50 mL portions contained in 50-mL conical tubes for a total of 30 samples. The tubes were transported on ice (4 °C) from University of Nebraska-Lincoln (UNL) in Lincoln, NE to the University of Nebraska Medical Center (UNMC) in Omaha, NE. The samples were exposed to gamma-irradiation using the RS-2000 X-Ray Irradiator (Rad Source Technologies, Suwanee, GA). The dose chart can be visualized in Table 1, but the length of exposure was calculated in order to generate 0, 50 Gray, and 150 Gray respectively. This was programmed using the control panel of the irradiator. The samples were placed in the center of the sample shelf at level 6 inside of the RS-2000. Due to the necessity to ensure uniform dosage, it was feasible to put two samples (50 mL conical tubes) on the sample shelf at a time. This required a total of 5 exposures of 50 Gray and 5 exposures of 150 Gray in order to irradiate all of the samples (Table 1). Immediately after irradiation, each culture was streaked on a fresh YPD plate and the remaining culture was flash frozen using liquid nitrogen. The samples were then transported back to UNL (Lincoln, NE) on dry ice. The YPD plates were transported using freezer packs to maintain a temperature of 4 °C. The travel time between Omaha and Lincoln was approximately 1 hour in length. Upon returning to UNL, the streaked YPD plates were incubated at 30 °C for 2-3 days to promote culture growth. The frozen liquid cultures were stored at -80 °C overnight prior to further analyses.

Harvesting Cells

The frozen yeast cultures were removed from storage at -80 °C and allowed to equilibrate to room temperature. After cultures were fully thawed, the cultures from the 5, 50 mL conical tubes were combined into a 500 mL culture flask, thus creating one combined sample for 0 Gray (No Exposure control), one for 50 Gray, and one for 150 Gray. The total volume of each sample was 250 mL (5 x 50 mL). The culture density of each culture was checked using a spectrophotometer. It is necessary for the cultures to still be at an optimal density or absorbance of around 0.6, this is read at 600 nm on the GENESYS 10S Vis Spectrophotometer (Thermo Fisher Scientific, Waltham, MA). To crosslink the protein to DNA, 5.4 mL of 37% formaldehyde was added to the culture for a final concentration of 1% formaldehyde. The samples were then incubated at room temperature for 15 minutes with occasional swirling by hand. Next, 1/19 of the total volume, 11.25 mL, of 2.5 M glycine was added to the culture, making the final concentration of glycine 125 mM. The addition of glycine is necessary to quench the excess formaldehyde (124). The cultures were incubated at room temperature for 5 minutes. To pellet the cells, the entire culture was transferred to a 250 mL Nalgene centrifuge bottle. The lids of the bottles were sealed with Parafilm laboratory film. The cultures were centrifuged for 5 minutes at 3,000 x g at 4 °C. The supernatant was removed and 250 mL of cold, sterile water was used to wash the cells. The cells were centrifuged for 5 minutes at 3,000 x g at a temperature of 4 °C. This wash step was repeated once. All centrifugation steps were performed in the Sorvall Super T-21 centrifuge, equipped with a Sorvall SS34 rotor.

Spheroplasting

After the final centrifugation step, the supernatant was removed and only the pellet remained. The cells were re-suspended in 19.5 mL of Buffer Z (1 M sorbitol, 50 mM Tris-HCl, pH 7.4, water). The re-suspension of cells was carefully done by pipetting the buffer up and down until the cellular pellet became homogenous in the liquid. The re-suspended cells were subsequently transferred to a sterile, 125-mL culture flask. Fourteen microliters of fresh 14.3 M β-mercaptoethanol (BME) was added to each culture to yield a final concentration of 10 mM. An enzymatic solution of zymolase was prepared by dissolving 100 mg of zymolase in 10 mL buffer (40% glycerol, 60% Buffer Z). The enzyme solution was divided into smaller portions and 0.5 mL of the zymolase solution was added to each culture. Zymolase is used as an enzymatic treatment in order to digest the cell wall present in yeast cells (129).

The cells were incubated at 30 °C with gentle shaking at 100 RPM for approximately 30 minutes. The time length of this digestion can be variable, but within the range of 15-60 minutes, and usually around 30-40 minutes. The success of the cell wall digestion can be confirmed via microscopy. To confirm that spheroplasts were obtained, one drop of culture was placed on a microscope slide and then mixed with one drop of sterile water. The cells that have lost their cells walls appear as swollen "ghosts" under the microscope (125). After spheroplasts had been successfully obtained, the digestion was complete, and the cultures were transferred from the 125 mL culture flasks to sterile, 50 mL VWR centrifuge tubes. To pellet the spheroplasts, the samples were centrifuged for 10 minutes at 3,000 x g, at 4 °C in the Sorvall Super T-21 centrifuge.

Micrococcal Nuclease (MNase) Digestion

After centrifugation, the spheroplasts were gently re-suspended in 3 mL of NPS

Buffer (0.5 mM spermidine, 0.075% NP-40, 50 mM NaCl, 10 mM Tris-HCl, pH 7.5, 5

mM $MgCl_2$, 1 mM $CaCl_2$, 1 mM β-mercaptoethanol (BME), water). To re-suspend cells,

the buffer was slowly added to the cells and a glass rod was used to gently mix the

spheroplasts. The re-suspended cell solution was divided into 3, 600 μl aliquots in new,

1.5 mL microcentrifuge tubes. Three aliquots were prepared in order to complete two

digestions at different concentrations of micrococcal nuclease (MNase), 30U and 45U, as

well as a 'No Digest' control. The samples included in this experiment are listed in Table

2. The amount of MNase was determined using a preliminary experiment that evaluated

both the amount of enzyme as well as the digestion time (Figure 10). In this experiment,

samples of yeast culture were prepared as described in this chapter, but without

irradiation exposure. We tested the incubation time for enzymatic digestion (30 minutes

vs. 40 minutes) as well as the amount of enzyme (15U MNase vs. 30U MNase). Based on

the results visualized in Figure 10, we found that there was no obvious difference in

results from 30 minutes compared to 40 minutes, so we decided upon a 30 minute

digestion time. Further, we found that 30U of MNase was necessary to obtain a larger

proportion of mononucleosomal DNA for further analysis. In the experiment discussed in

this chapter, we decided to digest with 30U and 45U of MNase to ensure we had enough

mononucleosomal DNA for downstream analyses. MNase (New England BioLabs,

Ipswich, MA) (15U/μl) was added to directly to the samples at a volume of 0, 2, or 3 μl

in order to add 0, 30U, or 45U of enzyme respectively. The samples were then incubated

at 37 °C for 30 minutes. To stop the digestion, the samples were shifted to ice (4 °C) and

18 μL 500 mM EDTA and 7 μL 200 mM EGTA were added to each sample.

Protein Degradation & DNA Purification

The samples were removed from the ice and 60 µl of 10% SDS, 10 µl of 10

mg/mL proteinase K, and 10 µl of 10 mg/mL DNase-free RNase A was added to each

sample. The samples were incubated at 56 °C for 5 hours. Following the incubation, a

standard phenol-chloroform extraction was performed as follows. Five hundred

microliters of phenol saturated with 0.1 M Tris-HCl, pH 7.5 was added to each sample

and mixed by inversion. The samples were centrifuged at 17,000 x g (high) for 5 minutes

at room temperature in the AccuSpin Micro 17 Centrifuge (Thermo Fisher Scientific,

Waltham, MA). Centrifugation causes the formation of two layers and the upper aqueous

layer containing the DNA was removed to a new 1.5 mL tube. This procedure was

repeated once with phenol (2 times total) and then once with chloroform, each time

removing the top, aqueous layer to a new, 1.5 mL tube (130). After the last separation, 40

µl of 3 M sodium acetate (NaAc) (0.1 volume) and 1 mL of 100% ice-cold ethanol (2.5

volume) were added to each sample. The samples were then moved to -20 °C (freezer)

and incubated overnight (12-18 hours). The conditions of cold temperature and salt are

required to precipitate the DNA and cause the formation of a DNA pellet (131).

After the overnight incubation, samples were centrifuged at 12,500 x g for 25

minutes at 4 °C in order to pellet the DNA. The DNA was in the form of a very small,

white pellet present on the side of the microcentrifuge tube (131). The supernatant was

removed and the pellet was washed with 500 µl of cold, 70% ethanol. The samples were

centrifuged at 17,000 x g for 5 minutes. The supernatant was removed and the samples

were allowed to dry for 10 minutes at 56 °C, with the lids of the tubes open. The pellet

was re-suspended in 40 µl of TE Buffer (10 mM Tris-HCl, pH 8.0, 0.5 mM EDTA) and

solubilized by incubation overnight (12-18 hours) at 56 °C. The samples were

subsequently stored at 4 °C until further analysis.

Deoxyribonuclease (DNase) Digestion

　　　Yeast cultures were prepared and irradiated as described earlier in this section

(Preparation and Maintenance of Culture and Irradiation Exposure) and according to

Table 1. After the cultures were removed from storage at -80 °C and allowed to

equilibrate to room temperature and combined to generate 3, 250 mL cultures, they were

transferred to a 250 mL Nalgene bottle and centrifuged at 3,000 x g for 4 minutes at 4 °C.

The supernatant was discarded and the cells were re-suspended in 7.5 mL of DNase

Buffer 1 (40 mM EDTA, 90 mM β-mercaptoethanol, water). The samples were

transferred to 50 mL conical tubes (VWR) and incubated at room temperature for 5

minutes. After incubation, samples were centrifuged at 3,000 x g for 4 minutes at 4 °C

and the supernatant was discarded. The cells were re-suspended in 8 mL of

Spheroplasting Buffer (1 M sorbitol, 1 mM EDTA, 3 mM DTT) and 800 μl of zymolase

(10 mg/ml). The cell suspension was transferred to a 125 mL culture flask and incubated

at 30 °C for 40 minutes with shaking at 100 RPM. The cells were transferred back to a 50

mL conical tube and centrifuged for 4 minutes at 3,000 x g at 4 °C. The supernatant was

removed and the cells were gently re-suspended in 2 mL of Lysis Buffer (100 mM NaCl,

10 mM Tris, pH 7.4, 10 mM $MgCl_2$, 5 mM β-mercaptoethanol, 0.075% NP-40, water)

(132). Similar to the preliminary experiments performed to optimize the experimental

conditions and amount of MNase necessary for digestion, we also performed preliminary

experiments to optimize the DNase digestion. Ultimately, we found that 25U and 35U of

DNase and an incubation time of 10 minutes were optimal to digest the DNA for

downstream analyses. In this experiment, the cell suspension was divided into 300 µl

aliquots to allow for No Digest, 25U DNase, and 35U DNase samples (Table 2). The

appropriate volume, 0, 25, or 35 µl of DNase enzyme (1U/µl) was added to each sample

to generate samples containing 0U, 25U, and 35U of DNase respectively (Table 2). All

samples were incubated at 37 °C for 10 minutes.

The reactions were stopped by adding 300 µl of Stop Solution (50 mM Tris (pH

7.4), 1 M NaCl, 2% SDS, 50 mM EDTA, water), vortexing, and incubating at 65 °C for

10 minutes. The DNA was purified using the phenol-chloroform extraction method

previously described in this section (Protein Degradation and DNA Purification). After

the last removal of the aqueous layer to a new 1.5 mL tube, 500 µl of 2-propanol was

added and samples were incubated at room temperature for 10 minutes. To pellet the

DNA, the samples were centrifuged at 17,000 x g for 5 minutes. The supernatant was

removed to isolate the DNA pellet. The pellet was washed with 500 µl of 70% ethanol

and centrifuged at 17,000 x g for 5 minutes. The supernatant was removed and the pellet

was allowed to dry by leaving the caps of the tubes open for about 10 minutes and

incubating the samples at 56 °C. The pellet was re-suspended in 150 µl of HEPES Buffer

(10 mM HEPES, 0.1 mM EDTA, water, pH 7.9) and 10 µl of RNase A. The samples

were then incubated overnight (12-18 hours) at 37 °C to remove any RNA present in the

sample (132).

The DNA was re-precipitated by adding 0.1 volume (15 µl) of 3 M sodium

acetate and 2.5 volume (375 µl) of 100% ethanol. The samples were incubated at room

temperature for 10 minutes and then centrifuged at 17,000 x g for 10 minutes. The pellet

was washed with 500 µl of 70% ethanol and centrifuged at 17,000 x g for 5 minutes. The

DNA pellet was dried and re-suspended in 75 µl of TE Buffer with an overnight

incubation at 56 °C (132). All DNA samples were then stored at 4 °C until further

analysis.

DNA Quantification (Qubit Fluorometer)

After re-suspension, samples were quantified using the Qubit HS dsDNA Kit on

the Qubit Fluorometer (Thermo Fisher Scientific, Waltham, MA). The Qubit assay works

with the use of a molecular dye, PicoGreen, that will bind to a specific target (133). In

this case, the specific target is double stranded DNA (134). Initially, the samples were

diluted 1:100 in order to get a reading that was within the quantification range of the kit.

This dilution step was based on preliminary experiments that found the concentration of

DNA in the samples was too high to be read using this kit. The 1:100 dilution was made

by combining 2 µl of each sample with 198 µl of TE Buffer. The Qubit Fluorometer was

calibrated using two manufacturer-supplied standards, Standard 1 and Standard 2.

Standard 1 is at 0 ng/µl of DNA and Standard 2 is at 10 ng/µl of DNA. The fluorescence

generated by these two standards is used to produce a standard curve and ensure that the

instrument is properly calibrated. Ten microliters of each standard is combined with 190

µl of a working solution, which contains the manufacturer-supplied, Qubit dsDNA HS

Buffer and Qubit dsDNA HS Reagent, PicoGreen dye (Thermo Fisher Scientific,

Waltham, MA). The calibration can be checked directly on the instrument and the value

difference between Standard 1 and Standard 2 should be at least 50-fold, but was usually

around 200-300 fold for these experiments, which is acceptable. To quantify the samples,

2 µl of each sample was combined with 198 µl of the working solution previously

described. Additionally, a positive control of standard, genomic DNA (PowerQuant Male

gDNA Standard, Promega, Madison, WI) at a concentration of 1 ng/µl was prepared and

a negative control of water combined with the working solution was quantified. The

samples were incubated for five minutes at room temperature after addition to the

working solution to allow the dye to bind. At least two minutes is necessary for the

molecular dye to bind the DNA (133). The positive control read at approximately 1 ng/µl

and the negative control read at 'Out of Range, Too Low'. The DNA quantifications of

the original samples were calculated by accounting for the volume of the sample added, 2

µl, and then multiplying the concentration read on the Qubit Fluorometer by the dilution

factor, which was 100.

Gel Electrophoresis

After the samples were quantified, the enzymatic digestion was confirmed using

native gel electrophoresis. To prepare the 1% gel, 5 µl of ethidium bromide (EtBr) was

combined with 50 mL of 1X Tris/Borate/EDTA (TBE) buffer and 0.5 g of agarose was

added to this solution. The solution was mixed and then heated to boiling in a standard

microwave in order to dissolve the agarose. The solution was then cooled to a point that it

was safe to pour into the casting tray (~56 °C). The gel was poured into the casting tray

containing a comb that created eight, 40 µl wells. The gel was allowed to solidify for

approximately thirty minutes. The comb and barriers were removed and the gel was

placed in a gel tank and 300 mL of 1X TBE (with 30 µl of EtBr added) was added as the

running buffer. All of the gel apparatus supplies were from the IBI Scientific Gel

Electrophoresis System (Peosta, IA).

To prepare the samples for gel electrophoresis, 2 µl of each sample was combined

with 3 µl of nuclease-free water, and 1 µl of 6X loading dye (New England Biosystems,

Waltham, MA). Additionally, ladders of λ DNA-HindIII Digest and 100 bp (New

England Biosystems, Waltham, MA) were prepared by taking 1 µl of the ladder, 4 µl of

nuclease-free water, and 1 µl of the 6X loading dye. A positive control of previously

extracted, genomic yeast DNA was also prepared in this manner. The entire volume, 6 µl,

was loaded directly on the gel. The gel was run at 50V for 3 hours. The gel was

visualized on the Gel Doc XR+ System (Bio-Rad Laboratories, Hercules, CA). The

purpose of running this gel was to ensure that the MNase treatment yielded

mononucleosomal DNA. The results of gel electrophoresis can be visualized in Figures

10 and 11. Mononucleosomal DNA is the band that is approximately at 147 bp, which is

located on the gel between the 100 and 200 bp bands that are part of the 100 bp ladder

(Figures 10 and 11) (125).

After the enzymatic digestion was confirmed, another gel was prepared as

previously described in this section (Gel Electrophoresis), with the exception of using

low-melting point agarose in place of regular agarose. The purpose of running the second

gel was to purify the mononucleosomal DNA by directly excising it from the gel. For this

gel, 25 µl of each MNase-digested sample was combined with 5 µl of 6X loading dye.

All ladders, standards and samples were prepared to yield a total volume of 30 µl and the

total volume was loaded on to the gel. The previously described procedure of running and

visualizing the gel was repeated according to this section, Gel Electrophoresis. This gel

image can be visualized in Figure 12.

Additionally, gel electrophoresis was used to evaluate the success of the DNase

digestion. To prepare the 1% gel, 5 µl of ethidium bromide (EtBr) was combined with 50

mL of 1X Tris/Acetate/EDTA (TAE) buffer and 0.5 g of agarose was added to this

solution. The solution was mixed and then heated to boiling in a standard microwave in order to dissolve the agarose. The solution was then cooled to a point that it was safe to pour into the casting tray, at a temperature of approximately 56 °C. The gel was poured into the casting tray that contained a comb that created eight, 40 µl wells. The gel was allowed to solidify for approximately thirty minutes. The comb and barriers were removed and the gel was then placed in a gel tank and 300 mL of 1X TAE (with 30 µl of EtBr added) was added as the running buffer.

To prepare the samples, 350 ng (5-20 µl) of each sample was combined with the appropriate volume of sterile water to yield a total volume of 20 µl, and 4 µl of 6X loading dye (New England Biosystems, Waltham, MA). Additionally, ladders of λ DNA-HindIII Digest and 100 bp (New England Biosystems, Waltham, MA) were prepared by taking 1 µl of each ladder, 18 µl of sterile water, and 4 µl of the 6X loading dye. A positive control of previously extracted, genomic yeast DNA was prepared as well as a positive control for the DNase digestion. The entire volume, 24 µl, was loaded directly on the gel. The gel was run at 200V for 30 minutes. The gel was visualized on the Gel Doc XR+ System (Bio-Rad Laboratories, Hercules, CA). These gel images can be visualized in Figure 13.

Purification of Mononucleosomal DNA

From the second gel that was run with a larger volume of the MNase-digested samples, the mononucleosomal DNA was cut out and purified. To accomplish this, the gel was placed on a transparent, plastic sheet on the Gel Doc XR+ System. The tray was pulled out and the UV light turned on to allow for the bands to be visualized. Using a sterile scalpel, the band of mononucleosomal DNA between the 100 and 200 bp DNA

size markers was cut out and placed into a sterile, pre-weighed, 2 mL microcentrifuge tube. A post-cut gel image can be visualized in Figure 12 to illustrate the region of the gel that was excised.

After the mononucleosomal DNA band was excised from the gel, it was purified with the Qiagen QIAquick Gel Extraction Kit (Qiagen, Valencia, CA) and according to the manufacturer's protocol. Each cut gel sample was weighed to confirm that the weight was between 100 and 400 mg for proper purification. Three volumes of Buffer QG were added to one volume of gel. For this calculation, 100 mg=100 µl. For example, if the gel portion weighs 200 mg, 200 µl x 3= 600 µl of Buffer QG. The samples were incubated at 50 °C for ten minutes with gentle shaking and occasional vortexing in order to completely dissolve the gel in the buffer. After the gel was successfully dissolved, one volume of isopropanol was added to each sample. The samples were then vortexed and briefly centrifuged to remove any liquid from the lid. The samples were added to the manufacturer-provided spin column in 700 µl portions. The samples were centrifuged for 1 minute @ 17,000 x g and the flow-through was discarded after each centrifugation step. Seven hundred and fifty microliters of Buffer PE were added to the spin column and the samples were centrifuged at 17,000 x g for 1 minute. The flow-through was discarded and the sample was centrifuged for an additional minute to remove any excess buffer. The spin column was placed in a sterile, 1.5 mL microcentrifuge tube and 30 µl of Buffer EB was added to the center of the column. The samples were incubated at room temperature for 10 minutes, then centrifuged for 1 minute at 17,000 x g. The spin column was discarded and the eluted DNA was kept in the 1.5 mL tube. The purified mononucleosomal DNA was quantified using the Qubit HS dsDNA Kit and the Qubit

Fluorometer, as previously described in the DNA Quantification (Qubit Fluorometer) section of this chapter. The purified mononucleosomal DNA samples were stored at 4 °C until further analysis.

Primer Optimization

The primer sequences to analyze the first yeast locus, the promoter region of ADH2, were obtained from *Analysis of Nucleosome Positioning Using a Nucleosome-Scanning Assay* by Infante et al (125). The sequences of the primers are contained in Table 3. The primers were obtained as lyophilized oligonucleotides from Sigma Aldrich (St. Louis, MO). The primers were re-suspended in the appropriate amount of nuclease-free water to obtain stock primers at a concentration of 200 pmol/µl. The stock primers were diluted 1:10 in nuclease-free water to obtain working primer solutions at a concentration of 20 pmol/µl.

To optimize the PCR conditions for the primers, traditional PCR was utilized, but a temperature gradient of 45-60 °C was used for the annealing temperature. The 25 µl reaction contained 1X GoTaq Flexi Buffer (Promega), 2.5 mM $MgCl_2$, 2.5 µM dNTPs, 10 µg BSA, 2.5 units of GoTaq DNA Polymerase (Promega), and 40 picomoles of each primer (forward and reverse). To each reaction, ten nanograms of genomic yeast DNA was added. The PCR cycling conditions were as follows: 95 °C for 5 minutes, 40 cycles of: 95 °C for 15 seconds, (45-60 °C) for 30 seconds, 72 °C for 30 seconds, and a final extension for 30 minutes at 72 °C. This was performed on the C1000 Thermal Cycler (Bio-Rad Laboratories, Hercules, CA).

Five microliters of the final PCR product were analyzed on a native, agarose gel. The gel was prepared by combining TAE Buffer, EtBr, and agarose according to the methodology previously described in the section, Gel Electrophoresis, earlier in this chapter. The goal was to obtain the optimal annealing temperature to generate the desired PCR product, which is visualized on a gel as a single band, right around 100 bp, but is dependent on the size of the amplicon that the primers were designed to amplify. As indicated in Figure 14, if the annealing temperature is two low, this will permit non-specific binding of the primers and amplification by PCR will generate multiple products. For example, the optimal annealing temperature for A12.25 was determined to be 60 °C, based on the results displayed in Figure 14. All 21 primer sets designed to amplify ADH2 (Table 3) were optimized using this technique. The optimization techniques described in this section were repeated for each set of primers designed to cover three additional loci, CYS3, DED1, and CHA1. The sequences of these primers can be found in Tables 4, 5, and 6 respectively.

Quantitative Real-Time PCR (qPCR) Analysis

After all primer sets were optimized to determine the correct annealing temperature, they were subsequently tested using quantitative real-time PCR (qPCR) and a set of yeast genomic DNA standards. The total reaction volume was 10 µl (8 µl of reaction mix and 2 µl of DNA). The reaction mix was composed of 5 µl of iTaq Universal SYBR Green SuperMix (Bio-Rad Laboratories, Hercules, CA), 250 nM (0.125 µl) of each primer (forward and reverse), and 2.75 µl of nuclease-free water. This master mix was prepared in excess and 8 µl was subsequently pipetted into the appropriate wells of a Hard-Shell Low-Profile Thin-Wall 96-Well Skirted PCR Plate (Bio-Rad

Laboratories, Hercules, CA). A standard curve was prepared with yeast genomic DNA

and serially diluting (1:10) from 17.8 ng/µl down to 1.78 x 10^{-4} ng/µl in order to generate

six data points (17.8, 1.78, 0.178, 0.0178, 0.00178, and 1.78 x 10^{-4}). Two microliters of

each standard was added to the appropriate well. A no template control (NTC) was also

included that contained 2 µl of nuclease-free water in place of DNA. A 96-well plate seal

was positioned on the top of the plate and the plate was centrifuged to ensure no air

bubbles were present in the wells. The cycling conditions used for qPCR were as follows:

95 °C for 10 minutes, then 40 cycles of 95 °C for 15 seconds, 60 °C for 30 seconds, and

72 °C for 30 seconds. At the conclusion of the run, a melt curve was generated by heating

the samples from 60 to 95 °C at a rate of 0.1 °C/second. This was performed on the CFX

Connect Real-Time PCR Detection System (Bio-Rad Laboratories, Hercules, CA) and

data was generated in the CFX Manager Software. To ensure that the qPCR conditions

were optimal for each primer set, certain parameters were evaluated (Figure 15) (135). It

was ensured that the standards amplified accordingly to generate a standard curve with an

R^2 value close to 1, that there was no amplification in the NTC, and that the melt curve

had a single peak, which is indicative of a single PCR product. An example of these

parameters are exhibited in the plots contained in Figure 15.

All samples were analyzed for each primer set using this qPCR method. Prior to

qPCR analysis, the undigested samples were diluted 1:500 and the mononucleosomal

DNA samples were diluted 1:100. This allowed for all samples to be proximal in DNA

concentration and to fall within the range of the standard curve (17.8 ng/µl to 1.78 x 10^{-4}

ng/µl) (125). The samples were prepared in the same method as the standards, by adding

2 µl of each DNA sample to 8 µl of the master mix (iTaq Universal SYBR Green

SuperMix, primers, and water). The cycling conditions used for each primer set were the same as previously described, however the annealing temperature of 54.5 °C was used (rather than 60 °C) for primer sets A4 and A20 for locus ADH2. These annealing temperatures were based on the results of the primer optimization experiments. A representative plot from the qPCR analysis using the CFX Manager Software can be viewed in Figure 15. Further, the data collected on this program can be exported in the form of Microsoft Excel spreadsheets.

Results

Data Analysis

All qPCR data were exported into Excel. The first step in analysis was to calculate the relative amount of each amplicon. It was necessary to correct for the input DNA concentration because the amount of input DNA varied between samples, which will ultimately affect the amount of amplicon detected. This normalization was done by taking the amplicon starting quantity (SQ) (determined from qPCR) and dividing by the input DNA concentration (determined from the measurement on the Qubit Fluorometer). The amplicon SQ is calculated based on the standard curve and the corresponding quantification cycle (Cq) of each standard data point. The Cq of the unknown samples is experimentally measured and then plotted on the standard curve to calculate the SQ (Figure 15) (125). The relative amount of each amplicon could then be compared between the MNase digested sample and its corresponding undigested control sample and the DNase digested sample and its corresponding undigested control sample. Comparisons could also be made across the different radiation exposures: 0, 50, and 150

Gray. This was done for each primer set and for each of the four loci, ADH2, CYS3, DED1, and CHA1.

The next step in analysis was to calculate the relative protection value of each amplicon. The relative protection value is the fold-enrichment of a particular amplicon in the digested DNA over the undigested DNA (125). This was done by dividing the corrected, digested amplicon (either MNase or DNase) by its corresponding no digest sample. The protection of an amplicon by either a nucleosome or a protein can be determined because if an amplicon is not protected, it will be digested by the corresponding enzyme. If an amplicon is protected by a histone or other protein, it will not be digested and will still be present in the digested samples after DNA purification (125). In a preliminary analysis, the relative protection values obtained from the two different amounts of enzyme, 30U and 45U for MNase and 25U and 35U for DNase, were analyzed and evaluated separately. The relative protection values did not exhibit significant differences and indicated an identical pattern of protection. For a secondary analysis of the data, the relative protections between the two MNase treatments (30U and 45U) were averaged and the relative protections between the DNase treatments (25U and 35 U) were also averaged. These are the relative protection values that were used for the data discussed in the remainder of this chapter. The relative protection of each amplicon can then be compared across the radiation exposures (0, 50, and 150 Gray). This was done for the four loci, ADH2, CYS3, DED1, and CHA1.

ADH2 Results

The first locus analyzed was the Alcohol Dehydrogenase (ADH2) promoter region (YMR303C) located on Chromosome XIII (874,203-874,977). ADH2 has an important role in catalyzing the conversion of ethanol to acetaldehyde and can result in the production of certain carboxylate esters (136). This region was previously characterized to have one strongly positioned nucleosome and two other nucleosomes that aren't as strongly positioned, but cover the TATA box and RNA initiation site (125). From the mapping results of our experiments exhibited in Figure 16, we found that there was nucleosome protection centered at amplicons A3-A4 (874,794-874,923), A8-A9 (874,627-874,748), A12-A13 (874,467-874,617), and A18-A19 (874,246-874,399). Figure 16 was generated in Ensembl by mapping the relative protection values of the amplicons against the chromosomal location of the amplicons (137). In this study, the primers were designed to produce amplicons that overlapped to allow for determination of precise locations of bound proteins. The relative protection values were mapped against non-overlapping regions, which required determining the region that was unique to a particular amplicon and did not overlap with the previous amplicon. The non-overlapping region was distinguished based on the genomic location of the primers and therefore the resulting amplicon. This mapping technique shows four distinct regions of nucleosome protection indicated by the fold-enrichment of the mononucleosomal DNA in the samples. Furthermore, the regions protected are right around ~150 bp in size, which is consistent with the length of DNA known to associate with histones as a nucleosome. Previous literature, indicated that the protection found at 874,627-874,748 was actually a well-positioned protein rather than a nucleosome (125). This result was consistent for the

No Exposure sample, 50 Gray Exposure sample, and 150 Gray Exposure sample in our experiment, as seen in the consensus pattern in the three panels present in Figure 16.

The DNase digestion was used to analyze regions that are bound to histone and non-histone proteins alike. Theoretically, it should exhibit the pattern of protection resulting from the MNase digestion, but supplemented with any additional DNA-binding proteins that are bound in this region. This digestion showed that there was protection at amplicons 1-4 (874,794-874,977), 12-16 (874,361-874,617), and 18-20 (874,203-874,399). There is a slight decrease in the relative protection value from approximately 874,627 to 874,748. This is the region that was protected in the MNase digestion, but was characterized as a well-positioned protein rather than a nucleosome by the previous literature (125). For this digestion, there wasn't fold enrichment as seen in the MNase digestion, but rather the protection was indicated by a relative protection value right around 1 and a decrease in protection was indicated by a lower, fractional relative protection value. The resulting DNase digestion pattern was consistent for the No Exposure, 50 Gray, and 150 Gray samples. Figure 16 depicts the map of such protection by proteins. The pattern of the protection is the same across exposures, however there seems to be a decrease in the relative protection values from around 1 to around 0.7 after exposure to 150 Gray of radiation.

CYS3 Results

The second locus analyzed was the Cystathionine gamma-lyase (CYS3) (YAL012W) promoter region. CYS3 catalyzes a reaction involved in the transsulfuration pathway and the abundance of the protein encoded by this gene increases in response to DNA replication stress (138). The CYS3 promoter region was previously characterized

as "fuzzy" due to its containment of nucleosomes that are not well localized (123). Additionally, a research group recently found three nucleosomes positioned in 20 different conformations (139). Two nucleosomes were strongly positioned and one showed variable positioning, with some individual cells lacking the nucleosome completely (139). The existence of multiple conformations may explain the previous characterization of "fuzzy" in this region.

The results of this experiment indicated the presence three distinct regions of protection by nucleosomes. It was found that there was nucleosome protection at amplicons CYS3_1-CYS3_2 (130,185-130,329), CYS3_5-CYS3_6 (130,369-130,509), and partially at CYS3_10 (130,682-130,781). This protection result can be mapped out along the promoter region on Chromosome I as seen in Figure 17. The two strongly positioned nucleosomes are present at 130,185-130,329 and 130,369-130,500, and then there is a slightly protected region around ~137,000. There is also a distinct lack of protection in the CYS3 protein coding region (Figure 17). This result was consistent for the No Exposure sample, 50 Gray Exposure sample, and 150 Gray Exposure sample, as the maps in Figure 17 show the same pattern of protection. This result indicates that irradiation did not alter the positioning of nucleosomes or pattern of protection at this locus.

The DNase digestion was used to map the location of proteins in this region. In the 'No Exposure' sample, the DNase digestion produced fractional amounts for the relative protection values, but most values were between 0.8 and approached 1, indicative of potential protection. However, there was a slight decrease in the fractional relative protection value at amplicons 8-9 (130,492-130,689), with a value around ~0.6,

potentially indicating a decrease in protection. The '50 Gray' sample also showed this similar pattern of protection with majority of amplicons producing a relative protection value around ~0.8, but with a decrease in protection at amplicon 8-9 with a value around ~0.6. Lastly, the '150 Gray' sample resembled this pattern, however most amplicons were at a relative protection value of around ~0.6-0.7 and the decrease around 8-9 was right around ~0.4-0.5. The region that showed a decrease in relative protection values resulting from the DNase digestion (130,492-130,689) was also depleted and unprotected according to the MNase digestion. This pattern is presented in Figure 17 and shows consistent protection by proteins, but an overall, slight decrease in the fractional relative protection value at the exposure to 50 and 150 Grays of radiation alike.

DED1 Results

The Dead-box protein (DED1) promoter region was also analyzed. DED1 (YOR204W) codes for an ATP-dependent DEAD (Asp-Glu-Ala-Asp)-box RNA helicase and is an essential enzyme required for translation initiation in all yeast mRNAs (140). Previous literature describes four nucleosomes in the regions that flank the promoter and the distinct DED1 promoter region that is depleted of nucleosomes (141). There is a distinct nucleosome at the 3' end of the HIS3 coding regions and other proximal nucleosomes cover the DED1 coding region. In this experiment, we found that four particular regions on Chromosome XV were protected 1 (722,386-722,486), 3-4 (722,510-722,694), 9-10 (722,845-723,000), and 12 (723,079-723,174). The mapping of this region can be visualized in Figure 18. This map indicates four potential nucleosomes with a distinct, unprotected region (722,694-722,845) that lacks nucleosomes, which is the DED1 promoter region. There is also the nucleosome positioned at the 3' end of the

HIS3 protein coding region and the two nucleosomes present in the DED1 coding region. This result was consistent across all exposures, No Exposure, 50 Gray, and 150 Gray, as their maps are consistent as seen in Figure 18.

The DNase digestion produced consistent protection of this region by other proteins. The majority of the region analyzed exhibited protection due to the DNA being bound by proteins and thus protected from enzymatic digestions. The region from amplicons 5-8 (722,694-722,845) exhibited a lower fractional relative protection value, which was consistent with the results of the MNase digestion. The result was consistent across all three exposures, however the 150 Gray exposure showed a lower, fractional relative protection value of all amplicons. The No Exposure and 50 Gray samples showed relative protection values right around 1 in protected regions and then around 0.6 in the unprotected region. However, the 150 Gray sample showed a relative protection value of around 0.7 in the protected region and a value of 0.2-0.4 in the unprotected region. These maps can also be viewed in Figure 18.

CHA1 Results

The final locus analyzed was the gene that codes for catabolic L-serine deaminase, CHA1. CHA1 (YCL064C) catalyzes the degradation of L-serine and L-threonine (142). Previously, the CHA1 promoter region has been characterized as "fuzzy", with nucleosomes that are not well localized, suggesting that there is a cell-to-cell variability of nucleosome positioning (123). Another research group found that there were two potential nucleosomes at the 5' end of the gene followed by a nucleosome-free region (139). Analysis of 481 individual cells resulted in the discovery of 68 different nucleosome conformations, with a total of 4 potential nucleosomes (139). With such a

high number of different nucleosome conformations, there is an expectation that nucleosome mapping results may vary.

Analysis of this locus produced some interesting results. For the 'No Exposure' sample, the MNase-digested sample produced all fractional relative protection values for the 15 different amplicons analyzed; the relative protection values were all less than one and did not show the fold enrichment that was demonstrated in the other loci that we analyzed. When comparing the MNase digested samples to the no digest sample, there seems to be a higher relative protection value at amplicons 6-9 (15,976-16,157), but all values are less than one; there was no fold enrichment of mononucleosomal DNA. Additionally the '50 Gray' sample also presented evidence of protection at amplicons 6-9 (15,976-16,157), with fold enrichment visualized in the digested samples. The '150 Gray' sample closely resembled the 'No Exposure' sample with fractional relative protection values of all amplicons. However, higher fractional relative protection values were visualized at amplicons 6-9 (15,976-16,157). These patterns can be visualized in Figure 19 and appear to indicate a consensus pattern of relative protection in this region. This may suggest the positioning of nucleosome(s) in this region. In all three exposures, there was also a lack of protection from about 16,157-16,400 as seen by the sharp decrease in the relative protection value right about 16,100 (Figure 19).

The DNase digestion at CHA1 revealed consistent protection of all amplicons with relative protection values between 0.8 and 1 for all amplicons. There was no fold enrichment visualized at any of the amplicons analyzed. This result was also visualized in the 50 and 150 Gray irradiated samples. However, in the 150 Gray exposure, the relative protection value was slightly lower, around 0.6-0.8. In Figure 19, there are no regions

that appear to lack protection by proteins according to the DNase digestion. If this region lacks strong association with nucleosomes, it may allow for other, non-histone proteins to bind consistently, which may be what we are potentially seeing in this experimental result.

Discussion

The purpose of this experiment was to optimize the protocols necessary to map the positions of nucleosomes and proteins at four specific loci in *S. cerevisiae*. Furthermore, the effects of 50 Gray and 150 Gray doses of irradiation on the positioning of nucleosomes and other proteins were evaluated. As described in the methods section of this chapter, the techniques that were optimized and utilized allowed this goal to be achieved. By using a standard workflow for all samples and loci, this analysis system can be further developed and applied to evaluate other systems. The protocols that we used in these experiments followed established and published protocols that were referenced throughout this chapter (125, 132). However, in any experiment, there will always be modifications that have to be made. We found in this study that it is essential to optimize every parameter of an experiment. This requires determining reaction conditions by taking into account all variables; necessary reagents, specific concentrations of reagents, potential inhibitors, temperature, duration, etc. For example, the success of any enzymatic digestion is contingent on supplying the enzyme with the correct reaction conditions as they require particular co-factors and their activity is optimal at a specific temperature. Alternatively, enzymes will have inhibitors, so it is essential that these are not present in the reaction environment. This optimization was accomplished by breaking down every step in this protocol and evaluating all necessary components. Once in a working

condition, the experimental protocols can then be modified for other experiments, as demonstrated in the experiments discussed Chapters 3 and 4. The success of the protocols in this experiment is illustrated by our ability to map the locations of nucleosomes and other proteins in four different loci in yeast, under three different exposures to radiation.

From this study, we were able to conclude that there was no obvious effect of radiation exposure on the positioning of nucleosomes and other proteins at the four loci we analyzed. The first locus that analyzed was ADH2, which was previously characterized to have three well-positioned nucleosomes and a well-positioned protein that protected associated DNA from MNase digestion (125). The results of our experiment aligned with this previous characterization, as we saw four distinct regions of DNA that were protected from enzymatic digestion due to their association with histones (Figure 16). Based on the protection pattern we observed in our control sample as well as the two different radiation-exposed samples, there is no apparent effect of radiation on nucleosome positioning at this locus. The results of the DNase digestion also lead us to believe that this locus contains additional DNA-binding proteins in addition to the histones that are bound. This interpretation is based on the consistent protection illustrated in the second map of Figure 16, showing protection at regions supplementary to those protected in the MNase digestion. An interesting consideration about this particular locus is the unknown protein approximately located between 874,600 and 874,800. This protein appears to protect the amount of DNA known to associate with the histone octamer as a nucleosome (~147 bp) and was protected from the MNase digestion. However, this region of DNA showed a decrease in the relative protection value obtained from the DNase digestion when compared to other regions of the locus. Initially, we

would need to determine if the decrease in relative protection value is a significant difference or if the decrease was still within the expected region of difference in these values. Again, this result warrants further investigation into the identity of this protein. The goal would be to understand why this particular region appears to be sensitive to the DNase enzyme, but protected from the MNase enzyme. Again, future experiments may help us to determine what we are seeing with the protein-association at this region of the locus.

The second locus we evaluated was CYS3. One of the reasons that we chose to analyze the positioning of proteins at this locus was because it was previously classified as poorly characterized in terms of its nucleosome positioning. Single cell analysis of this locus revealed that there were two well-positioned nucleosomes and a third potential nucleosome that was not as strongly positioned. Also, there were multiple nucleosome configurations that varied in terms of the number of nucleosomes as well as the positioning locations (139). Our mapping results, as seen in Figure 17, show a distinct pattern of two regions protected from MNase digestion due to their association with histones as nucleosomes. The regions protected are approximately ~150 bp in size (Figure 17). Additionally, there is a third region of DNA (~25 bp) that indicates a third potential nucleosome. However, due to the smaller size of this protected region, this may suggest that this region is only partially protected or alternatively that there may be movement of this nucleosome. This result also raises the question of cell to cell variability that was addressed in previous studies (139). In this experiment, we analyzed a bulk population of cells and our mapping result is an average or snapshot of the positioning among the cells. At a region that we are seeing partial protection, this result

may be attributed to multiple configurations of nucleosomes and our result showing a combination of these patterns. It may also be helpful to design additional primer sets that analyze this region further to help understand why a smaller region appears to be protected. In CYS3, there is also a very distinct region that was unprotected from digestion, which may be indicative of a nucleosome-free region (~130500-130650) at the promoter region. The protection patterns obtained from the MNase digestion at this locus were consistent between the no exposure control sample and the two radiation-exposed samples. The results of the DNase digestion again showed consistent protection from enzymatic digestion by proteins bound at this locus. We did see a slight decrease in relative protection value at the unprotected region found in the MNase digestion (~130,500-130,650), regardless of exposure to radiation.

We selected our third locus, DED1, for analysis because it has been characterized to have four well-positioned nucleosomes and a distinct region that is nucleosome-free (141). The region that is nucleosome-free may be useful in down-stream experiments in which we hope to analyze both unprotected and protected regions for lesions associated with DNA damage. When we experimentally determined the nucleosome positioning at this locus, we found a pattern that mimicked that described by another research group (141). There was a distinct region that was unprotected and presumably nucleosome-free. This region was distinguishable at a genomic location of 722,694-722,845 in our results, as seen in Figure 18. There were also four regions protected by four nucleosomes that were proximal to the boundaries of the nucleosome-free region. We see in Figure 18 that the pattern of nucleosome positioning does not appear to be affected by exposure to radiation. The analysis of DED1 based on the DNase digestion shows a pattern of

consistent protection by other proteins, but a slight decrease in the relative protection value at the nucleosome-free region indicated by the MNase digestion. We hope that future experiments may provide insight into what types of additional proteins are protecting this locus and the other loci analyzed. An investigation into DNA-bound proteins and correlation with the cell cycle may aid in our understanding of what types of proteins may be bound.

Lastly, we analyzed CHA1 for the same reasoning behind our analysis of CYS3. CHA1 was previously poorly characterized and single cell analysis revealed four potential nucleosomes and multiple configurations ranging from 2-4 nucleosomes positioned at different locations (139). In our relative protection maps in Figure 19, we see that there is a region from 15,976-16,157 that appears to be protected and a region from 16,157-16,400 that seems to lack such protection. The analysis of CHA1 is unique from the other loci examined in that we did not see fold enrichment of the relative protection values at protected regions. Rather, we saw a higher fractional relative protection value. It is important to keep in mind that we are analyzing a bulk population of cells that are expected to show cell to call variation in nucleosome positioning. Our mapping result being an average of the configuration may explain this distinct, but fractional relative protection value. If some cells exhibit nucleosome positioning at a particular region of DNA, but others do not, our result is then an average of these configurations. We do note that we did see a similar pattern of protection regardless of radiation exposure, as exhibited in Figure 19. There was also a consistent pattern of protection from DNase digestion, as shown in Figure 19, in all three samples. We

speculate that this may be due to the association of other DNA-binding proteins in this region, in addition to the association of DNA with histone proteins.

Looking at the results of these experiments, it is important to point out features of this experimental design that factor into our interpretation of the results. As pointed out earlier, we performed our experiments using a bulk population of cells. We expect that there is cell to cell variation due to shifts in nucleosome positioning. With this realization in mind, our end result is somewhat of a snap shot of all of the cells analyzed. If numerous nucleosome configurations exist, our end mapping result could be contingent on the number of cells with a particular protein positioning pattern. If we see a very distinct region of protection, this may indicate that a greater percentage of cells have this nucleosome strongly-positioned. However, if the region is either not as distinct or there are differences in the relative protection values, it may indicate that this nucleosome positioning is more variable and multiple configurations exist.

A similar consideration is the stage of the cell cycle that the yeast were in when analysis was performed. As described in the Materials and Methods section of this chapter, the yeast were in the exponential growth phase (budding) when they were irradiated and then immediately flash frozen. Looking at microscopy results (Figure 9), it is apparent that although majority of cells are budding, some are not at that moment. We infer that all of the cells aren't at the exact same point in the cell cycle at a given point in time. Further, being in the midst of growth may give rise to differences in chromatin organization, thus affecting the relative protection values we may obtain. In the future, it may be insightful to analyze single cells to get a more precise look into the nucleosome configurations that exist (139). Although this analysis would be more difficult than

working with a population of many cells, it may indicate a prevalent nucleosome configuration in the population. We might then be able to distinguish if this configuration also exists in samples that were exposed to radiation. Future experiments might also include the analysis of yeast cells after they have been synced at different stages of the cell cycle. The transitions between cell cycle stages will influence chromatin organization and subsequently, nucleosome positioning (4).

The experimental results of our DNase digestion suggest that the four loci analyzed are consistently protected from DNase digestion due to their association with histones and non-histone proteins. While we saw fold enrichment in the relative protection values of the MNase digested samples, we only saw relative protection values right around 1 or higher, fractional relative protection values in the DNase digested samples. The reasoning behind this difference in relative protection values may be due to the difference in sample preparation, post-digestion. In our experiments, post-MNase digestion, we purified the mononucleosomal DNA by excising it from a gel, thus producing a sample that only contained mononucleosomal DNA. This isolation may then explain the fold enrichment exhibited in the digested samples. For the DNase digestion, we did not perform any purification or isolation of DNA; native gel electrophoresis was only used to confirm that the enzymatic digestion was successful. The DNA sample that we are analyzing downstream is digested by the enzyme, but not purified, so it contains varying degrees of digestion. If feasible, it may be interesting to purify fragments of DNA at particular or even a range of fragment sizes, resulting from DNase digestion. The purified and isolated fragments could then be analyzed for protection according to the methods discussed in this chapter.

The results of our experiment suggest that exposure to radiation does not appear to have an obvious effect on the pattern of protein protection we observed at four specific loci, ADH2, CYS3, DED1, and CHA1 in *Saccharomyces cerevisiae*. The chromosomal maps of the relative protection values show a distinct protection pattern that appears to exist at these four loci regardless of exposure to radiation (Figures 16-19). Exposing the cells to irradiation and then analyzing the positions of nucleosomes at four different loci illustrates that there is a distinct pattern of nucleosome positioning that is conserved, even in conditions that are known to stress the cell and could potentially damage DNA. Given that nucleosome positioning is complex, this result may suggest that the nucleosomes we observed are strongly positioned. Such conservation of positioning may be associated with the protective role that histones and other proteins play in protecting DNA from radiation-induced lesions. It is also possible that the four loci we analyzed may not be involved in any damage response, so we may not see a reaction to radiation exposure. However, we need to investigate this relationship further.

We hope to continue our research endeavors with future experiments that comprehensively evaluate the genomic environment and its ability to protect DNA. To further investigate the protective capabilities of the genomic environment, it would be necessary to also consider DNA sequence along with the positioning of histone and non-histone proteins. Now that we have experimentally mapped out regions that are protected and unprotected by protein association, this data can be used in conjunction with future experiments. These mapping techniques can also be used to evaluate particular loci that play essential roles in processes such as DNA repair (72). Taking a closer look at the regions that are bound to a protein as well as those that lack such association may reveal

particular sequences motifs that protect DNA from damage. We may find that the

sequence and structure of DNA work synergistically to protect regions of DNA from

damage, thus forcing the sites of damage to be non-random throughout the genome.

There are still many experiments and analyses to be carried out as we work towards

understanding such relationships at the molecular level.

Table 1. Dose Chart for RS-2000.
This table contains the level the samples were placed at inside the instrument (RS-2000), which was the level closest to the radiation source, level 6. All samples were placed in the center of the sample shelf. Two samples contained in 50 mL conical tubes were irradiated per sample run, totaling to five runs and ten samples per radiation dose. The dose rate is calculated based on previous calibration experiments conducted by UNMC and this rate determines the programmed time to deliver a desired dose.

Sample Run	Dose	Level	Dose Rate	Time
1A	0 Gray	N/A	N/A	N/A
1B	0 Gray	N/A	N/A	N/A
1C	0 Gray	N/A	N/A	N/A
1D	0 Gray	N/A	N/A	N/A
1E	0 Gray	N/A	N/A	N/A
2A	50 Gray	6	8.5 Gy/Min	5 min. 53 sec.
2B	50 Gray	6	8.5 Gy/Min	5 min. 53 sec.
2C	50 Gray	6	8.5 Gy/Min	5 min. 53 sec.
2D	50 Gray	6	8.5 Gy/Min	5 min. 53 sec.
2E	50 Gray	6	8.5 Gy/Min	5 min. 53 sec.
3A	150 Gray	6	8.5 Gy/Min	17 min. 39 sec.
3B	150 Gray	6	8.5 Gy/Min	17 min. 39 sec.
3C	150 Gray	6	8.5 Gy/Min	17 min. 39 sec.
3D	150 Gray	6	8.5 Gy/Min	17 min. 39 sec.
3E	150 Gray	6	8.5 Gy/Min	17 min. 39 sec.

Table 2. List of Experimental Samples.
This table contains the samples that were analyzed in this study. The variable of this experiment was radiation exposure, including a no exposure control, 50 Gray, and 150 Gray exposure. To determine the positioning of proteins, we performed enzymatic treatments using MNase and DNase, with two different enzyme amounts, and also maintaining a no digest control.

Sample #	Radiation Exposure	Enzymatic Treatment
1	No Exposure	No Digest (M)
2	No Exposure	30 U MNase
3	No Exposure	45 U MNase
4	50 Gray	No Digest (M)
5	50 Gray	30 U MNase
6	50 Gray	45 U MNase
7	150 Gray	No Digest (M)
8	150 Gray	30 U MNase
9	150 Gray	45 U MNase
10	No Exposure	No Digest (D)
11	No Exposure	25 U DNase
12	No Exposure	35 U DNase
13	50 Gray	No Digest (D)
14	50 Gray	25 U DNase
15	50 Gray	35 U DNase
16	150 Gray	No Digest (D)
17	150 Gray	25 U DNase
18	150 Gray	35 U DNase

Table 3. ADH2 Primer Sequences.

These primers were originally published in *Analysis of Nucleosome Positioning Using a Nucleosome Scanning Assay* by Infante et al. in 2012 (125). The primers were obtained from Sigma Aldrich (St. Louis, MO) in the form of lyophilized DNA oligos. Primers were optimized accordingly.

Forward Primer Name	Sequence	Reverse Primer Name	Sequence
A1_F	GAAGAGACTAATCAAAGAAT CGTTTTC	A1_R	CGTTTGTTTGCCCCTACG
A2_F	CGTTTTCTCAAAAAAATTAAT ATCTTAAC	A2_R	TCTTGGCATCAGAAAATTT GAG
A3_F	GTTTGATCAAAGGGGCAAAACG	A3_R	CGGATCATAAGGCAATTTT TAGATAAG
A4_F	AAATCGTTTCTCAAATTTTC TGATG	A4_R	CAGGCTGTAACCGGAGAGA C
A5_F	TCTAACCAGTCTTATCTAAAAAT TGCC	A5_R	TGAAGACAAAATCCCTTA ATTAAAAC
A6_F	CCGTCTCTCCGGTTACAGC	A6_R	ATGAGCGAAAGCCGTTAAT G
A7_F	CCTGCCTTTCTAATCACCATTC	A7_R	GCGGGCAAAACGTCATAAC
A8_F	AATTAAGGGATTTTGTCTTCATTA ACG	A8_R	GGATGGTTTCCCGCCTG
A9_F	AAAATGTTATGACGTTTTGCCCG	A9_R	AGATGCCCGGTGTTCCG
A10_F	GAAACCATCCACTTCACGAGACT G	A10_R	TTTTTTTTCATTCTCTCAAT CTGAAAT
A11_F	CCTCTGCCGGAACACCG	A11_R	CCATTTCTATGCTCTCCTCT GC
A12_F	AAGTTGGAGAAATAAGAGAATTT CAGATTG	A12_R	GCTTTACCAAAAAGTGAAC CCC
A12.25_F	GAGAATTTCAGATTGAGAGAATG AA	A12.25_R	GCTTTACCAAAAAGTGAAC CCC
A12.25_2_F	AAAAAAAAAAAAAAAAAAAAAGG CAGAGG	A12.25_2_R	TGAAAAAAGTCGCTACTGG CAC
A13_F	AAAAGGCAGAGGAGAGCATAGA AATG	A13_R	TGAAAAAAGTCGCTACTGG CAC
A15_F	ATCACATATAAATAGAGTGCCAG TAGCGAC	A15_R	TTACCAAGAAGAAACAAG AAGTGATAAA
A16_F	CACTCGAAATACTCTTACTACT GCTCTC	A16_R	GTTGATAGTTGATTGTATG CT TTTTG
A17_F	GTTGTTTTTATCACTTCTTG TTTCTTC	A17_R	TTGAGTTTCTGGAATAGAC ATTGTG
A18_F	GAATATCAAGCTACAAAAAGC ATACAATC	A18_R	ACTTGCCGTTGGATTCGTA G
A19_F	TATCGTAATACACAATGTCT ATTCCAGAAA	A19_R	GGCTTTGGCTTTGGAACTG
A20_F	CTCAAAAAGCCATTATCTTCTAC G	A20_R	GTGGCAGACACCAGAGTAC

Table 4. CYS3 Primer Sequences.

These primers were originally published in *Single-cell nucleosome mapping reveals the molecular basis of gene expression heterogeneity* by Small et al. in 2014 (139). The primers were obtained from Sigma Aldrich (St. Louis, MO) as lyophilized DNA oligos and were optimized accordingly.

Forward Primer Name	Sequence	Reverse Primer Name	Sequence
Cys3_1F	CCACGTCCCCATCAAACT	Cys3_1R	GCTTTCGCAAGCGAGGTC
Cys3_2F	GACGCTGAGCTGTATCACG	Cys3_2R	CACCGGGTTGGCTCTGTA
Cys3_3F	GGCAGAGGACCTCGCTTG	Cys3_3R	GGCCTTCGAGGTCGCTAA
Cys3_4F	CCAACCCGGTGGACAAAC	Cys3_4R	GAGCACCCGGGAAGGAGT
Cys3_5F	AACGAGATTAGCGACCTCGAA	Cys3_5R	GGCCCACTGGTGGAAGTC
Cys3_6F	ACTCCTTCCCGGGTGCTC	Cys3_6R	GGTATGGGGTCCAGTGTGG
Cys3_7F	CAACGACGACTTCCACCA	Cys3_7R	AGGGTGGAATTACATAGCGTTAC
Cys3_8F	CACACTGGACCCCATACCA	Cys3_8R	CGCCACAACTGGCTGAGA
Cys3_9F	TCACGTGATCTCAGCCAGTT	Cys3_9R	ACCTGGCATCTTATGCTTTAAATA
Cys3_10F	TGCCAGGTAGATGGAACTTG	Cys3_10R	CTTGTGTGTATATGTATAAGGTGCAAA
Cys3_11F	GTGCCGTGCCAGATTGAA	Cys3_11R	TGGTAGCAAATTTATCAGATTCTTG
Cys3_12F	TTGAGGCCTATACACATAGACATTT	Cys3_12R	GGCCTTGGTAGCAAATTTATCA
Cys3_13F	TGCTACCAAGGCCATTCA	Cys3_13F	TGCTACCAAGGCCATTCA
Cys3_14F	CCATTCATGCCGGTGAAC	Cys3_14R	ACCGATAGGGTTAGCTGGAG
Cys3_15F	CCCATTTCTTTGTCCACCA	Cys3_15R	CGGCAACTGCTCTTTCCA
Cys3_16F	CAGAGAGAACTTGGAAAGAGCA	Cys3_16R	GAAGCGATTGCAAGATTGTGG

Table 5. DED1 Primer Sequences.

These primer sequences were graciously provided by the laboratory of Dr. Kevin Struhl at Harvard Medical School. The primers were obtained from Sigma Aldrich (St. Louis, MO) and as lyophilized DNA oligos and were optimized accordingly.

Forward Primer Name	Sequence	Reverse Primer Name	Sequence
DED1_1F	TGCAAAGGGAGAAAGTAGGAGATC	DED1_1R	CAGACAATCAACGTGGAGGG
DED1_2F	AATTACCCTCCACGTTGATTGTCTG	DED1_2R	GCGAGGTGGCTTCTCTTATGGC
DED1_3F	TAGTGAGAGTGCGTTCAAGGC	DED1_3R	GTCACTACATAAGAACACCTTTGG
DED1_4F	CCAACGATGTTCCCTCCACC	DED1_4R	CGTATACATACTTACTGACATTCATAGG
DED1_5F	GCAGCATACGATATATATACATGTGTAT	DED1_5R	GCATTACCTTGTCATCTTCAGTATC
DED1_6F	CCTATGAATGTCAGTAAGTATGTATACG	DED1_6R	CGCCTCGTTCAGAATGACACG
DED1_7F	TTCTATACGTGTCATTCTGAACGAGG	DED1_7R	CCATCTCTTTTATATTTTTTTTCTCG
DED1_8F	CGAGAAAAAAAATATAAAAGAGATGG	DED1_8R	AATGCTTTTCTTGTTGTTCTTACG
DED1_9F	AAGTTAGTTGTGGTGATAGGTGGC	DED1_9R	CTTAAATTTTGCACTTGTTCGC
DED1_10F	TATTATGGCTGAACTGAGCGAAC	DED1_10R	CACTTCTTGGTTTTCCTCTTAAGTGAG
DED1_11F	AGAGGAAAACCAAGAAGTGCCAG	DED1_11R	TTGTTGCTAAAGAAGCTGCCAC
DED1_12F	CTTTAGCAACAACCGTCGTG	DED1_12R	CATCTACCACCAGAACGGC
DED1_13F	CTTCGGTGGAAACAACGG	DED1_13R	CCTTTTCGTTTCTTGGAGCTG
DED1_14F	CGATGGCAAACATGTCCC	DED1_14R	GTTATCGAAGTTAATACCAGAAGATTGG
DED1_15F	GAGATCGCCATATTTGGTGTCC	DED1_15R	CAGGAACATCCTTACCAGAGG
DED1_16F	TACGATGATATTCCAGTGGACGC	DED1_16R	TTGATGTTTTCCAATAACAATCCG
DED1_17F	TCCTGAACCAATCACAGAATTTACC	DED1_17R	ATTTTTGCACAGGTGTTGGC
DED1_18F	CGTTTCACCAAGCCAACACC	DED1_18R	CCCACCAGTCTTACCAGAACC

Table 6. CHA1 Primer Sequences.
These primers were originally published in *Single-cell nucleosome mapping reveals the molecular basis of gene expression heterogeneity* by Small et al. in 2014 (139). The primers were obtained from Sigma Aldrich (St. Louis, MO) and as lyophilized DNA oligos and were optimized accordingly.

Forward Primer Name	Sequence	Reverse Primer Name	Sequence
Cha1_1F	CCGGAAAGGCTTCTGCAC	Cha1_1R	TGGCACTTTTCATGATGAGATT
Cha1_2F	CCGGAAAGGCTTCTGCAC	Cha1_2R	TTTTGAATTCGAATGGCACT
Cha1_3F	CAACCAAGTGGCTCCTTCA	Cha1_3R	CGCCAGAACTAGCGAAAAC
Cha1_4F	CAACCAAGTGGCTCCTTCA	Cha1_4R	GCAGCAAAACCGGCATTA
Cha1_5F	TCATGAAAAGTGCCATTCG	Cha1_5R	CAGTCTTTGACATGCTGTTGC
Cha1_6F	CCTCAGGTTTTCGCTAGTTCTG	Cha1_6R	TCGCTGTAGGAACCACGAC
Cha1_7F	AATGCCGGTTTTGCTGCT	Cha1_7R	GGCACCGGTGTTCCTGAT
Cha1_8F	TGCTGCAACAGCATGTCA	Cha1_8R	GGCACCGGTGTTCCTGAT
Cha1_9F	GTACAGTCGTGGTTCCTACAGC	Cha1_9R	GTATCTGCTTCTTTCCAGTAGGC
Cha1_10F	ACACCGGTGCCCAGGTTA	Cha1_10R	GGGCTCAATGACCTGAGAG
Cha1_11F	ACACCGGTGCCCAGGTTA	Cha1_11R	CCGGATTATCGAAGGGATG
Cha1_12F	TGCCTACTGGAAAGAAGCAG	Cha1_12R	CCGGATTATCGAAGGGATG
Cha1_13F	TGAGCCCATTTATGTTCATCC	Cha1_13R	CACGGAAATATGTTGCGATT
Cha1_14F	CCGGATATTTGGGAAGGAC	Cha1_14R	CCTCCACCAACGCTGCAT
Cha1_15F	TCGCAACATATTTCCGTGA	Cha1_15R	CAGCTAAACCATACCTTTCCAA

Figure 7. Standard YPD plate containing *S. cerevisiae*.

This shows the colony growth on a standard YPD plate streaked with *S. cerevisiae* after 2-3 days incubation at 30 °C. Standard technique was used to isolate a single colony.
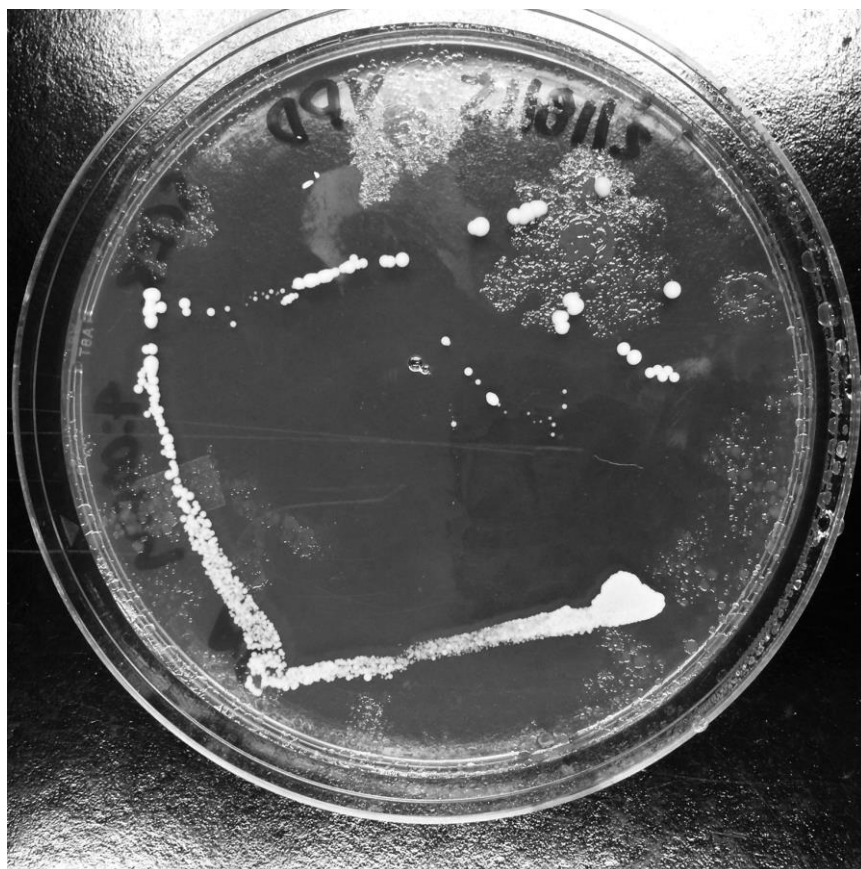
Figure 8. Culture Density of S288C *Saccharomyces cerevisiae*.

This plot was obtained by measuring the absorbance of a culture of *S. cerevisiae* in YPD broth. The culture originated from a single colony and was incubated at 30 °C in an incubator with shaking at 250 RPM. Absorbance readings at 600 nm were taken every hour from 0-54 (except 34-48 hours) hours using a spectrophotometer and YPD broth as a blank. At around 13 hours, it was necessary to dilute samples 1:10 using YPD broth in order to get a more accurate reading. This plot shows the culture density in the format of absorbance versus time (hours).
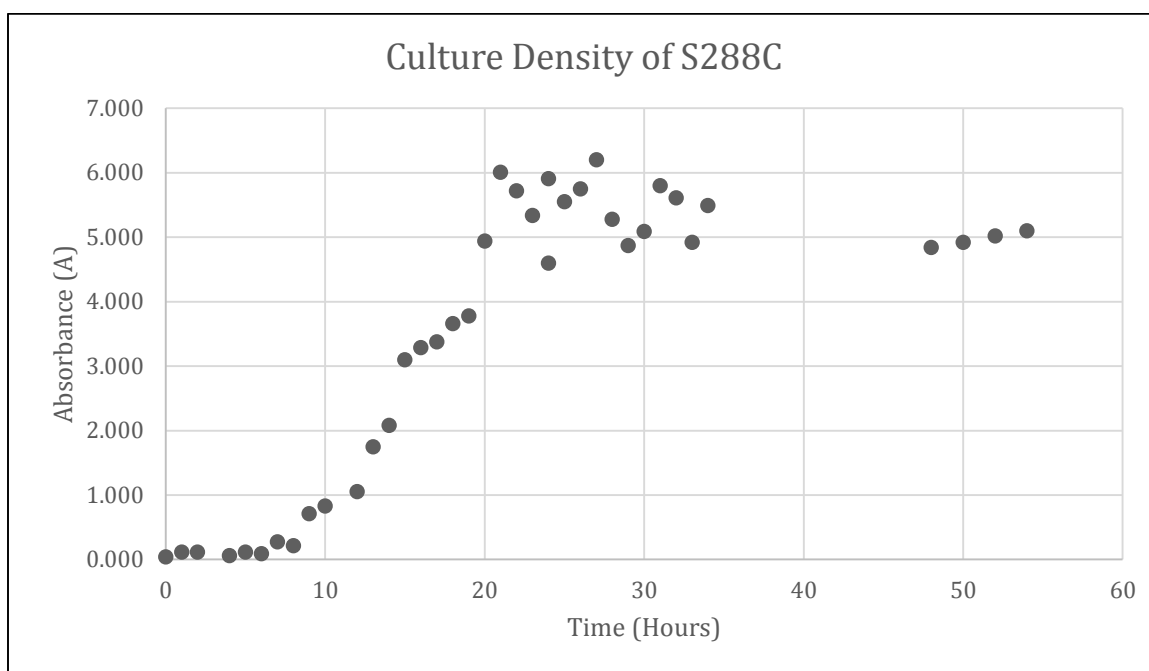
Figure 9. Yeast cells in growth phase.

This image was captured while visualizing yeast cells under the microscope under the 60X objective. The growth phase is indicated by the budding visualed.
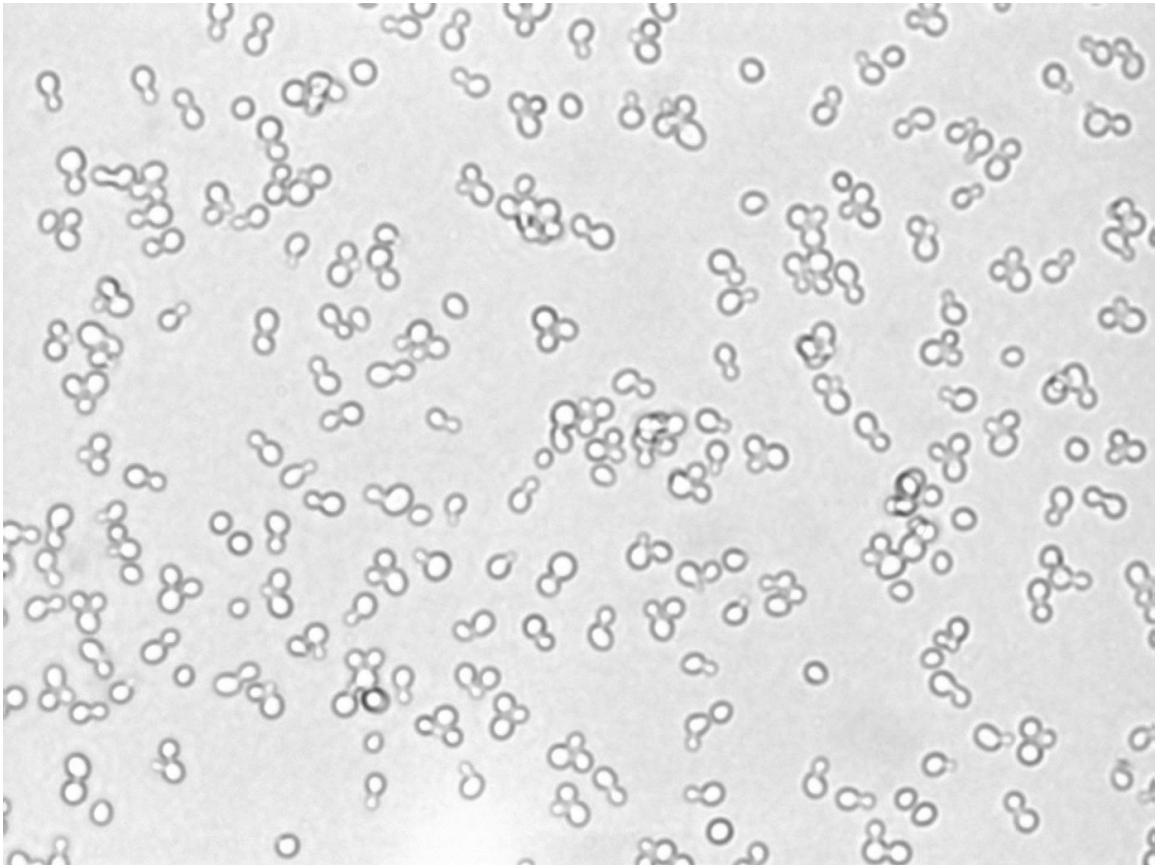
Figure 10. MNase Native Gel Electrophoresis.

This 1% gel was prepared using 50 mL of 1X TBE, 5 µl of EtBr, and 0.5 g agarose. The gel was run in 1X TBE Buffer (with EtBr) for 3 hours at 50 volts. The ladders included in the first two lanes are λ-DNA-HindIII Digest Ladder and 100 BP Ladder (New England Biosystems, Waltham, MA). This experiment tested 15U vs. 30U of MNase as well as a digestion time of 30 vs. 40 minutes.
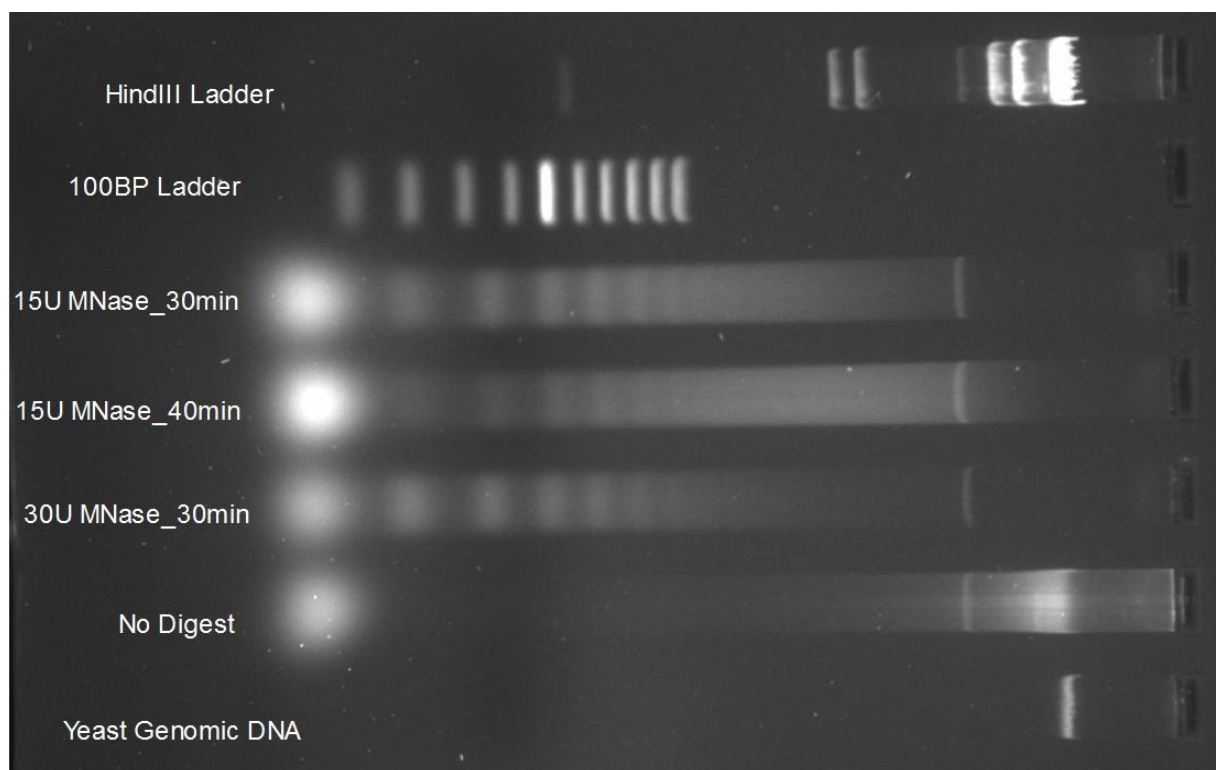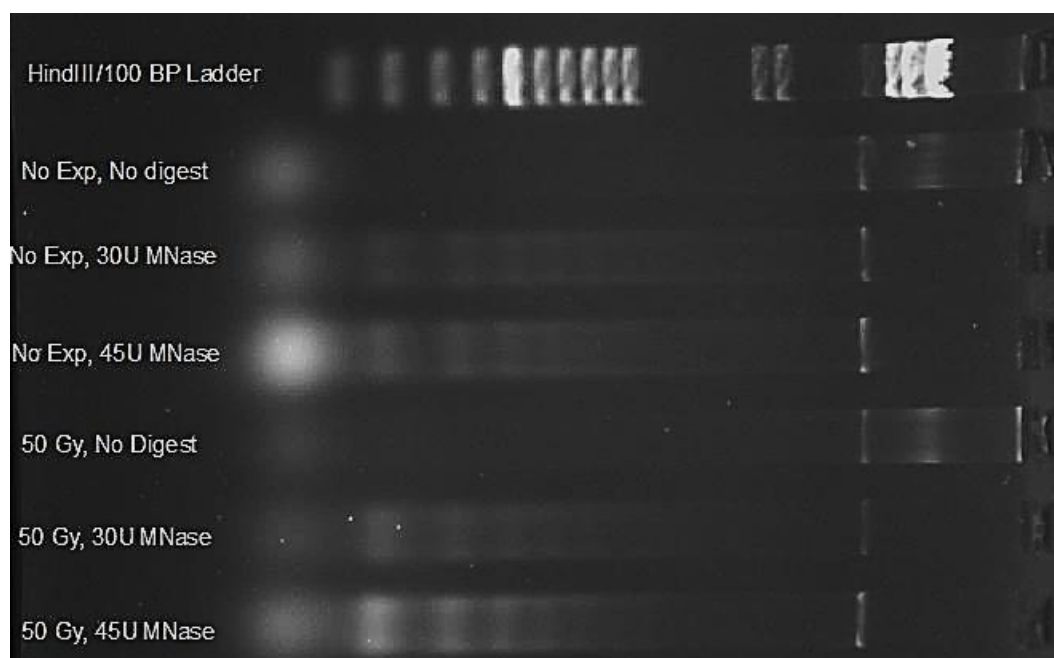
Figure 11. MNase Native Gel Electrophoresis of Irradiated Samples.

The 1% gel was prepared using 50 mL of 1X TBE, 5 µl of EtBr, and 0.5 g agarose. The gel was run in 1X TBE Buffer (with EtBr) for 3 hours at 50 volts. The ladder in the first lane is a combination of λ-DNA-HindIII Digest Ladder and 100 BP Ladder (New England Biosystems, Waltham, MA). These gels were used to confirm the enzymatic digestion and no digest control for the No Exposure, 50 Gray (A), and the 150 Gray samples (B).
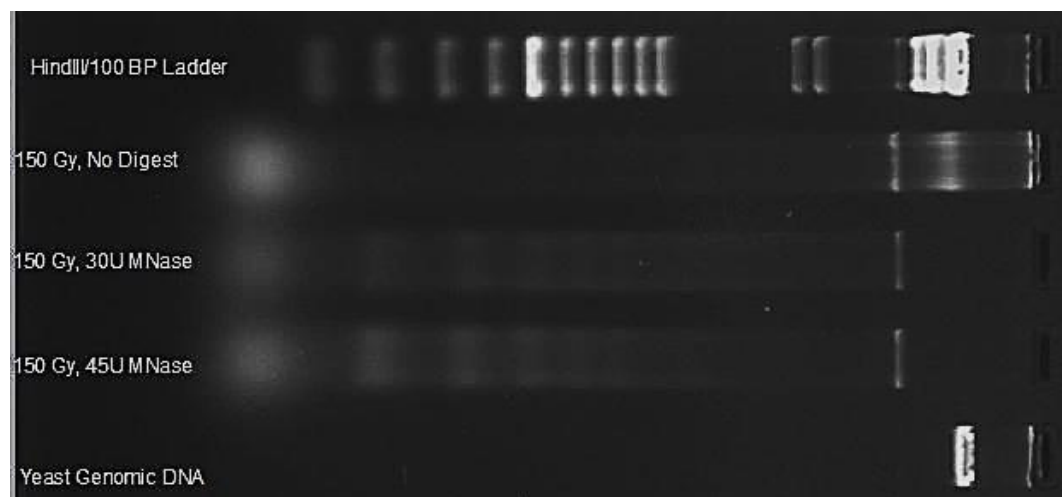
A)

B)

Figure 12. Gel Electrophoresis to Purify Mononucleosomal DNA.

The 1% gel was prepared using 50 mL of 1X TBE, 5 μl of EtBr, and 0.5 g low-melting point agarose. The gel was run in 1X TBE Buffer (with EtBr) for 3 hours at 50 volts. The ladder in the first lane is a combination of λ-DNA-HindIII Ladder and 100 BP Ladder (New England Biosystems, Waltham, MA). This gel was used to purify the mononucleosomal DNA from the digested samples for the No Exposure, 50 Gray, and 150 Gray samples. The gel can visualized before (A) and after the mononucleosomal DNA was excised (B).
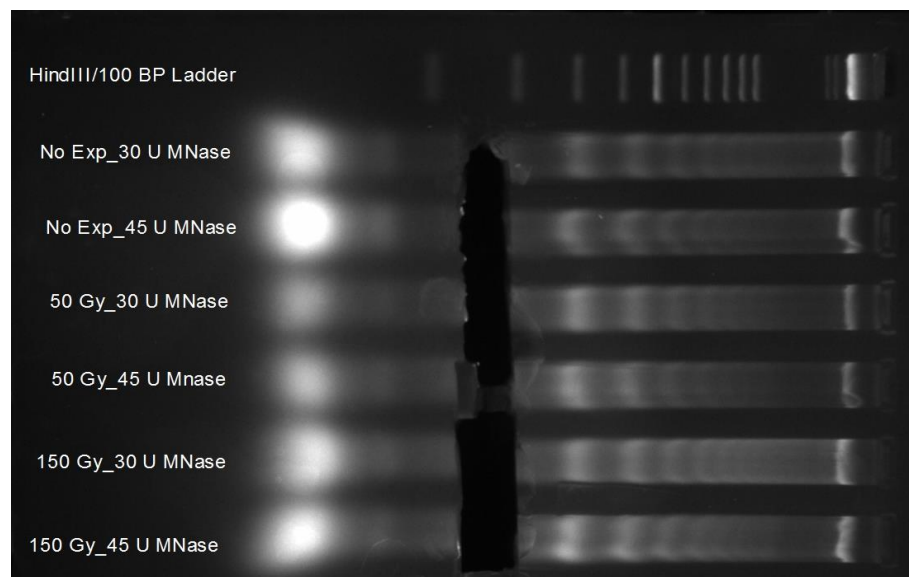
A)
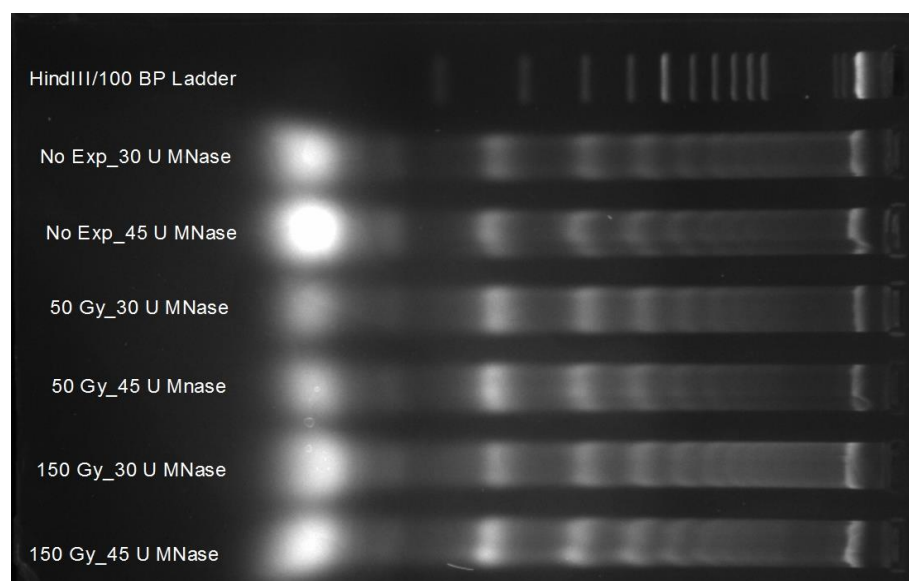
B)

Figure 13. Gel Electrophoresis to Confirm DNase Digestion.

The gels were prepared using 50 mL of 1X TAE, 5 μl of EtBr, and 0.5 g agarose. The gel was run in 1X TAE Buffer (with EtBr) for 30 minutes at 200 V. The ladder in the first lane is a combination of λ-DNA-HindIII Digest Ladder and 100 BP Ladder (New England Biosystems, Waltham, MA). These gels were used to visualize the DNase digestion and no digestion for the No Exposure (A), 50 Gray, and 150 Gray samples (B).

A)
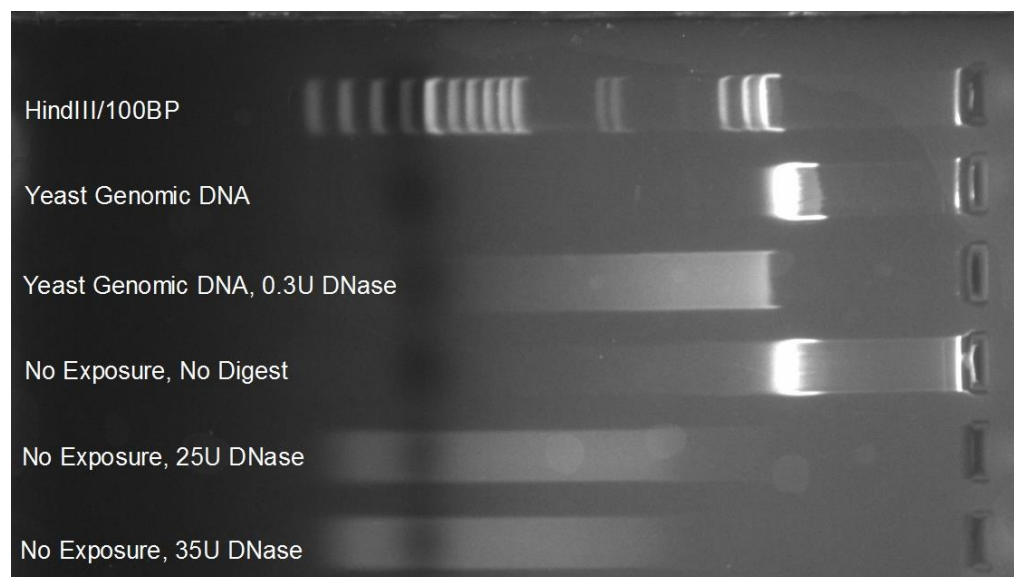
B)

Figure 14. Primer Optimization Gel Electrophoresis.

The primers to analyze all loci were optimized using a temperature gradient for the annealing temperature and traditional PCR. After amplification, 5 µl of the PCR product combined with 1 µl of 6X loading dye was analyzed on a native agarose gel. The gel was run at 100 V for 60 minutes. The size of the desired amplicon is around 100 bp. In the first two lanes, λ-DNA-HindIII and 100 bp ladders were run alongside the samples. The numbers below the lanes indicate the annealing temperature, in degrees Celsius, used from the temperature gradient PCR. This analysis indicated non-specific binding at lower temperatures by the presence of multiple bands, however a single band was obtained at 60 °C.
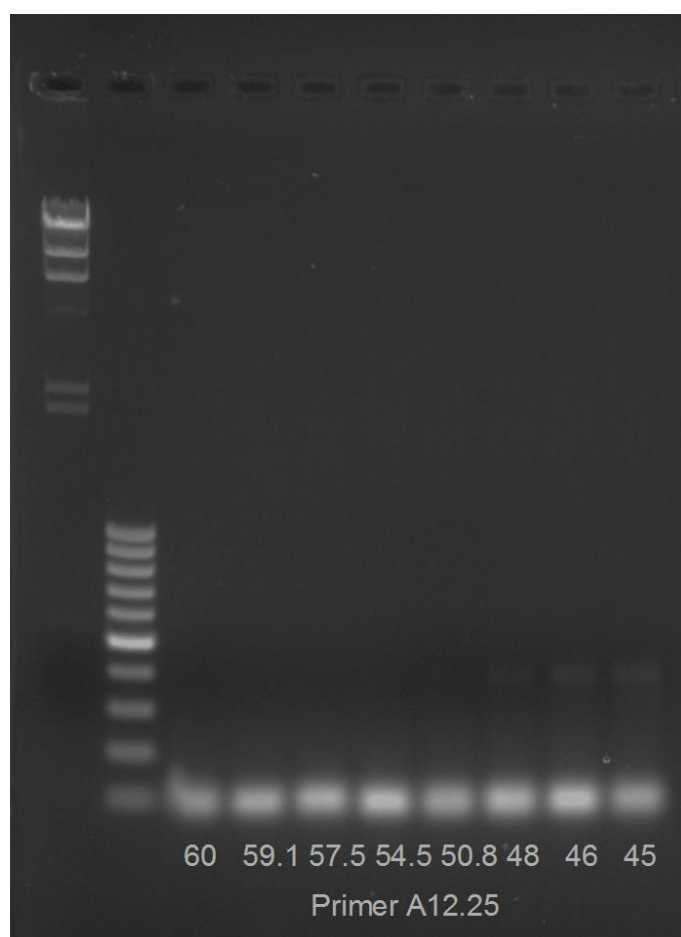
Figure 15. qPCR Plots from CFX Software.

Representative plots obtained from the CFX software. These plots are generated from the RFU detected after each PCR cycle (A), then using the standards to generate a standard curve of Cq versus the log of the starting quantity (B) and the unknown samples are plotted on the curve (x). Lastly, a melt curve is generated by heating the samples from 60 to 95 °C and ensuring a single product is obtained by the presence of a single peak (C).

A)
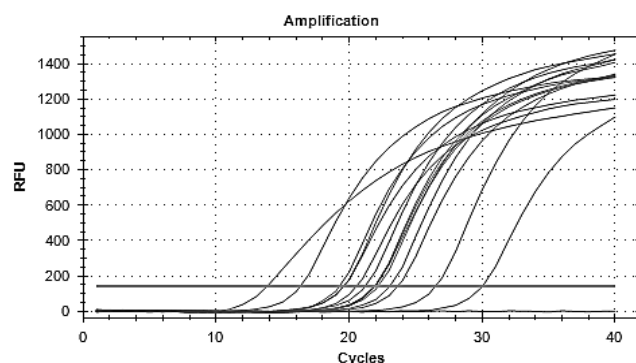
B)
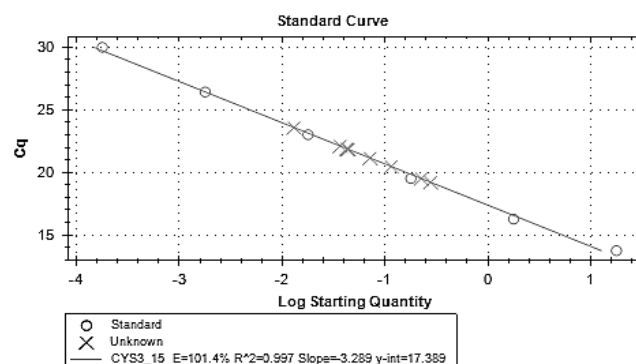
C)

Figure 16. Relative Protection Plots of ADH2.

The relative protection value was calculated by dividing the digested value by the no digest value for each amplicon. These values were then mapped along the chromosomal location in Ensembl (137). The four regions of the locus that were protected appear as a distinct black rectangular shape in the first panel. The second panel shows the DNase digestion to map all proteins. The three maps are from the No Exposure, 50 Gray, and 150 Gray samples (from top to bottom).
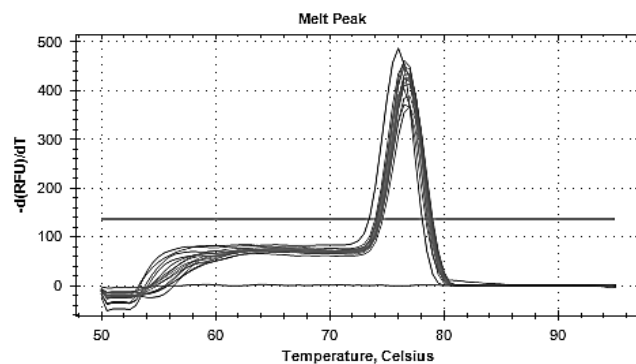
A)

B)

Figure 17. Relative Protection Plots of CYS3.

The relative protection value was calculated by dividing the digested value by the no digest value for each amplicon. These values were then mapped along the chromosomal location in Ensembl (137). The three regions that are protected at this locus appear as a distinct black rectangular shape. There are two very clear nucleosomes positioned and then slight protection indicated at the third location around 130,700. The second panel shows the DNase digestion to map all proteins. The three maps are from No Exposure, 50, and 150 Gray from top to bottom.
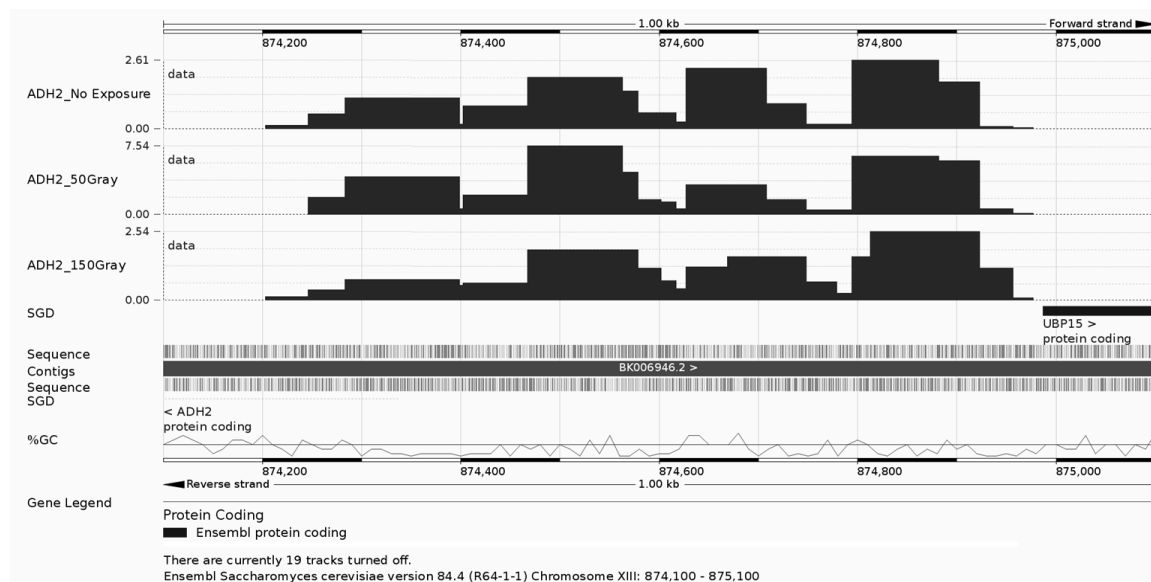
A)

B)
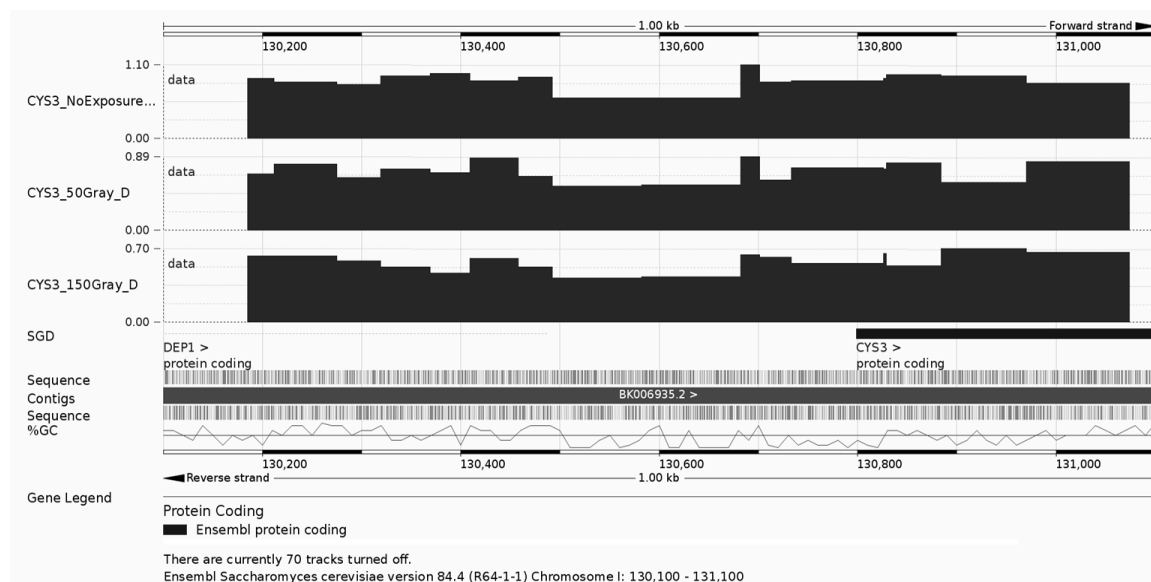
Figure 18. Relative Protection Plots of DED1.

The relative protection value was calculated by dividing the digested value by the no digest value for each amplicon. These values were then mapped along the chromosomal location in Ensembl (137). The four regions that are protected at this locus appear as a distinct black rectangular shape. There are four nucleosomes positioned with a distinct lack of protection between 722,650 and 722,840. The second panel shows the DNase digestion to map all proteins. The three maps are from No Exposure, 50, and 150 Gray, from top to bottom.
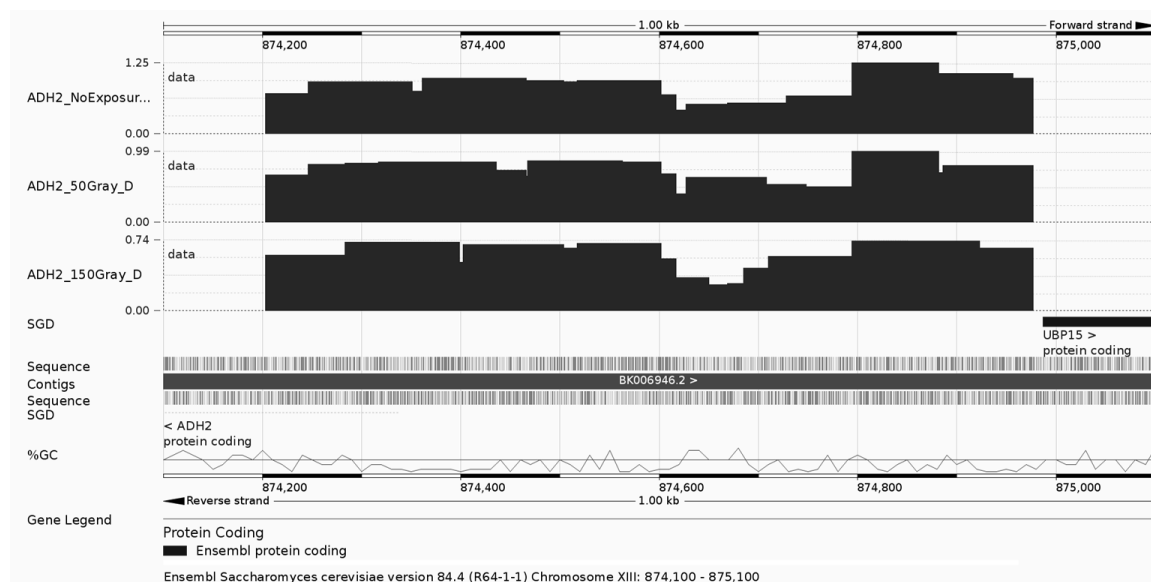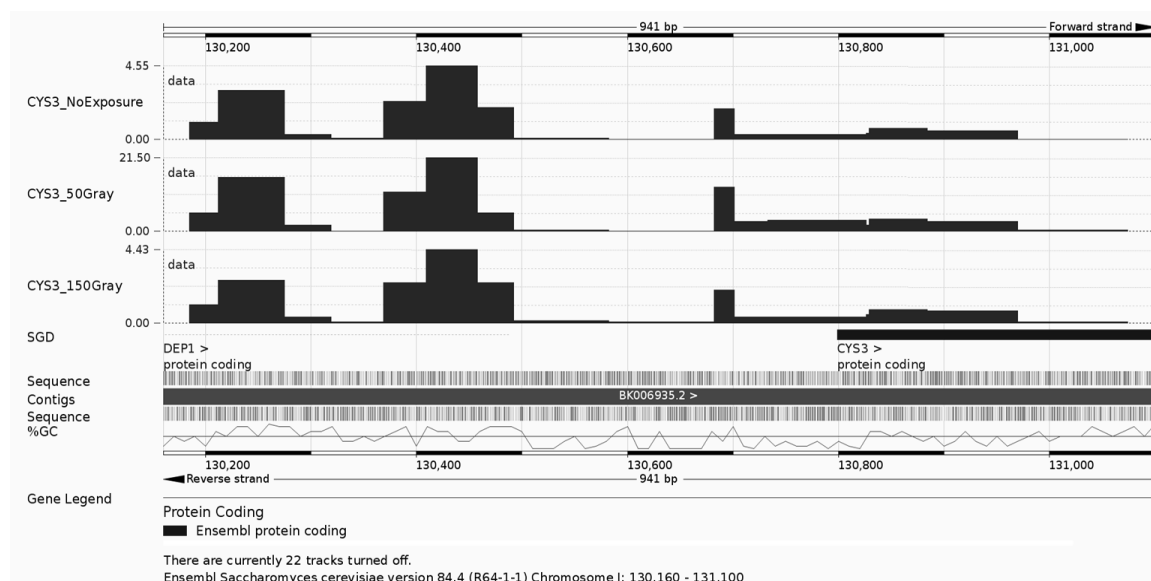
A)

B)

Figure 19. Relative Protection Plots of CHA1.

The relative protection value was calculated by diving the digested value by the no digest value for each amplicon. These values were then mapped along the chromosomal location in Ensembl (137). There appears to be protection 15,976-16,157 by the distinct black rectangular shapes. There is also a distinct lack of protection at 16,157-16,400. The second panel shows the DNase digestion to map all proteins. The three maps are from No Exposure, 50, and 150 Gray, from top to bottom.
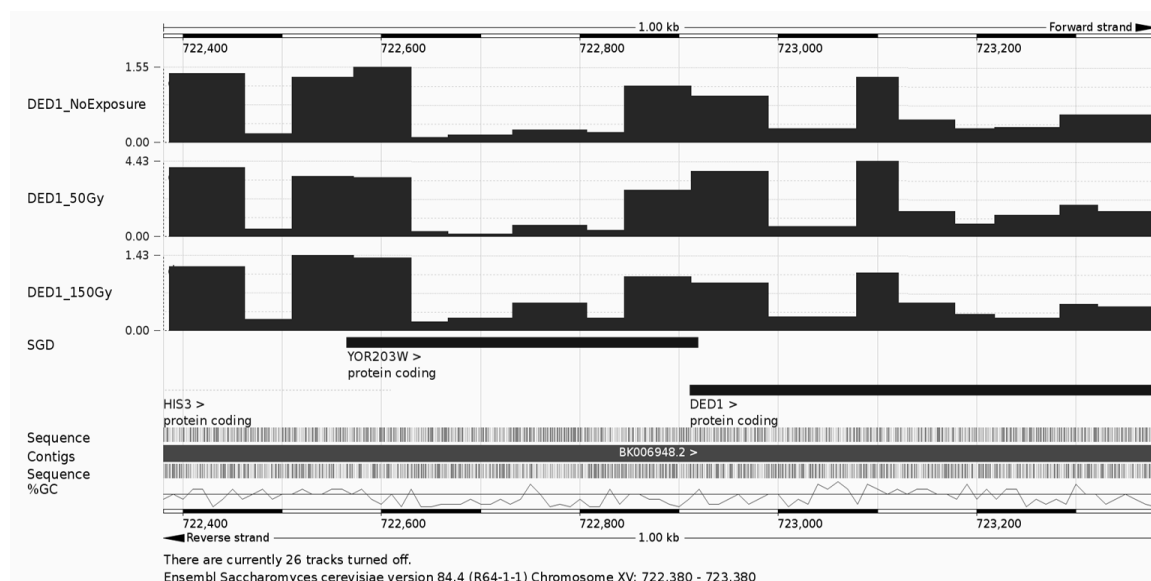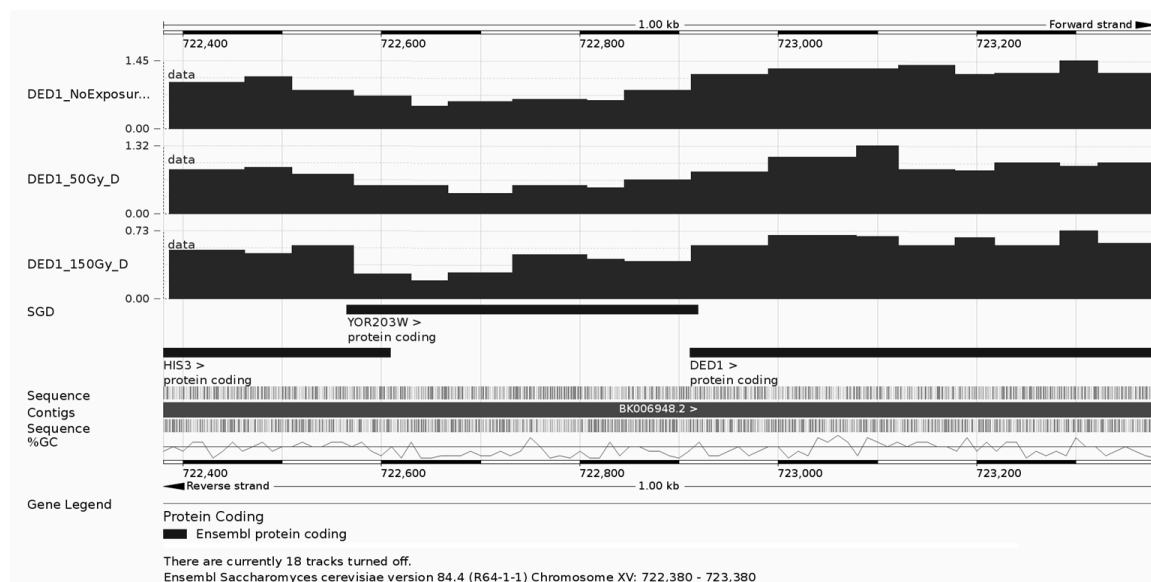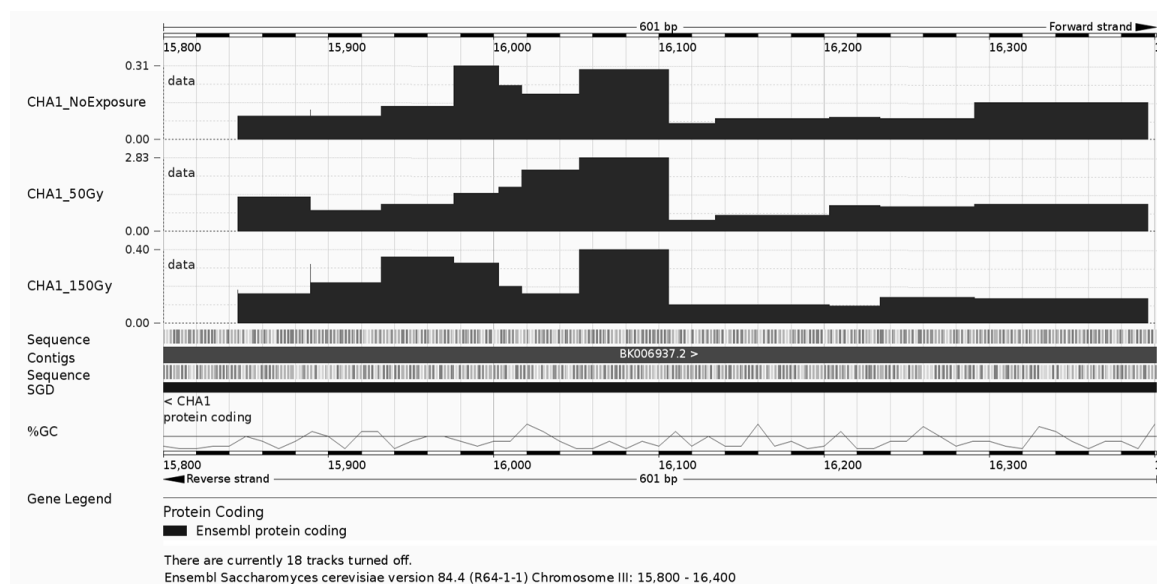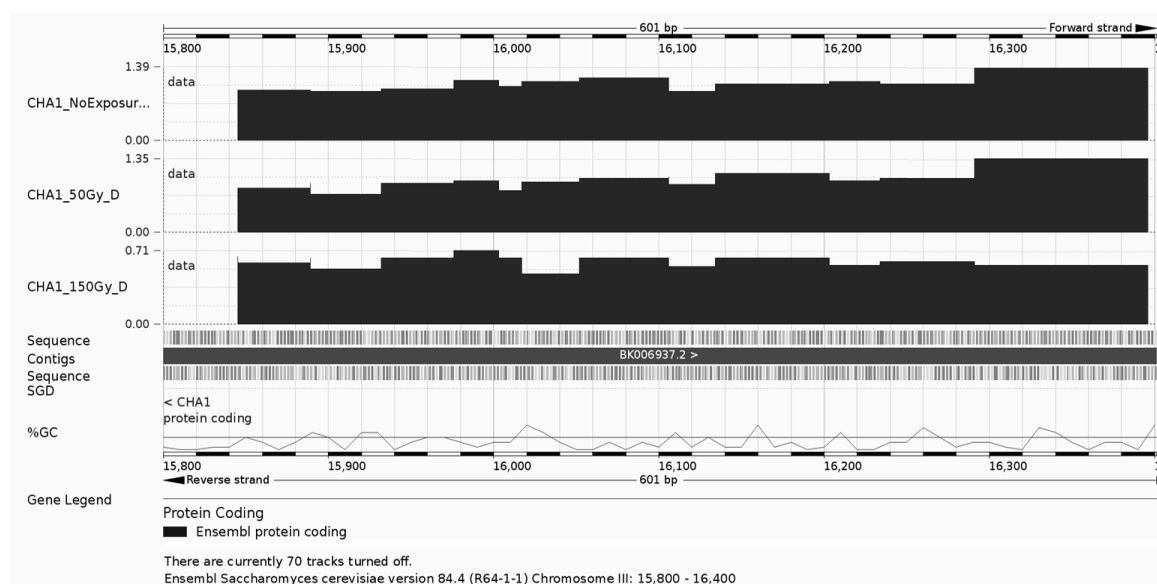
A)

B)

CHAPTER 3:

EVALUATION OF THE EFFECTS OF MULTIPLE DOSES OF IRRADIATION ON *SACCHAROMYCES CEREVISIAE*

Introduction

Based on previous experiments conducted involving yeast cells exposed to various doses of irradiation, it was found that higher doses of irradiation, specifically 250 Gray and higher, negatively affected the growth of yeast by causing a delay in the time it took for colonies to grow on the YPD plate and additionally caused a decrease in the number of colonies. After samples were subjected to a dose of irradiation, they were immediately streaked on YPD plates and incubated at 30 °C. After an ample time period was given for growth (approximately three days), the plate was evaluated visually by looking at the growth of colonies. Plates from the organisms exposed to higher doses of irradiation showed diminished growth, however some cells were still able to survive. The number of colonies visualized on a plate from a high-dose irradiated sample was much lower than a control plate streaked from culture that was not exposed to irradiation.

To evaluate how these increased levels of irradiation and chronic exposure can impact yeast, cultures were subjected to 250 Gray of irradiation. Immediately after the period of irradiation, part of the culture was streaked on YPD plates in triplicate and incubated at 30 °C for 2-3 days to allow for culture growth. One milliliter of each culture was flash frozen using liquid nitrogen and stored at -80 °C. After the growth period, a single colony that survived the irradiation was inoculated in YPD broth for 15-18 hours. The survival samples were subjected to another dose of irradiation at 250 Gy and the protocol was repeated to evaluate the effects of continuous irradiation exposure for the viable cultures. It is important to note that after irradiation exposure, there was a loss of growth observed and the number of colonies diminished. Further, the colonies were very small and circular in shape. This procedure was repeated for eight rounds of irradiation.

Additionally, after the third round of irradiation, two different colored colonies appeared on the plate. One was light yellow in color, designated to be the "light" mutant and one was a darker yellow in color, designated to be the "dark" mutant. The only difference observed phenotypically was the color of the colony. For rounds 4-8, there were three different culture lines that were maintained, which we called: Wild Type (WT), Light, and Dark. All results of the time of growth were recorded after each round of irradiation.

A standard protocol for nucleosome and protein mapping was modified from the protocol detailed in Chapter 2 in order to work with 1 mL of starting culture, which was the amount that was saved after each round of irradiation. After the appropriate enzymatic digestion protocol was followed and DNA was purified, the DNA was quantified, and the samples were then analyzed using qPCR with the primers for the loci, ADH2, CYS3, DED1, and CHA1 (Chapter 2). The protocols discussed in the Materials and Methods section of Chapter 2 were implemented to analyze the samples in this study. This study provides an additional evaluation of the effects of radiation on the positioning of nucleosomes and other proteins. By taking samples of yeast culture through additional rounds of irradiation exposure, we can attempt to understand if the effects may be cumulative. Further, we introduce the question of whether or not this continued radiation exposure may alter the positions of nucleosomes and other proteins.

Materials and Methods

Culture Preparation and Chronic Irradiation Exposure

To begin, an aliquot of the laboratory-maintained culture-line of S288C

Saccharomyces cerevisiae was removed from the -80 °C freezer. Using aseptic technique,

the culture was streaked on an YPD plate and the plate was incubated at 30 °C for two

days. A single yeast colony was isolated from the plate and subsequently inoculated into

100 mL of YPD broth. The liquid culture was grown overnight for approximately 14-15

hours at 30 °C with shaking at 150 RPM. After the overnight growth, the absorbance of

the culture was measured at 600 nm to ensure that the culture was in the growth stage

(Figure 8). Furthermore, a small portion of the culture was also visualized under the

microscope (40X and 60X objectives) to ensure this (Figure 9).

From the culture, a 1 mL portion was transferred to a sterile, 1.5 mL

microcentrifuge tube. This sample was then irradiated using the RS-2000 Irradiator

(Reddy Lab, University of Nebraska-Lincoln, NE). To obtain an exposure of 250 Gray,

the duration was set to 38 minutes, 34 seconds based on the dose rate of 6.84 Gy/minute

at level 6. This dose rate was previously calibrated by the Reddy Lab. This exposure time

was entered and saved on the control panel of the RS-2000. To set up the instrument, the

adjustable sample shelf was placed at level 6, which is the level that is closest to the

radiation source at the top of the instrument. The closer the shelf is placed to the radiation

source will increase the radiation dose obtained. The sample was contained within a 1.5

mL tube and the tube was placed on its side directly in the center circle of the sample

shelf. This placement in the center of the sample shelf is to ensure dose uniformity. After

the irradiation cycle, part of the culture was streaked out on three YPD plates and the

plates were then incubated at 30 °C. The remainder of the culture was immediately flash frozen in the 1.5 mL tube using liquid nitrogen. The frozen culture was then transferred on dry ice to the -80 °C for long-term storage.

The time required for growth to appear on the YPD plates was recorded and the plates were allowed to incubate. These time periods can be visualized in Table 7. After growth was visualized, a single colony was isolated and inoculated in YPD broth. The same protocol for irradiation and sample preparation was repeated through eight rounds of irradiation. A sample of the original culture as well as a sample after each round of irradiation was preserved at -80 °C for storage until further analysis.

Modified MNase Protocol

The protocol described in detail in the Materials and Methods section of Chapter 2 was modified in order to apply the analysis techniques to a starting volume of 1 mL, which differs from the original protocol that had a starting volume of 250 mL. The reagents utilized were identical unless noted and majority of the protocol modification was in terms of the volume of reagents. To begin, the samples of yeast were removed from the -80 °C freezer and allowed to thaw at room temperature. Each sample was divided into two, 500 µl aliquots; one aliquot was used for MNase analysis and the other aliquot was used for DNase analysis, which is described in detail in the next section. To the 500 µl of yeast culture for MNase analysis, 24.5 µl of 37% formaldehyde was added and the sample was incubated at room temperature for 15 minutes with occasional inversion in order to mix. Subsequently, 51.1 µl of 2.5 M glycine was added and the sample was incubated at room temperature for five minutes. The sample was centrifuged for 5 minutes at 16,000 x g at 4 °C in order to pellet the cells. The cell pellet was washed

twice with 1 mL of cold sterile water. In each wash step, the water was added, the sample was centrifuged at 16,000 x g at 4 °C for 5 minutes, and the supernatant was removed.

After the final water wash, the pellet was re-suspended in 1 mL of Buffer Z. The cell suspension was added to an additional 8.75 mL of Buffer Z in a 125 mL culture flask. Furthermore, 250 µl of Zymolase solution and 7 µl of BME were added. The sample was incubated at 30 °C with shaking at 100 RPM for 30 minutes in order to generate spheroplasts. The spheroplasts were confirmed using microscopy to ensure digestion of the cell wall. The entire cell solution was transferred to a 15 mL conical tube and centrifuged for 10 minutes at 5,500 RPM at 4°C. The supernatant was discarded and the cellular pellet was re-suspended in 800 µl of NPS Buffer. The solution was divided into two, 400 µl portions in 1.5 mL microcentrifuge tubes (No Digest (M) and + MNase). Three microliters of 15U/µl was added to the +MNase sample to add 45U of MNase and 3 µl of nuclease-free water was added to the No Digest sample. The samples were incubated at 37 °C for 30 minutes to allow the enzyme digestion to proceed.

The reaction was stopped by shifting the samples to ice and 18 µl of EDTA and 7 µl of EGTA were added. Additionally, 60 µl of 10% SDS, 10 µl of Proteinase K, and 10 µl of DNase-free RNase A were added. The samples were incubated at 56 °C for 5 hours. A standard phenol-chloroform extraction was performed as previously described in the Materials and Methods section of Chapter 2. To precipitate the DNA, 40 µl of 3M sodium acetate and 1 mL of 100% ethanol was added to the samples and they were incubated in the freezer (-20 °C) overnight (12-18 hours). The next day, the samples were removed from the freezer and centrifuged for 25 minutes at 12,500 RPM at 4 °C. A small white pellet of DNA formed on the side of the 1.5 mL tube. The supernatant was

removed carefully as to not disturb the pellet. The pellet was then washed with 500 µl of 70% ethanol. The samples were centrifuged on high (17,000 x g) for five minutes. The supernatant was removed and the pellet was allowed to dry for approximately 10 minutes at room temperature with the lids of the 1.5 mL tubes open. The pellet was re-suspended in 40 µl of TE Buffer with an overnight incubation at 56 °C. The samples were then stored at 4 °C until further analysis.

Modified DNase Protocol

The remaining 500 µl of the yeast culture was used to perform a modified DNase digestion protocol. Once again, the reagents used in this protocol were identical to those described in the Materials and Methods section of Chapter 2 unless otherwise noted. The sample was centrifuged for five minutes at 16,000 x g at 4 °C in order to pellet the cells. Taking care not to disturb the pellet, the supernatant was removed. The cellular pellet was re-suspended in 1 mL of DNase Buffer I followed by a five minute incubation at room temperature. The sample was centrifuged for five minutes at 16,000 x g at 4 °C. The supernatant was discarded and the pellet was re-suspended in 1 mL of Spheroplasting Buffer. The entire cell suspension was transferred to a 125 mL culture flask and an additional 3 mL of Spheroplasting Buffer was added along with 800 µl of Zymolase Solution. The sample was incubated at 30 °C with shaking at 100 RPM for 30 minutes followed by confirmation of spheroplasts by microscopy. The entire cell solution was transferred to a 15 mL conical tube and centrifuged for 10 minutes at 5,500 RPM at 4°C. The supernatant was discarded and the pellet was re-suspended in 600 µl of NPS Buffer. From this suspension, two, 300 µl aliquots were transferred to 1.5 mL tubes (No Digest (D) and + DNase). To the + DNase sample, 25 µl of 1U/µl DNase were added and then

25 µl of water was added to the No Digest sample. The samples were incubated at 37 °C

for 10 minutes. In order to stop the reaction, 300 µl of Stop Solution were added and the

samples were incubated at 65 °C for 10 minutes. To purify the DNA, a standard phenol-

chloroform extraction was performed according to the protocol outlined in the Materials

and Methods Section of Chapter 2. To precipitate the DNA, 40 µl of 3M sodium acetate

and 1 mL of 100% ethanol was added to the samples and they were incubated in the

freezer (-20 °C) overnight (12-18 hours). The next day, the samples were removed from

the freezer and centrifuged for 25 minutes at 12,500 RPM at 4 °C. A small white pellet of

DNA formed on the side of the 1.5 mL tube. The supernatant was removed carefully as to

not disturb the pellet. The pellet was washed with 500 µl of 70% ethanol. The samples

were centrifuged on high (17,000 x g) for five minutes. The supernatant was removed and

the pellet was allowed to dry for approximately 10 minutes at room temperature with the

lids of the 1.5 mL tubes open. The pellet was re-suspended in 40 µl of TE Buffer with an

overnight night incubation at 56 °C. After the re-solubilization, the samples were stored

at 4 °C until further analysis.

Gel Electrophoresis & DNA Quantification

After the samples from all rounds of irradiation were prepared according to both

the MNase and DNase modified protocols, the samples were evaluated as previously

described in Chapter 2. After the enzymatic digestions, all DNA samples were quantified

using the Qubit High-Sensitivity double-stranded DNA Kit on the Qubit Fluorometer.

After quantification, the gel electrophoresis protocols were performed to confirm the

success of the enzymatic digestions as well as the no digestion, negative controls. A

second, 1% TBE gel was used to further purify the mononucleosomal DNA along with

the Qiagen QIAquick Gel Extraction Kit (Qiagen, Valencia, CA). The gel-purified

mononucleosomal DNA was then quantified using the Qubit High-Sensitivity double-

stranded DNA Kit and the Qubit Fluorometer. All samples were stored at 4 °C until

further analysis.

qPCR Analysis

The primer sets that were optimized and utilized in the Materials and Methods

section of Chapter 2 were also used to analyze the loci ADH2, CYS3, DED1, and CHA1

of the samples in this experiment. Based on the total number of samples, which was 76,

and the inclusion of a standard curve and no template control (NTC), it was necessary to

run one plate for each primer set. This made the total number of plates/runs 70. To

prepare the samples for analysis, 20 µl of each sample was combined with 180 µl of TE

Buffer in order to dilute the sample 1:10. The samples were then transferred to a 96-well

plate so that they could be easily transferred to the qPCR, 96-well plate using a multi-

channel pipette. The total reaction volume was 10 µl (8 µl of reaction mix and 2 µl of

DNA). The reaction master mix of reagents was composed of 5 µl of iTaq Universal

SYBR Green SuperMix (Bio-Rad Laboratories, Hercules, CA), 250 nM (0.125 µl) of

each primer (forward and reverse), and 2.75 µl of nuclease-free water. This master mix

was prepared in excess and 8 µl was subsequently pipetted into the appropriate wells of a

Hard-Shell Low-Profile Thin-Wall 96-Well Skirted PCR Plate (Bio-Rad Laboratories,

Hercules, CA) using a multi-channel pipette. A standard curve was prepared using yeast

genomic DNA and serially diluting (1:10) from 17.8 ng/µl down to 1.78×10^{-4} ng/µl in

order to generate six data points on the standard curve. The data points of the standard

curve were: 17.8, 1.78, 0.178, 0.0178, 0.00178, and 1.78×10^{-4} ng/µl. Two microliters of

each standard was added to the appropriate well. A no template control (NTC) was also

included that contained 2 µl of nuclease-free water in place of DNA. A 96-well plate seal

(Bio-Rad Laboratories, Hercules, CA) was then used to cover and seal the wells on the

plate. The plate was centrifuged and placed on the CFX Connect Real-Time PCR

Thermal Cycler (Bio-Rad Laboratories, Hercules, CA). The cycling conditions used were

as follows: 95 °C for 10 minutes, then 40 cycles of 95 °C for 15 seconds, 60 °C for 30

seconds, and 72 °C for 30 seconds. A melt curve was generated by heating the samples

from 60 to 95 °C at a rate of 0.1 °C/second. These are the cycling conditions that were

determined to be optimal in Chapter 2. This was performed on the CFX Connect Real-

Time PCR Detection System (Bio-Rad Laboratories, Hercules, CA) and data was

generated in the CFX Manager Software.

Results

Data Analysis

As discussed in Chapter 2, a protection assay was used to determine particular

regions of DNA that are bound to proteins. Specific regions of DNA were protected from

enzymatic digestion and successfully amplified during qPCR analysis. Alternatively,

regions of DNA that were not bound to protein were digested by the enzyme and these

regions of DNA weren't amplified during qPCR analysis. All qPCR data were exported

into Excel. The first step in analysis was to calculate the relative amount of each

amplicon. This step is necessary to correct for the input DNA concentration because the

amount of input DNA varied between samples, which will ultimately affect the amount of

amplicon detected. It is important to note that the DNA input varied due to the amount of

DNA extracted from each particular sample and it being necessary to keep a consistent

reaction volume. The DNA concentration among samples varied, but within a reasonable

range that allowed the samples to fall on the standard curve used in our qPCR analysis.

To keep the protocols feasible and standardized, 2 µl of DNA was added to each reaction

for qPCR analysis. By keeping the volume of DNA identical, this makes the total amount

of DNA added variable among samples. However, this variation can easily be corrected

for. This normalization was done by taking the amplicon starting quantity (SQ)

(determined from qPCR) and dividing by the input DNA concentration (determined from

the measurement on the Qubit Fluorometer) (125). The relative amount of each amplicon

can then be compared between the MNase digested sample and its corresponding no

digest control sample as well as the DNase digested sample and no digest control sample.

Comparisons can also be made across the rounds of radiation, round 0 (starter culture that

was not exposed) through round 8. This was done for each primer set and for all primer

sets of each of the four loci, ADH2, CYS3, DED1, and CHA1.

The next step in analysis was to calculate the relative protection value of each

amplicon. The relative protection value is the fold-enrichment of a particular amplicon in

the digested DNA over the undigested DNA (125). This was done by dividing the

corrected, digested amplicon (either MNase or DNase) by its corresponding no digest

sample. If an amplicon is protected by a histone or other protein, it will not be digested

and will still be present in the digested samples after DNA purification (125). The

relative protection of each amplicon can then be compared between treatments (MNase

and DNase) as well as across each of the eight rounds of radiation and comparing back to

the pre-radiation culture. This was done for all amplicons of the four loci, ADH2, CYS3,

DED1, and CHA1.

ADH2 Results

From the mapping results exhibited in Chapter 2, Figure 16, we found that there

was nucleosome protection centered at amplicons A3-A4 (874,794-874,923), A8-A9

(874,627-874,748), A12-A13 (874,467-874,617), and A18-A19 (874,246-874,399). The

previous literature as well as our experimental results indicated four, distinct regions of

DNA that were protected by three nucleosomes and an additional unknown protein,

regardless of exposures to 50 and 150 Gray of radiation alike (125). In this experiment,

we expanded our analysis to evaluate increased exposure at a dose of 250 Gray as well as

increasing the number of rounds of irradiation from a single round to eight rounds. By

using identical evaluation techniques as described in the Results Section of Chapter 2, we

plotted the relative protection values for all amplicons in the ~800 bp region of the ADH2

promoter region (874,203-874,977). As depicted in Figure 20, the four regions protected

by nucleosomes were conserved through all eight rounds of radiation exposure. This is

visualized by the same pattern that was exhibited in this region in Chapter 2, Figure 16.

The four protected regions encompass 874,794-874,923, 874,627-874,748, 874,467-

874,617, and 874,246-874,399. We did see differences in the fold enrichment of

mononucleosomal DNA in this experiment, which will be discussed later, but the

consensus pattern of protection indicative of four nucleosomes, or three nucleosomes and

an unknown protein, was still present, showing a conservation of nucleosome positioning

after eight doses of 250 Gray of radiation.

The DNase digestion to map additional proteins in this region left us with

interesting results. As evident in Figure 21, it appeared that there was an overall decrease

in the relative protection values obtained after exposure to radiation. The pre-radiation

culture showed evidence of protection, but then by eighth round of exposure, it seemed that the sample lacked protection completely. This result warrants further investigation because it conflicts the result of the nucleosome mapping experiment in this study. The regions that are bound to nucleosomes were protected in the MNase-digestion, but the DNase-digestion showed no evidence of consistent protection in the later rounds of irradiation. The protection pattern in the maps of Figure 21 shows differences in relative protection values across rounds of radiation exposure. The relative protection values were much lower than those obtained in the experiment discussed in Chapter 2. This result will be discussed later on in this chapter.

CYS3 Results

The experimental results obtained for CYS3, outlined in Chapter 2, indicated the presence of three distinct regions of protection by nucleosomes. It was found that there was nucleosome protection at amplicons CYS3_1-CYS3_2 (130,185-130,329), CYS3_5-CYS3_6 (130,369-130,509), and partially at CYS3_10 (130,682-130,781), as seen in Figure 17. The two strongly positioned nucleosomes are present at 130,185-130,329 and 130,369-130,500, and then there is a slightly protected region around ~137,000. This pattern of protection was found in the No Exposure sample, 50 Gray Exposure sample, and 150 Gray Exposure sample. In this study, the increased dose of 250 Gray and increased number of doses to eight, produced comparable results to those reported in Chapter 2. There was indication of strong nucleosome protection from 130,185-130,329 and 130,369-130,509 after each of the eight rounds of exposure. There was also evidence of a region of protection at 130,682-130,781, however the region showed more variability, as visualized in Figure 22. There was also a very clear region that was

depleted of nucleosomes located at 130,509-130,682, with a lack of protection visualized as a flat line in Figure 22. This region that lacked nucleosomes is the CYS3 promoter region. Similar to the results of ADH2, there were differences in the fold enrichment values between rounds, but again, a similar pattern of protected regions was distinguished.

Again, the DNase digestion to map the locations of regions protected by proteins produced variable results as depicted in Figure 23. However, in the pre-radiation and multiple rounds of radiation, there was indication of protection at some regions of DNA, but this protection was not consistent. The majority of relative protection values generated by the DNase digestion were very low, fractional values. These results warrant further investigation because these results do not align with the protection results of the MNase digestion, which is illustrated when comparing Figures 22 and 23.

DED1 Results

In the experimental analysis of DED1 outlined in Chapter 2, we found that four particular regions on Chromosome XV were protected, 1 (722,386-722,486), 3-4 (722,510-722,694), 9-10 (722,845-723,000), and 12 (723,079-723,174). The mapping of this region can be visualized in Figure 18 and a consensus pattern is illustrated in the no exposure, 50 Gray, and 150 Gray samples. This map also illustrates a distinct unprotected region that lacks nucleosomes, the DED1 promoter. The experimental results in the present study also showed a consensus pattern of protection. There are two potential nucleosomes located at 722,386-722,694. This is visualized on the left side of each panel of Figure 24. Although the fold enrichment patterns do show differences, there is a region of about ~300 bp that is protected by what appears to be two nucleosomes in every round

of radiation and in the pre-radiation, control culture. Another distinct feature of the map

of relative protection (Figure 24) is the lack of protection from about 722,694-722,845.

This is the DED1 promoter that is characterized as a nucleosome-free region and our data

further supports this. We also saw the second set of two nucleosomes following the

nucleosome-free region on the right side of the panels in Figure 24. Heightened relative

protection values were indicated at 722,845-723,000 and 723,079-723,174 in all eight

rounds of radiation exposure. There also appears to be a potential fifth region of

protection at the 3' end, around 723,200 that was not illustrated in the previous study.

However this additional region of protection was exhibited in every round including the

starter culture, showing a conservation of nucleosome protection for this experiment

(Figure 24).

The DNase digestion produced variable results in terms of protection for this

locus, as seen in Figure 25. It appeared that all relative protection values obtained were

fractional and did not necessarily support the data obtained from the MNase digestion.

The relative protection values that were calculated using the DNase digestion and

associated no digest data appeared to result in low, fractional values. Looking at Figure

25, we do however see that across all rounds of radiation, the relative protection value is

higher at around 722,400, on the far left side of the maps. By the eighth round of

exposure, the relative protection values dropped to below 0.04 (Figure 25). The

conflicting results obtained from the DNase digestion were also illustrated in the loci

ADH2 and CYS3, again warranting further investigation.

CHA1 Results

The results of CHA1 discussed in detail in Chapter 2 were somewhat variable, but nonetheless indicated a consensus pattern of protection. For the no exposure, 50 Gray, and 150 Gray exposures alike, there was a heightened relative protection value at region encompassed within amplicons 6-9 (15,976-16,157), as visualized in Figure 19. This may suggest the positioning of nucleosome(s) in this region indicated by partial protection. In all three exposures, there was also a lack of protection from about 16,157-16,400 as seen by the sharp decrease in the relative protection values right about 16,100 (Figure 19). In this study, the samples collected after each round of exposure to 250 Gray of radiation were analyzed and illustrated a similar pattern of protection. As seen in Figure 26, there is a region that displays heightened relative protection values from about 15,950-16,100 in all samples from the starter culture, which was not exposed to irradiation, through the eighth round of irradiation. This was in agreement with the protection pattern obtained in Chapter 2, Figure 19. However, there was a difference in the positioning after 16,100 in this experiment. Rather than a lack of protection as seen in Chapter 2, there appeared to be a small region that was protected at about 16,200 and from about 16,290-16,400 (Figure 26). Although this pattern differed from the results discussed in Chapter 2, the pattern of nucleosome positioning in this experiment was consistent across all rounds of radiation and in the starter culture (no exposure). Therefore, the difference in pattern protection visualized when comparing Figure 19 and Figure 26 can't be attributed to radiation exposure.

The DNase digestion produced variable results for this experiment, but a lack of protection was indicated by very low, fractional relative protection values. As visualized

in Figure 27, the relative protection values appeared to decrease from the starter culture through the eighth round of irradiation. The starter culture (round 0) and the first two round of irradiation appeared to indicate some protection by proteins with relative protection values in the range of 0.5-0.9. After 8 rounds of irradiation, it appears that protection by proteins is non-existent, with extremely low relative protection values (Figure 27). These data seem to conflict the results obtained from MNase digestion (Figure 26) as we did not see the pattern of protection. The DNase digestion results at CHA1 warrant further investigation, as stated for all loci analyzed in this study.

Discussion

The goal of this experiment was to evaluate the effects of an increased exposure of radiation on the survival of yeast cells and additionally, the positioning of nucleosomes and other proteins at four loci. Building off of the study discussed in Chapter 2, we increased the dose of irradiation to 250 Gray and also increased the number of doses to eight. We took the established protocols (125, 132) and optimizations obtained in our laboratory (Chapter 2) and applied them to this study. A major success of this study was that we were able to perform our analysis with only 1 mL of starting yeast culture. The majority of established protocols call for at least 200 mL of yeast culture to perform mapping experiments, but we have illustrated that it is possible to perform analyses with an initial volume of 1 mL. Slight modifications to the protocols had to be made and the final 1:100 dilution step prior to qPCR analysis was replaced with a 1:10 dilution. This experimental modification may be useful for labs that are looking to work with smaller sample sizes.

The results that we obtained in this experiment showed that increased exposure to radiation appears to have an effect on the survival and growth patterns of yeast cells when grown on YPD plates at 30 °C after exposure (Table 7). Our results were variable, but after three doses of 250 Gy, we saw an increase in the growth time for colonies to appear on the plate to about six days. Further, after four doses, this time increased to about eleven days and after seven rounds, the time increased to about twelve days. However, after six doses, the growth time seemed to return to normal, about two-three days. The growth patterns are presented in Table 7. These results may suggest that the exposure to radiation has a negative impact on the survival and growth rates of yeast. Given these results, we would want to begin to look for a potential genetic explanation for this phenomenon in our future experiments. This would begin with investigating loci that are known to be essential for pathways associated with cell growth. There are specific genes in *S. cerevisiae* that encode proteins that process nutrients as well as proteins that ensure functional transitions between stages in the cell cycle. An example would be the SWE1 gene in *S. cerevisiae*. The SWE1 gene codes for a protein kinase directly involved in mediating the transition between stages of the cell cycle (143). Although we did not see an effect on protein positioning in the particular four loci analyzed in this experiment, this is not to say that there will not be an effect on other loci. If we expanded our analysis to loci that play a functional role in cell growth, we might potentially see variation in protein binding. The loci we analyzed do not appear to play a role in cell growth, but there are over 200 genes in *Saccharomyces cerevisiae* that are important for this process to be successful (143, 144).

Future studies will hopefully repeat this experiment and we will see if these results are corroborated. We would like to see if delay in growth is consistent and potentially extend this experiment for a longer duration of time and additional rounds of radiation exposure. Ultimately, we would hope to investigate to the extent that yeast cells can no longer survive due to chronic radiation exposure, if possible. Future experiments would seek to characterize potential loci affected. It may be possible to use next-generation sequencing technologies to evaluate different regions of the yeast genome, with a comparison to the reference sequence of S288C (145). It is known that there are numerous genes that are essential to growth and overall survival. Yeast cells have a large, but distinct group of genes that are part of its environmental stress response. The environmental stress response is coordinated and involves the up- and down- regulation of particular genes. These genes are characterized to offer cellular protection during oxidative stress, heat shock, osmotic shock, and starvation. Further, they are involved in the processes of DNA damage repair, cell wall modification, metabolism, and intracellular signaling (146). Analyzing these specific loci in cells obtained after we see delayed growth time may allow us to identify if particular genes are up- or down-regulated. To evaluate the up- or down- regulation of genes, we could potentially analyze RNA extracted from these cells for gene expression using RNA sequencing and/or qPCR (147). Investigation and research into gene expression techniques would be required in order to select the best method for our particular analysis.

Overall, the results of this study suggest that exposure to radiation does not appear to have an obvious effect on the positioning of nucleosomes at the four loci we analyzed, ADH2, CYS3, DED1, and CHA1. The mapping patterns illustrated in Figures 20, 22, 24,

and 26 all show that there are highly similar relative protection patterns for nucleosomal occupancy for all samples from the starter culture that was not exposed to radiation through the eighth round of radiation exposure. The results of our experiments convey that nucleosome positioning is conserved at these loci regardless of exposure to radiation.

In this experiment, our results showed differences in the fold enrichment of the mononucleosomal DNA, which are the relative protection values that are mapped along the genomic location, as seen in Figures 20, 22, 24, and 26. The fold enrichment values are obtained from taking the corrected amount of digested DNA and dividing it by the corrected amount of undigested, control DNA (125). This phenomenon was observed on multiple occasions for all four loci and at multiple positions within the specific regions analyzed. The protection patterns across rounds of radiation were similar, but the differences were seen in the relative protection values. Relative protection values greater than one are indicative of protection at that region, but what might differences in these values indicate? We are hoping to work towards understanding this trend and what the differences in relative protection values can be attributed to. This result must be further investigated to determine if it is potentially due to any experimental variation. A step in the procedure that is dependent on histone concentration is the crosslinking of protein to DNA. The crosslinking is carried out by a standard formaldehyde treatment and was presumed to be complete after a fifteen minute incubation period, followed by an incubation with glycine to quench any excess formaldehyde (124, 125). However, in the event that the crosslinking was not complete, this could leave regions with higher histone concentration with incomplete crosslinking between the protein and DNA.

In the future, we could evaluate the crosslinking step specifically by performing the formaldehyde treatment and rather than continuing on with our normal procedure, we can test the DNA-protein crosslink. A potential method to do this would be to go directly to a phenol-chloroform extraction without any further treatment. If the DNA is crosslinked with proteins, it will be located in the organic layer rather than in the aqueous layer, where DNA that is not crosslinked is found. If the crosslink is complete after the treatment, we would not find any DNA in the aqueous layer. Alternatively, we could compare our formaldehyde treated crosslinked DNA to a DNA control (that has not been crosslinked) using a sonication method. Post-sonication, we would purify the DNA and analyze by gel electrophoresis. If the DNA has not been completely crosslinked, it will be sheared by the sonication and would exhibit a similar pattern to the un-crosslinked DNA when analyzed using gel electrophoresis. However, if the crosslink was complete, the DNA should have been protected by the crosslink to proteins. These methods of evaluation are only suggestions and additional consideration must be given to the sensitivity of these detection methods. Ultimately, how can we be certain that we have completely crosslinked the protein and DNA? If we are able to determine a method and successfully confirm that crosslinking was complete, this would rule out that this experimental step is responsible for the differences in relative protection values that we are seeing. The thorough evaluation of the crosslinking step illustrates the necessity to consider every step in our procedure that might be responsible for the differences in relative protection values. After experimental variation is ruled out as a contributor, this would allow us to work towards determining the biological sources that differences in relative protection values at particular regions of DNA may be attributed to.

At this point in time, we have not evaluated all potential sources of experimental variation so we can only speculate on the reasoning for such differences in relative protection values. One explanation may be that this relative protection value is proportional to the strength of association with DNA or how strongly a nucleosome is positioned. We must also consider that this experiment was evaluating a population of cells and thus our results are a survey of the configurations present across many cells. If majority of cells have a said nucleosome positioned, this may correlate with a higher relative protection value. Contrary, if multiple configurations exist for a cell, the relative protection value may be lower due to a nucleosome's presence in some cells and the lack of this nucleosome at a particular position in other cells. We know that particular nucleosomes are characterized as strongly positioned whereas others are not as strong and exhibit variable positioning. Nucleosome occupancy may vary and thus the differences in fold enrichment and exact position would be expected to exhibit slight variation in where the nucleosomes are positioned at a given point in time.

Additionally, the DNase digestion to map all proteins did not support the data obtained from our MNase digestion in this particular study. The DNase digestion in this study produced very low relative protection values even at regions that exhibited protection in the MNase digestion. This result was illustrated in all four loci analyzed and can be visualized when comparing pairs of Figures, 20 and 21, 22 and 23, 24 and 25, and, 26 and 27. This is an interesting result because we were able to successfully analyze these four loci after DNase digestion in our previous experiments in Chapter 2. We know that we can't directly compare the enzymatic digestions because of the post-digestion purification techniques. However, in Chapter 2, we saw that the DNase digestion still

appeared to support the MNase digestion due to relative protection values close to 1. Because of the sample size modification in these experiments, the protocols for enzymatic digestions were tested with yeast culture samples prior to running the experiments with collected samples of interest. The enzymatic digestion was successful under the reaction conditions described in the Materials and Methods section of this chapter and with an enzyme amount of 25U. This protocol was tested in multiple cultures and confirmed by gel electrophoresis. However, it appears that the application of these techniques in this particular experiment were not successful. This may be due to our method of detection and a potential inability to detect the particular region of DNA. We must also keep in mind the variance in post-digestion purification and the isolation of mononucleosomal DNA prior to analysis. We did not employ any further purification of the DNase digested DNA, which may be necessary to successfully detect regions of protein-bound DNA. Even so, this warrants further investigation into what this lack of protection from digestion may be attributed to and why the relative protection values were low fractional amounts. In order to investigate this result, we would want to repeat this experiment and see if similar results are obtained. Further, we may need to consider a method to purify the DNA post-DNase digestion in order to apply our detection methods.

We hope that the experiments we performed as part of this study lead us to additional experiments and alternative investigations of the results. In this study, we found two variable or mutant colonies after the second round of irradiation. Phenotypically, we found that these strains varied due to their production of a yellow colony when grown on standard, YPD plates rather than the distinct white color of the wild-type S288C laboratory strain. One mutant colony was a lighter shade of yellow and

one was a darker shade of yellow. However, the shape and size was comparable between the mutants and the wild-type strain. We maintained separate culture lines for these colonies and continued to carry them through the remainder of the experiments, treating them as separate cultures. It would be an interesting future experiment to further analyze and identify these strains. Analysis techniques such as microsatellite typing and next-generation sequencing could be used to compare these strains back to the wild-type strain and potentially determine what is causing the phenotypic variation. A microsatellite typing technique has been established to use molecular markers to distinguish between strains of *Saccharomyces cerevisiae*. This technique is based on the genotype generated from a panel of seven polymorphic microsatellite loci, YKL172w, YKR072c, YKL139w, YLR177w, YDR289c, YMR057c, and ylr[b] (148). Microsatellite typing could be used to identify that the strains and compare to the genotype of our laboratory strain of S288C. This technique would be used initially to confirm the identity of the strains. Further, next-generation sequencing might be useful to detect any variations in the sequence of the strains. This technology can detect sequence variations within individual genomes. We can look for single-nucleotide polymorphisms (SNPs), insertions/deletions (indels), and potentially structural variants (149).

In these experiments, we identified regions of the loci that were protected and additionally those regions that were unprotected. Using sequence analysis techniques such as ligation-mediated PCR (LMPCR) would allow us to take closer look at the unprotected versus protected region and further evaluate the sequence features. One of the ultimate goals would be to evaluate both structure and sequence of DNA and characterize the incidence of damage at the molecular level. We would also hope to

evaluate additional loci in *Saccharomyces cerevisiae*, such as those involved in the DNA

repair pathways as discussed earlier in this chapter.

Figure 20. Relative Protection Plot of ADH2 (MNase Digestion).

The relative protection value was calculated by dividing the digested value by the no digest value for each amplicon. These values were then mapped along the chromosomal location in Ensembl (137). The four regions of the locus that are protected and thus bound as a nucleosome appear as a distinct black rectangular shape. The maps are from the starter culture through the 8th round of irradiation, from top to bottom.
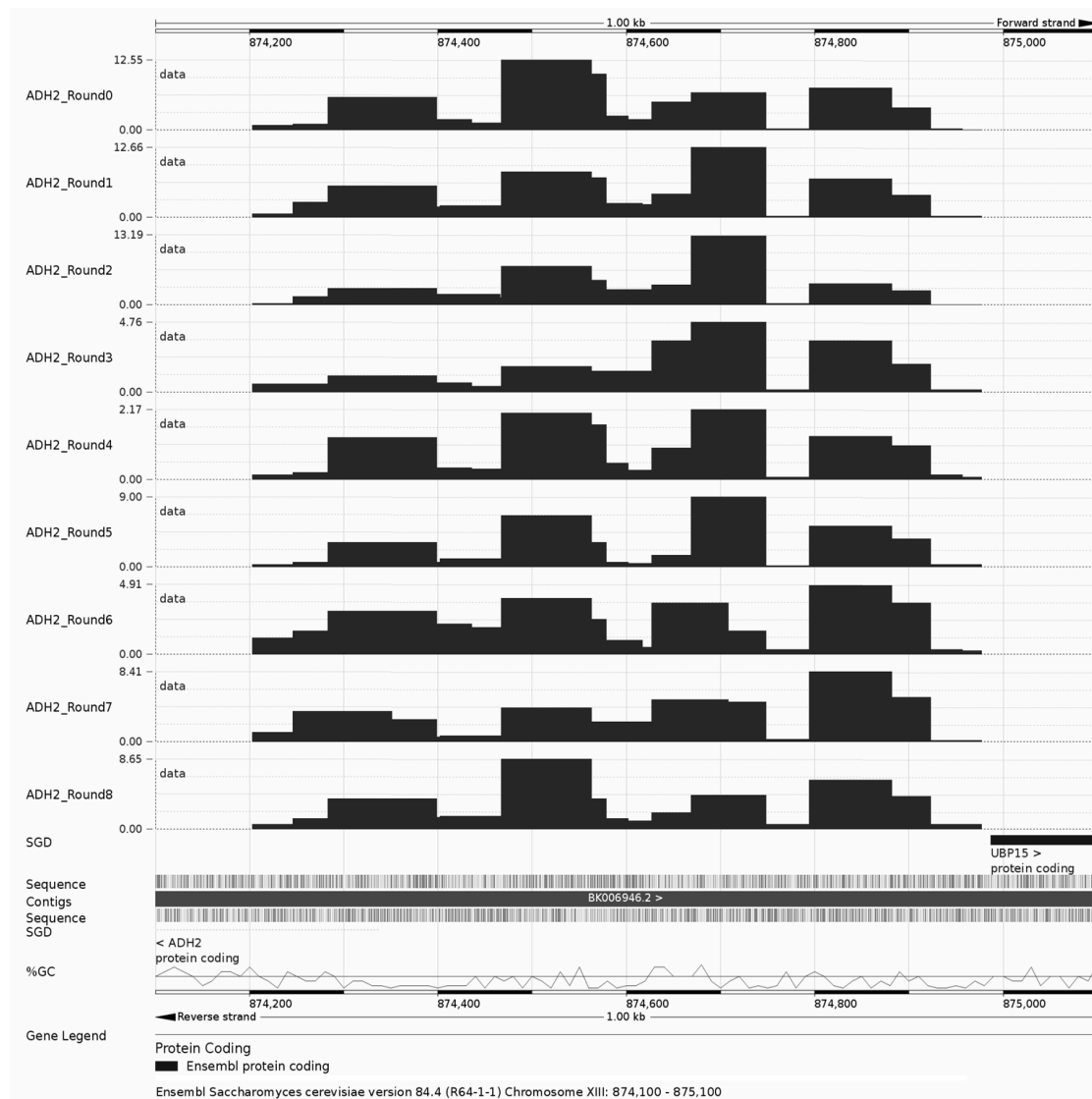
Figure 21. Relative Protection Plot of ADH2 (DNase Digestion).

The relative protection value was calculated by dividing the digested value by the no digest value for each amplicon. These values were then mapped along the chromosomal location in Ensembl (137). The maps are from the starter culture through the 8th round of irradiation (from top to bottom) for the results obtained from the DNase digestion.
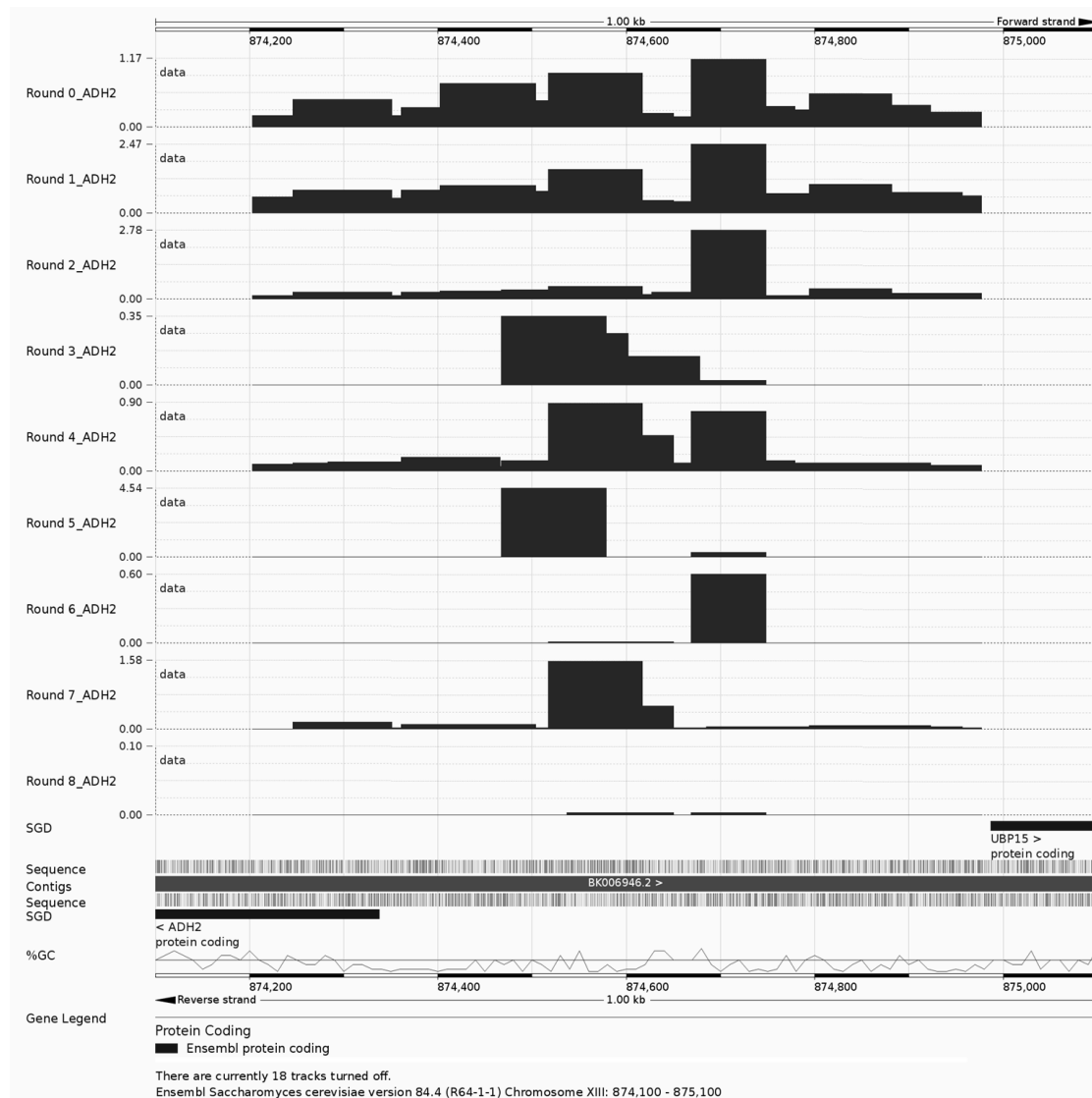
Figure 22. Relative Protection Plot of CYS3 (MNase Digestion).

The relative protection value was calculated by dividing the digested value by the no digest value for each amplicon. These values were then mapped along the chromosomal location in Ensembl (137). The maps are from the starter culture through the 8th round of irradiation, from top to bottom.
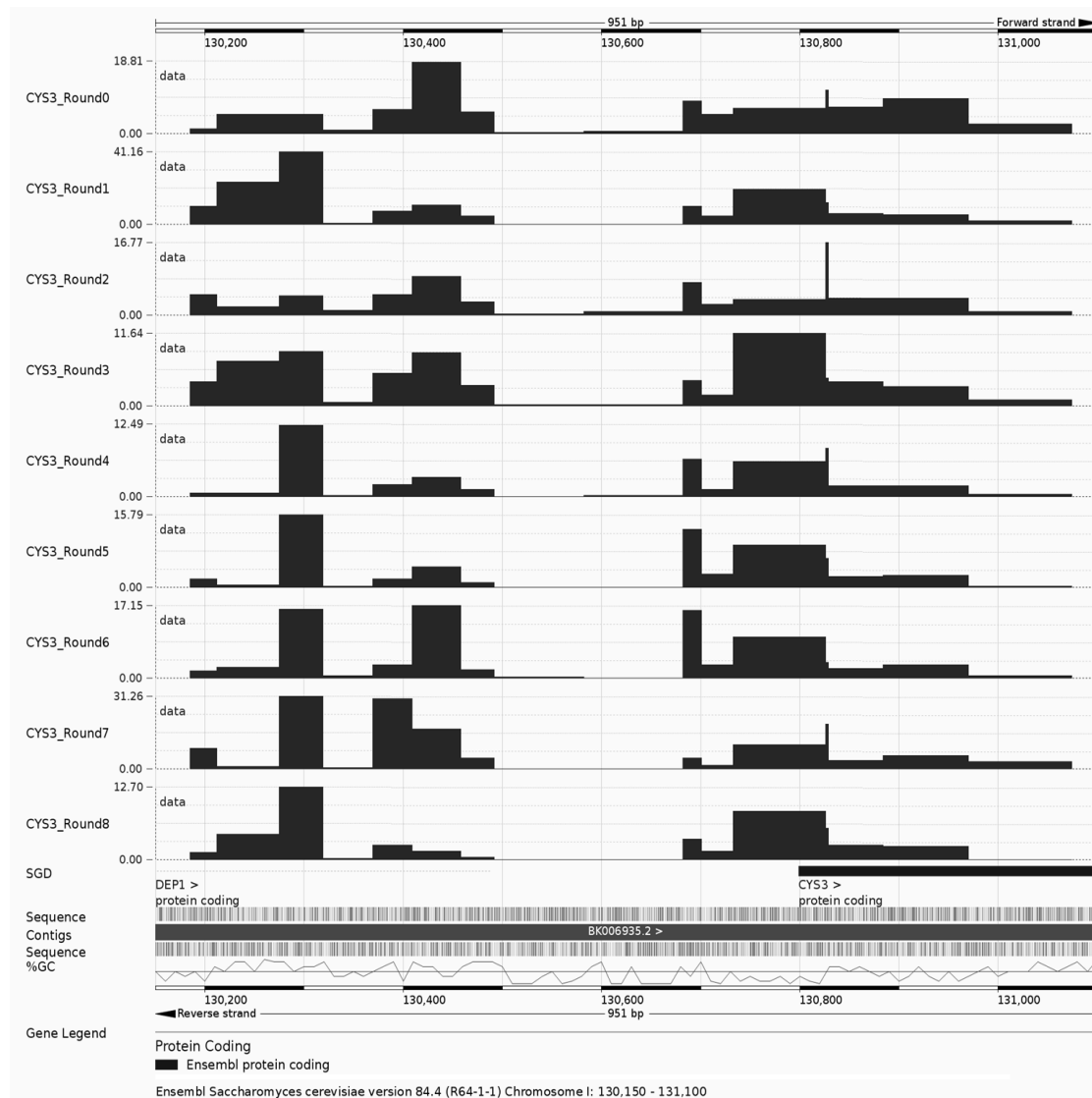
Figure 23. Relative Protection Plot of CYS3 (DNase Digestion).

The relative protection value was calculated by dividing the digested value by the no digest value for each amplicon. These values were then mapped along the chromosomal location in Ensembl (137). The maps are from the starter culture through the 8th round of irradiation (from top to bottom) for the results obtained from the DNase digestion.

Figure 24. Relative Protection Plot of DED1 (MNase Digestion).

The relative protection value was calculated by dividing the digested value by the no digest value for each amplicon. These values were then mapped along the chromosomal location in Ensembl (137). The maps are from the starter culture through the 8th round of irradiation, from top to bottom.
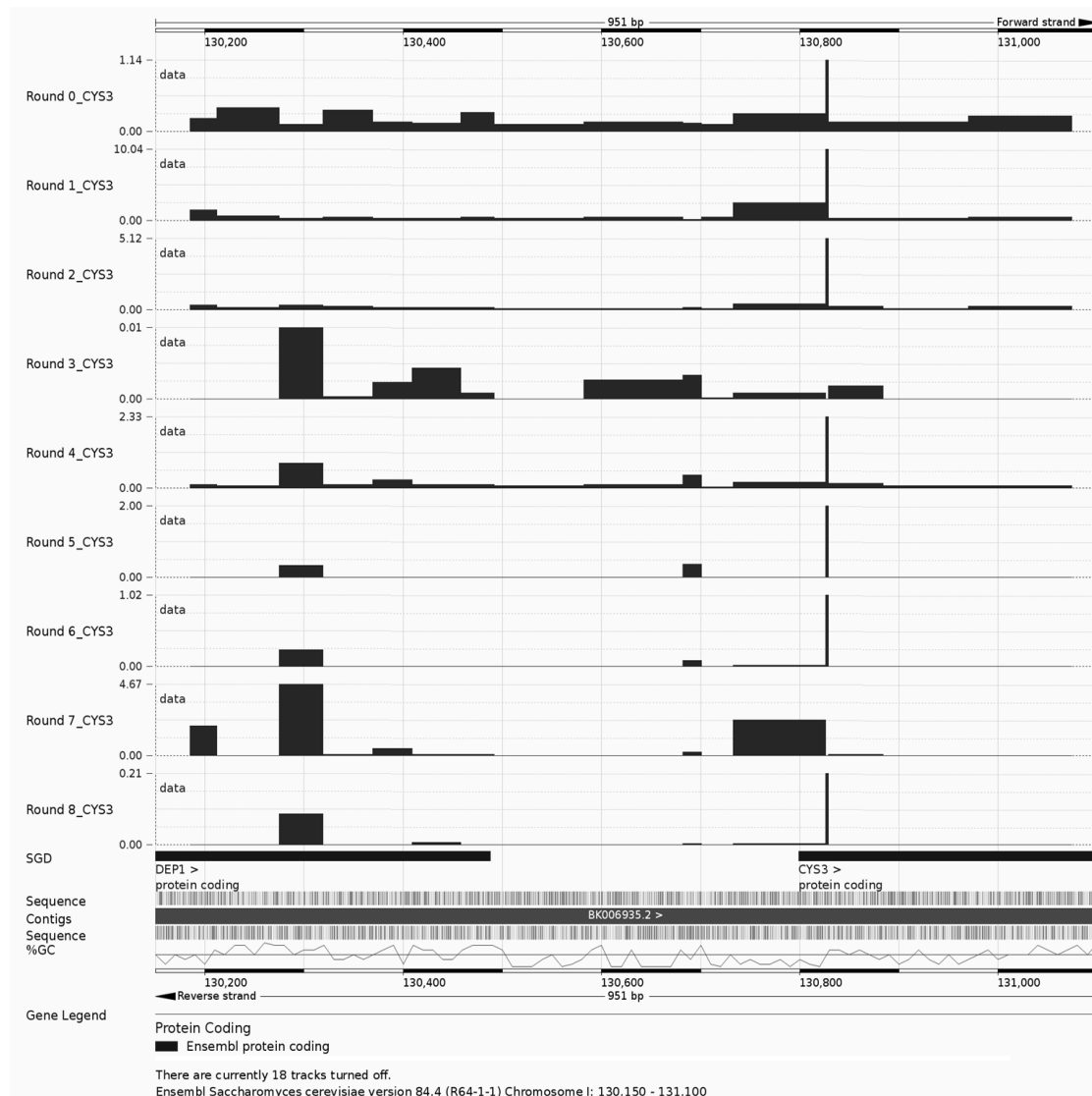
Figure 25. Relative Protection Plot of DED1 (DNase Digestion).

The relative protection value was calculated by dividing the digested value by the no digest value for each amplicon. These values were then mapped along the chromosomal location in Ensembl (137). The maps are from the starter culture through the 8th round of irradiation (from top to bottom) for the results obtained from the DNase digestion.
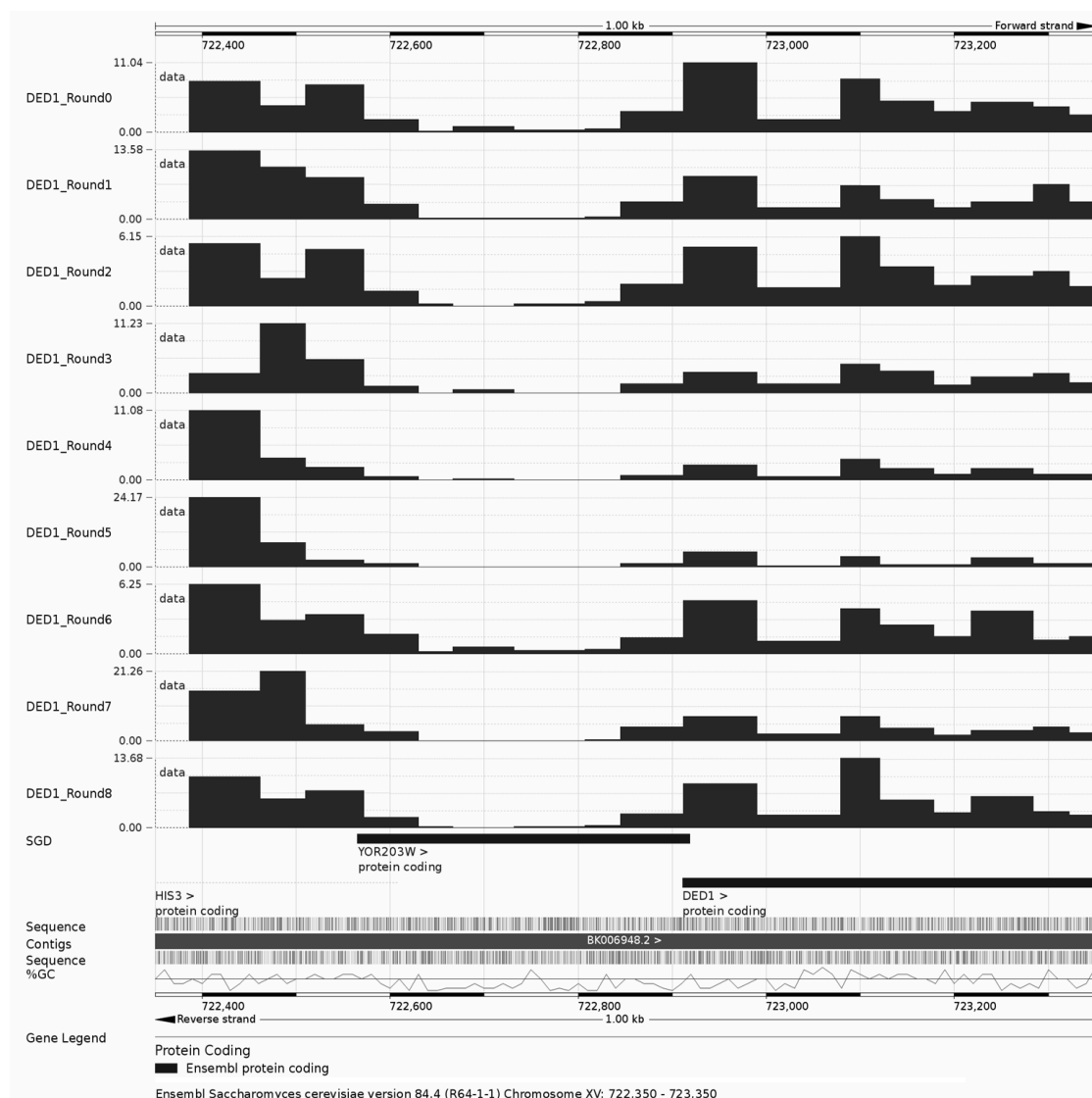
Figure 26. Relative Protection Plot of CHA1 (MNase Digestion).

The relative protection value was calculated by dividing the digested value by the no digest value for each amplicon. These values were then mapped along the chromosomal location in Ensembl (137). The maps are from the starter culture through the 8ᵗʰ round of irradiation, from top to bottom.
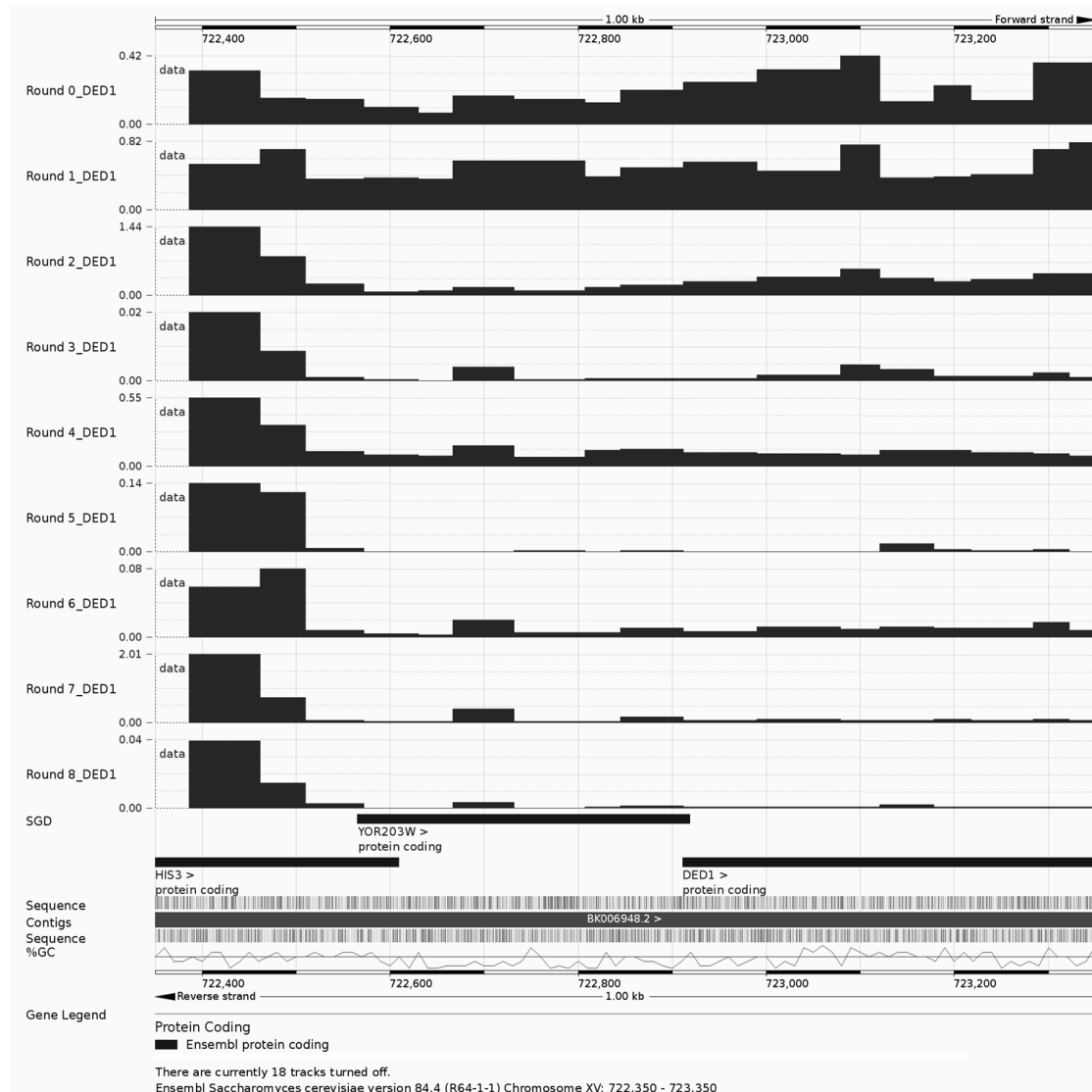
Figure 27. Relative Protection Plot of CHA1 (DNase Digestion).

The relative protection value was calculated by dividing the digested value by the no digest value for each amplicon. These values were then mapped along the chromosomal location in Ensembl (137). The maps are from the starter culture through the 8th round of irradiation (from top to bottom) for the results obtained from the DNase digestion.
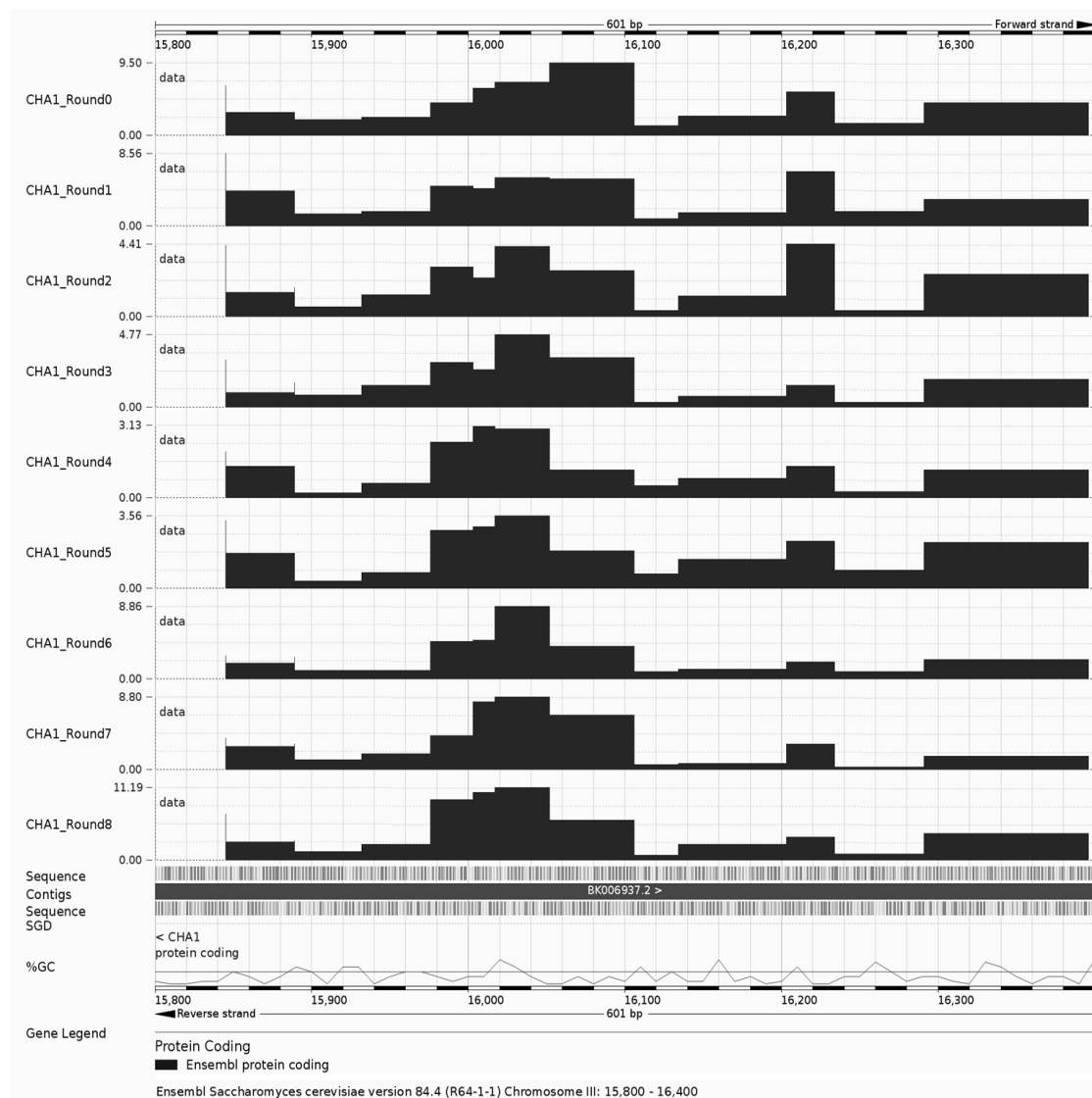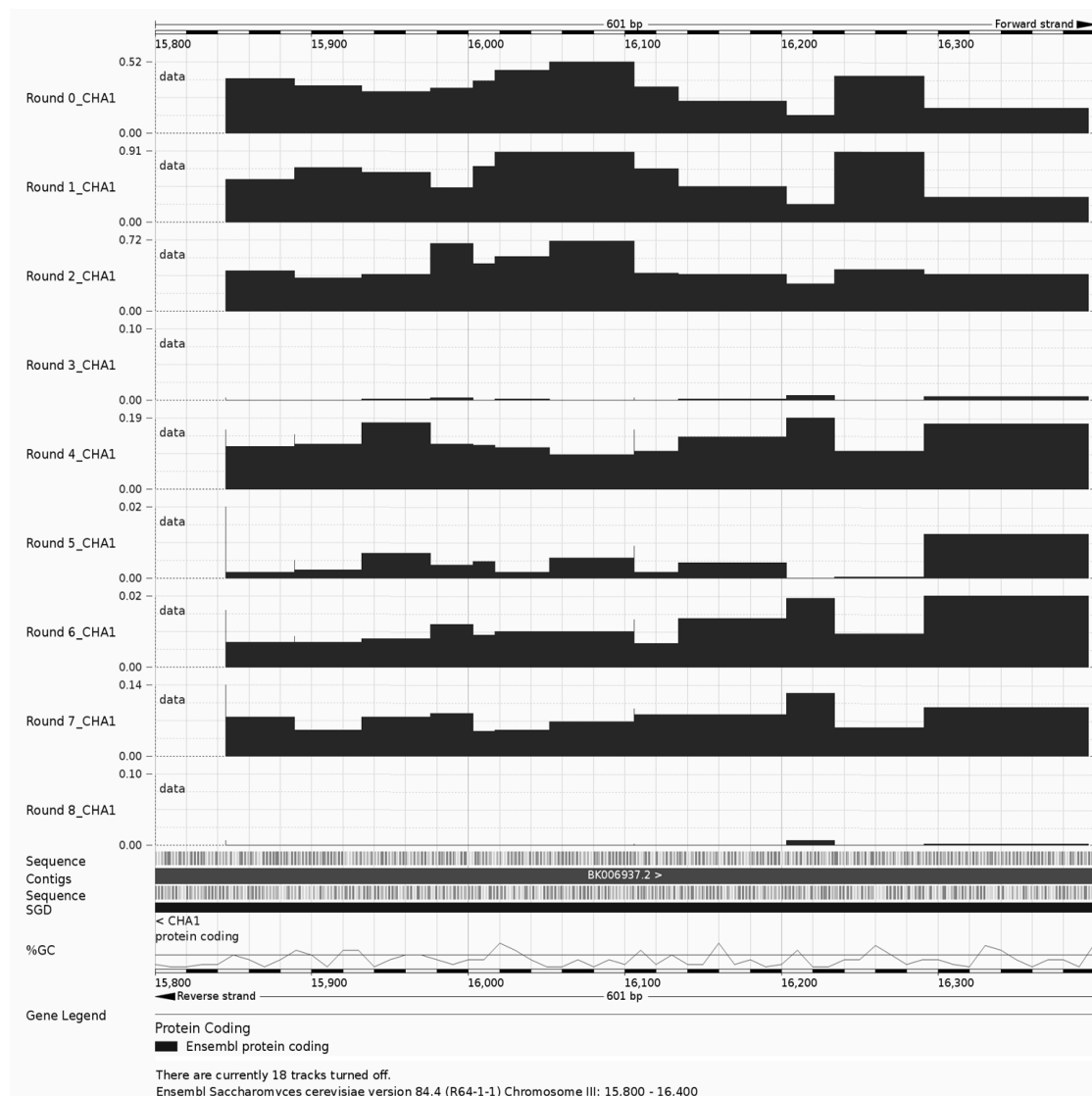
Table 7. Growth Observations after Multiple Rounds of Irradiation.
This table contains the growth observations for the YPD plates that were incubated after
each round of irradiation (0-8). Each culture sample was streaked out on three YPD
plates and then incubated at 30 °C.

Round	Observations	Time for Growth
0 (Starter Culture)	This was the culture that was used to start the experiment and was not exposed to irradiation.	Normal Growth (2-3 Days)
1	2 plates showed no growth, 1 plate showed a cluster of very small colonies, and 2 plates showed growth consisting of 3 colonies (*5 plates total)	3 Days
2	1 plate showed no growth, 1 plate had 3 colonies, 1 plate had 1 colony, 1 plate had 8 colonies, and 1 plate had 1 normal colony and 2 **abnormal yellow colonies**.	3 Days
3	3 plates had no growth, 1 plate had 3 colonies, and 1 plate had 3 colonies	6 Days
4	2 original, wild-type plates showed minimal growth (~5 colonies) after 11 days. Mutant plates showed normal growth after 2 days	2-11 Days (11 Days for original culture, 2 days for mutant plates)
5	After 3 days, light and dark mutant plates both showed normal growth Original, wild-type plates required 10 days of incubation for growth (~5 colonies)	2-10 Days (10 Days for original culture and 2 days for mutant plates)
6	After 2 days, light and dark mutant plates both showed normal growth. Original, wild-type plates took 3 days of incubation for growth	2-3 Days (Mutant plates showed growth after 2 days and it took 3 days for growth on the original culture plate)
7	After 2-3 days, light and dark mutant plates both showed normal growth. Original, wild-type plates took 4 days of incubation for growth on one plate and then 12 days for growth on the remaining two plates.	2-12 Days (Mutant plates showed growth after 2-3 days. The original culture took 4-12 days for growth)
8	After 2 days, light and dark mutant plates both showed normal growth. Original, wild-type plates took 3 days of incubation for growth	2-3 Days (Mutant plates showed growth after 2 days and it took 3 days for growth on the original culture plate)

CHAPTER 4:

APPLICATION OF NUCLEOSOME AND PROTEIN MAPPING TO EVALUATE THREE FORENSICALLY IMPORTANT STR LOCI

Introduction

In a final study, the techniques that were optimized in *Saccharomyces cerevisiae* were applied to evaluate human white blood cells. In this experiment, we analyzed three STR loci: D8, D13, and D21 that are found in human DNA. These three loci are all forensically important because they are part of the thirteen CODIS loci (109). The goal was to look at inherent properties of DNA organization in the form of nucleosomes and other proteins at the regions encompassing these STRs. This study experimentally determined regions of DNA that associate with said proteins and additionally evaluated how exposure to UV radiation may affect the association and/or positioning. Additionally, we evaluated the effects of UV radiation on STR profiling, which is the current and widely-accepted technique used in forensic DNA analysis (111).

Samples of whole blood were collected from five different individuals. White blood cells (WBCs) were isolated from the samples of whole blood. The WBCs were then exposed to UVC light at 0 hours to serve as a no exposure control (0 J/cm^2), 3 hours (27.4 J/cm^2), and 8 hours (73.1 J/cm^2). These exposure times were determined by evaluating the damaging effects of UV light on DNA using alkaline gel electrophoresis, as well as the polymerase chain reaction (PCR) and capillary electrophoresis on the 3130 Genetic Analyzer (Applied Biosystems, Foster City, CA). After the WBCs were exposed to UVC light for the appropriate exposure time, they were subjected to an enzymatic digestion using either micrococcal nuclease (MNase) or deoxyribonuclease (DNase) and the DNA was subsequently purified. Native gel electrophoresis of the purified DNA was used to confirm the success of the enzymatic digestion. For samples that were digested

with MNase, it is necessary to isolate the purified mononucleosomal DNA from the gel using the Qiagen QIAquick Gel Extraction Kit.

After the DNA was purified, qPCR with tiled primers to cover a region encompassing each of the three STR loci (D8, D13, and D21) was performed. This allowed for the determination of the positioning of nucleosomes and proteins in these regions of DNA and whether or not the exposure to UVC light appeared to influence their positioning. Experimental determination of protein positioning will aid in our understanding of these regions of DNA. Additionally, traditional PCR and capillary electrophoresis was used to evaluate the success of the techniques used in forensic analysis after the radiation exposure. Performing such experiments in five different individuals gave us a better idea of the consistency of positioning and any potential variability between humans with our use of biological replicates.

Materials and Methods

Collection of Human Blood Samples

Whole blood samples were collected from five different individuals. The individuals filled out volunteer paperwork according to the University of Nebraska-Lincoln Institutional Review Board. After filling out the paperwork, the individuals went to the University of Nebraska-Lincoln Health Center (Lincoln, NE) and had two, 4 mL EDTA tubes of blood drawn. After the blood was drawn, it was stored in a refrigerator set to a temperature of 4 °C. Each sample was assigned a randomized sample number that could not be associated with any personal or identification information.

Isolation of White Blood Cells

Four milliliters of whole blood was transferred to a 50 mL VWR conical tube and 8.5 mL of cold, 0.5% acetic acid was added. The sample was mixed by inversion and incubated at room temperature for five minutes. After the brief incubation period, 8.5 mL of cold 1.8% sodium chloride (NaCl) was added, and the sample was mixed gently. The sample was centrifuged at 1,500 RPM for 10 minutes at 4 °C in order to pellet the cells. The supernatant was discarded and the pellet was re-suspended in 8.5 mL of cold, sterile water. The sample was incubated for five minutes at room temperature. Another 8.5 mL portion of 1.8% NaCl was mixed into the sample and it was centrifuged at 1,500 RPM for 10 minutes at 4 °C. The supernatant was removed and the pellet of white blood cells remained. The pellet was re-suspended in 2 mL of freezing solution (0.093 M citric acid, trisodium salt, 0.017 M sodium phosphate (monobasic), 0.020 M sodium phosphate (dibasic), 40% glycerol, water). The white blood cells were stored at -80 °C. Alternatively, the white blood cells can be suspended in sterile 1X PBS rather than the freezing solution if the experiments are to be conducted immediately after isolation (150).

UV Radiation Exposure

Prior to experimentation, it was necessary to calibrate the UV Crosslinker lamp intensity (Table 8). The length of time to deliver a dosage of 1.0 J/cm^2 was experimentally measured and then the rate of energy delivery was calculated to be 0.1522 J/cm^2/minute. This calibration can be found in Table 8. In a preliminary experiment, white blood cells were exposed to UVC light in a Stratalinker 1800 UV Crosslinker (Stratagene, San Diego, CA) for various time periods ranging from 0 to 16 hours. After UVC exposure, DNA was extracted and purified from the white blood cells. The DNA

was analyzed using alkaline gel electrophoresis and PCR followed by capillary electrophoresis of STRs on a genetic analyzer. On the alkaline gel, the high pH environment denatures the double-stranded DNA and single strand breaks are detected as a smear pattern on the gel. The smear pattern is due to the resulting DNA fragments that are present, which vary in size (151). The results of this preliminary experiment are exhibited and summarized in Table 9, which contains the results of STR profiling and Figure 28, which contains the image of the alkaline gel. It was decided to evaluate the effects of 0, 3, and 8 hours of UVC exposure based on these results. The duration of exposures correlates to a dosage of 0 J/cm^2, 27.4 J/cm^2, and 73.1 J/cm^2 respectively (Table 8).

The samples of white blood cells were removed from the -80 °C freezer and allowed to equilibrate to room temperature. Aliquots of 500 µl from the stock samples of white blood cells were prepared in 1.5 mL tubes. The samples were centrifuged for 10 minutes at 12,500 RPM at 4 °C. The supernatant was removed and the pellet was re-suspended in 500 µl of sterile, 1X PBS. The samples were then exposed to UVC light in the Stratalinker 1800 UV Crosslinker for either 3 or 8 hours. Briefly, the 1.5 mL microcentrifuge tubes that contained the samples were placed on their sides directly on the base of the Stratalinker 1800 UV Crossslinker. The samples were places directly adjacent to one another to ensure uniform exposure. The samples that were not exposed to UVC light, referred to as 'No Exposure' or 0 hours, were stored in a covered microcentrifuge tube rack, at 4 °C during the time of exposure to UVC.

MNase Digestion & DNA Purification

Post-irradiation, the samples were centrifuged at 4 °C at 3,000 x g for 10 minutes to pellet the cells. The pellet was re-suspended in 1 mL of 0.5% NP-40/Buffer A (0.34 M sucrose, 15 mM Tris-HCl, 15 mM NaCl, 60 mM KCl, 2 mM EDTA, 0.5 mM EGTA, 0.2 mM PMSF, 15 mM β-mercaptoethanol, water) by pipetting the buffer up and down and the sample was incubated on ice for 10 minutes. The samples were centrifuged at 4 °C at 3,000 x g for 10 minutes. The supernatant was removed and the cells were re-suspended in 800 μl of Buffer A. $CaCl_2$ was added to the sample to a final concentration of 0.001 M. This sample was then divided into two, 400 μl portions in new 1.5 mL tubes. Fifteen microliters of MNase (1U/μl) was added to the sample to be digested and 15 μl of sterile water was added to the no digest sample. The samples were incubated at 37 °C for 3 hours. The reaction was stopped by adding 18 μl of EDTA and 7 μl of EGTA and shifting the samples to ice. Subsequently, 60 μl of 10% SDS, 10 μl of RNase A, and 10 μl of Proteinase K were added to the samples. The samples were incubated at 56 °C for 3 hours (1). A standard phenol-chloroform extraction was performed as previously described in the Materials and Methods Section of Chapter 2. The DNA was purified by ethanol precipitation (1 mL 100% ethanol and 40 μl of 3M sodium acetate) overnight (12-18 hours) at -20 °C.

After the overnight incubation, the samples were centrifuged at 4 °C at 12,500 RPM for 25 minutes. The supernatant was removed and the DNA pellet was washed with 500 μl of 70% ethanol. The samples were centrifuged at 17,000 x g for 5 minutes. The supernatant was removed and the pellet was allowed to dry at room temperature for approximately 10 minutes by leaving the lids of the 1.5 mL tubes open. The pellet was re-

suspended in 40 µl of TE Buffer with an overnight (12-18 hours) incubation at 56 °C. The samples were stored at 4 °C until further analysis.

DNase Digestion & DNA Purification

After the samples of white blood cells were allowed to equilibrate to room temperature and were exposed to the appropriate UV dosage as described earlier in this section, the samples were centrifuged at 4 °C at 12,500 RPM for 10 minutes to pellet the cells. The supernatant was removed and the pellet was re-suspended in 300 µl of NPS Buffer. To the samples that were to be enzymatically digested, 2 µl of DNase (1U/µl) was added. The samples were incubated at 37 °C for 10 minutes. To terminate the digestion, 300 µl of Stop Solution was added to each sample and the samples were incubated at 65 °C for 10 minutes. A standard phenol-chloroform extraction was performed according to the protocol outlined in the Materials and Methods Section of Chapter 2. The DNA was then purified by ethanol precipitation (1 mL 100% ethanol and 40 µl of 3M sodium acetate) overnight (12-18 hours) with an incubation at -20 °C. After the overnight incubation, the samples were centrifuged at 4 °C at 12,500 RPM for 25 minutes. The supernatant was removed and the DNA pellet was washed with 500 µl of 70% ethanol. The samples were centrifuged at 17,000 x g for 5 minutes. The supernatant was removed and the pellet was allowed to dry at room temperature for approximately 10 minutes with the lids of the tubes left open. The pellet was then re-suspended in 40 µl of TE Buffer with an overnight incubation at 56 °C. The samples were stored at 4 °C until further analysis.

DNA Quantification and Gel Electrophoresis

As previously described in the Materials and Methods section of Chapter 2, the amount of DNA in each sample was quantified using the Qubit HS dsDNA Kit and the Qubit Fluorometer. The samples were analyzed using native gel electrophoresis in order to confirm the success of the enzymatic digestions. Briefly, the 1% agarose gel was prepared using 0.5 g agarose, 5 µl ethidium bromide, and 50 mL of 1 X TBE. Ten microliters of each sample was combined with 2 µl of 6X loading dye and the total volume was loaded on the gel. A λ DNA-HindIII Digest and 100 BP combination ladder was also loaded on the gel. The gel was run at 50 V for 3 hours. The gels to confirm both the MNase digestion and the DNase digestion can be visualized in Figure 29. After the digestion was confirmed using this method, a larger, 25 µl portion of the MNase digested samples were run on a new 1%, TBE gel, prepared with low-melting point agarose. The mononucleosomal DNA was then excised directly from the gel and purified using the Qiagen QIAquick Gel Extraction Kit according to the manufacturer's protocol and as described in the Material and Methods Section of Chapter 2. After the mononucleosomal DNA was purified, it was quantified using the Qubit HS dsDNA Kit and the Qubit Fluorometer.

Primer Design and Optimization

In order to analyze three forensically important STR loci, tiled primers were designed to cover three distinct ~500 base pair regions of DNA. Each of the three regions encompassed one of three STRs, D8S1179, D13S317, and D21S11. The sequences of the STRs were obtained from the STRBase, which contains the sequence information for the CODIS STR loci (http://www.cstl.nist.gov/biotech/strbase/seq_ref.htm) (152). The

GenBank accession numbers are AF216671 (D8S1179), AL353628.7 (D13S317), and

AP00043 (D21S11). Primers were designed using Primer3 software

(http://bioinfo.ut.ee/primer3-0.4.0/) and specific parameters were set in order to optimize

the primers and standardize them. The parameters were set by our laboratory in order to

dictate the size of the amplicon desired, the specificity and self-complementarity, the

length of the primers, the GC content, and the melting temperature range of the primers.

Additionally, the alignment tools, BLAT and its associated In-Silico PCR, were used to

ensure the specificity of the primer pairs designed to amplify the regions of human DNA.

BLAT detects all regions in the human genome that a set of primers will bind to, thus

evaluating the specificity of a particular primer set. By using this software prior to

ordering and experimentally testing primers, one can eliminate some of the difficulties

associated with non-specific binding. However, this will neither eliminate nor replace the

experimental optimization that needs to be performed in the laboratory (153, 154). The

sequences of the primer sets designed to analyze D8, D13, and D21 can be found in

Tables 10, 11, and 12 respectively.

The primers were optimized in a method that was very similar to the technique

discussed in the Materials and Methods section of Chapter 2. Traditional, end-point PCR

was set up and the reaction contained 1X GoTaq Buffer (Promega), 2.5 mM $MgCl_2$, 2.5

µM dNTPs, 2.5U GoTaq Polymerase (Promega), 10 µg BSA, 0.8 µM of each primer

(forward and reverse), water, and 1 ng of human genomic DNA. The cycling conditions

were as follows: 95 °C for 5 minutes, then 30 cycles of 95 °C for 15 seconds, temperature

gradient (45-60 °C) for 30 seconds, and 60 °C for 30 seconds, and a final extension for 30

minutes at 60 °C. The thermal cycler was programmed to hold at 12 °C until the run was

manually stopped. This was performed on the C1000 Thermal Cycler (Bio-Rad

Laboratories, Hercules, CA). Five microliters of each PCR product was analyzed on a

native gel. Once again, the optimal annealing temperature was visualized by a single

product/band on the gel. In many cases, the lower annealing temperatures permitted

nonspecific binding and resulted in multiple products visualized on the gel. An example

of the electrophoretic analysis of the temperature gradient can be visualized in Figure 30.

This allowed for the determination of the optimal annealing temperature for each primer

set individually.

In cases where there was nonspecific binding at all temperatures in the range of

45-60 °C in the initial temperature gradient, additional optimization experiments were

performed. The second step in optimization for unsuccessful primer sets was running an

additional PCR temperature gradient that included an annealing temperature range from

60 to 75 °C. By increasing the annealing temperature, it is possible to increase the

specificity of primer binding to the DNA template (155). If necessary, primers were

redesigned using Primer3 to ensure that they amplified a single, specific product. When

primers were re-designed, the sequence of the primer was altered slightly and in some

cases, the length of the primer was increased in order to ensure specific binding. The

majority (25/28) of the primer sets for the human loci were optimized at an annealing

temperature of 60 °C. However, primer sets D8_2 and D21_2 required an annealing

temperature of 75 °C, whereas D8_3I required an annealing temperature of 76 °C. Both

primer sets D8_3 and D8_9 had to be redesigned and multiple primer sets were ordered

and tested. The letter after the primer set number indicates that it was the result of a re-

design, hence D8_3I and D8_9Z (Table 10). These annealing temperatures were

determined to produce a single product from the amplification by PCR. An example of

unsuccessful and successful primer sets can be viewed in Figure 30. Multiple bands are

visualized at all temperatures for D8_9Y, and although there are multiple bands at the

lower annealing temperature, at an annealing temperature of 60 °C, D8_9Z amplified the

desired, single product.

qPCR Analysis

　　After the primers were optimized using traditional PCR, a trial run of qPCR was

performed with each primer set to ensure that the reaction conditions translated properly

from PCR to the qPCR analysis. To test the primers, a standard curve including eight

standard data points ranging from 50 ng/µl serially diluted down to 0.023 ng/µl of

standard human genomic DNA (Control Human Genomic DNA- Human Male, BioChain

Institute, Newark, CA) was analyzed for each primer set (50, 16.7, 5.56, 1.85, 0.62, 0.21,

0.068, 0.023 ng/µl). The total reaction volume was 10 µl (8 µl of reaction mix and 2 µl of

standard DNA). The reaction mix of reagents was composed of 5 µl of iTaq Universal

SYBR Green SuperMix (Bio-Rad Laboratories, Hercules, CA), 250 nM (0.4 µl) of each

primer (forward and reverse), and 2.2 µl of nuclease-free water. This master mix was

prepared in excess and 8 µl was pipetted into the appropriate wells of a Hard-Shell Low-

Profile Thin-Wall 96-Well Skirted PCR Plate (Bio-Rad Laboratories, Hercules, CA).

Two microliters of each standard were added to the appropriate well. A no template

control (NTC) was also included that contained 2 µl of nuclease-free water in place of

DNA. A 96-well plate seal was used to seal the wells and the plate was centrifuged to

remove any air bubbles present in the wells of the plate. The cycling conditions used

were as follows: 95 °C for 5 minutes, then 35 cycles of 95 °C for 15 seconds, 60 °C for

30 seconds, and 60 °C for 30 seconds. A melt curve was generated by heating the

samples from 65 to 95 °C at a rate of 0.1 °C/second. For the primer sets that had a

different annealing temperature (not 60 °C), D8_2, D8_3I, and D21_2, the same cycling

conditions were used with the exception of either 75 °C or 76 °C for the annealing

temperature. This was performed on the CFX Connect Real-Time PCR Detection System

(Bio-Rad Laboratories, Hercules, CA) and data was generated in the CFX Manager

Software (Figure 31).

To ensure that the qPCR conditions were working properly, the data generated

were evaluated based on certain criteria. The resulting plots were visualized to ensure that

the efficiency was above 85%, that the R^2 value was close to 1, there was no

amplification in the NTC, and that the melt curve exhibiting a single peak due to the

presence of one product (135) (Figure 31). After the reaction and cycling conditions met

the necessary criteria, they were then applied to analyze the experimental samples.

The preparation of the samples for this study was described earlier in this chapter,

but included the 0, 3, and 8 hours of UVC exposure and enzymatic treatments of -/+

MNase and -/+ DNase for each exposure of five different individuals. In total, there were

60 DNA samples that required analysis. Each of these samples was diluted 1:10 by taking

20 µl of the sample and combining it with 180 µl of TE Buffer. Two technical replicates

of each DNA sample were analyzed in order to ensure the accuracy of analysis. The

samples were transferred into a 96 well plate and a multi-channel pipette was used to

transfer 2 µl of the sample to the appropriate well on a Hard-Shell Low-Profile Thin-Wall

96-Well Skirted PCR Plate (Bio-Rad Laboratories, Hercules, CA). The samples were

prepared in the same method as the standards, by adding 2 µl of each sample to 8 µl of

the master mix (iTaq Universal SYBR Green SuperMix, primers, and water). In addition

to the samples, a standard curve with seven data points was run with each plate, ranging

from 16.7 down to 0.023 ng/µl, and a NTC. The cycling conditions used were the same

as previously described in the first trial of qPCR analysis. Each primer set required two

plates and thus two qPCR runs to analyze all samples, which made the total number of

runs 56. Once again, the CFX Manager Software was used to evaluate the data and an

example of the plots generated can be viewed in Figure 31. Furthermore, the data

collected on this program can be exported in the form of Microsoft Excel spreadsheets.

STR Profiling

In addition to the qPCR analysis, the effect of UVC exposure on STR profiling

was also evaluated. To do so, one of the undigested samples from each of the three UVC

exposures (0, 3, and 8 hours) for each of five individuals was diluted to a concentration of

1 ng/µl. In addition to the experimental samples, a PCR positive control of standard

human genomic DNA (Control Human Genomic DNA- Human Male, BioChain Institute,

Newark, CA) and an amplification blank containing water in place of DNA were also

analyzed. End-point PCR was carried out in a 25 µl reaction containing: 1 ng template

DNA, 1X GoTaq Buffer, 2.5 mM $MgCl_2$, 250 µM dNTPS, 2.5U GoTaq DNA Polymerase

(Promega Corporation, Madison WI), 0.005 mg BSA (Thermo Fisher Scientific Inc.,

Waltham, MA) and using PowerPlex 16 primers (108) at the following concentrations:

D3S1358- 0.12 µM, TH01- 0.55 µM, D21S11- 0.20 µM, D18S51- 0.30 µM, PENTA E-

0.40 µM, D5S818- 0.135 µM, D13S317- 0.07 µM, D7S820- 0.16 µM, D16S539- 0.08

µM, CSF1PO- 0.08 µM, PENTA D- 0.55 µM, AMEL- 0.16 µM, VWA- 0.15 µM,

D8S1179- 1.0 µM, TPOX- 0.6 m µM, and FGA- 0.64 µM (Sigma Aldrich, St. Louis,

MO). The cycling conditions used in this study were those recommended by the manufacturer for use with the PowerPlex® 16 Commercial Kit (Promega Corporation, Madison, WI): 96°C for 5 minutes, 10 cycles of 94°C for 30 seconds (ramp 100%), 60°C for 30 seconds (ramp 29%), 70°C for 45 seconds (ramp 23%); 22 cycles of 90°C for 30 seconds (ramp 100%), 60°C for 30 seconds (ramp 29%), 70°C for 45 seconds (ramp 23%); and a 30 minute hold at 60 °C.

Amplified samples were analyzed using a 3130 Genetic Analyzer (Applied Biosystems, Carlsbad, CA). One microliter of PCR product was added to a combination of 9.5 µl of hi-di formamide (Applied Biosystems) and 0.5 µl of Internal Lane Standard-600 (Promega Corporation). Samples were heated to 95°C for 3 minutes and snap cooled to 4°C for 3 minutes in order to denature the DNA and render it single-stranded. Samples were run on the genetic analyzer with an injection time of 10 seconds at 5.0 volts and analyzed using GeneMapper software (Applied Biosystems). GeneMapper software produced an electropherogram that displayed the 16 loci in a representation of relative fluorescence units (RFU) versus size, in base pairs. The STR profiles were evaluated accordingly and representative electropherograms can be visualized in Figure 32.

Results

Data Analysis

All real-time data were exported into Excel. The first step of analysis required calculating the average of the two technical replicates that were run for each sample. It is important to note that technical replicates were run as a measure of any error due to the performance of the methods used. Initially, all of the qPCR data runs were reviewed to ensure that there was not variance between the two replicates. We evaluated the variance

between the technical replicates by looking at the Cq values directly obtained from our

qPCR analysis. Looking at the difference between the Cq values for a particular set of

technical replicates, we ensured that the difference was less than or equal to 0.5. In

majority of replicates, the Cq values only showed a difference of 0.01-0.1, which

illustrates that there is minimal performance error in these experiments. In a scenario in

which greater variance between the replicates was exhibited, as seen by a greater

difference in Cq values, the samples would need to be repeated and a third technical

replicate would be necessary to ensure accuracy of the analysis methods. This variance

was not exhibited in any of the pairs of technical replicates analyzed in our study. After

similarity was ensured, the average SQ of the two technical replicates was calculated

using the equation, $(T_1+T_2)/2$.

The second step in analysis was to calculate the relative amount of each amplicon.

It is necessary to correct for the input DNA concentration because the amount of input

DNA varied between samples and thus will impact the quantification value obtained from

qPCR. As discussed in previous chapters, this was due to differences in DNA

concentrations of samples and the necessity to add the same volume of each sample to the

qPCR reaction. This correction was done by taking the amplicon SQ (determined from

qPCR) and dividing by the input DNA concentration (determined from quantification

measurement on the Qubit Fluorometer) (125). The amplicon SQ is calculated based on

the standard curve of seven DNA data points (0.023-16.7 ng/µl) (Figure 31). The relative

amount of each amplicon can then be compared between the enzymatic treatment

(MNase or DNase) and it's corresponding 'no digest' sample, across exposures (No

Exposure, 3 Hour UVC, and 8 Hour UVC), as well as across the five biological

replicates.

The third step in analysis was to calculate the relative protection of each

amplicon. This was done by dividing the corrected, digested amplicon (either MNase or

DNase) by its corresponding undigested sample (125). The locations of nucleosomes and

proteins can be determined based on the resulting digestion patterns. If an amplicon is

protected by association with a protein, it will not be digested and will still be present in

the digested samples. However, if a region of DNA is not bound to a protein, it will be

digested by the enzyme. The relative protection of each amplicon can then be compared

across exposures (No Exposure, 3 Hour UVC, and 8 Hour UVC), as well as across

biological replicates. By calculating the relative protection of each amplicon, we are able

to determine the relative position of a nucleosome or other protein.

D8S1179 Results

Previously, web-based tools were used to characterize regions containing

forensically important STRs based on their likelihood to contain nucleosomes (156). Both

NXSensor and nuScore are software programs offer a "nucleosome likelihood prediction"

based on the sequence composition of a region analyzed. As discussed in the literature

review in Chapter 1, there are sequence motifs that will promote DNA-histone binding

and the formation of nucleosomes, but there are also motifs that will disfavor the

formation of nucleosomes, centered on the bendability of a particular region of DNA.

Based on the software prediction, the region containing the STR D8S1179 was classified

with a medium likelihood for nucleosome containment, with 3-5 potential positions for

nucleosomes to be located within the ~500 bp sequence analyzed (156). Given that other

factors in addition to sequence influence nucleosome positioning, it is important to experimentally determine where nucleosomes are located in a particular region of DNA. We know that sequence doesn't act alone to determine nucleosome positioning and an experimental determination allows all factors of the cellular environment to be considered. Factors such as histone variants, post-translational modifications, high order chromatin structure, and non-histone proteins can also influence nucleosome positioning in addition to DNA sequence (21).

From our experiments, we found that there appeared to be strong protection by a potential nucleosome located at 124,894,666-124,894,818, which showed a heightened relative protection value due to fold enrichment in the mononucleosomal DNA, as seen in Figure 33. This protection result was consistent across the five individuals analyzed, but we did see variance in the fold enrichment among our biological replicates and exposures as visualized by the analysis of variance depicted in Figure 34. The relative protection values are contained within a range of just above a value of 1 to above 6. This specific region was also consistent for fold-enrichment in the mononucleosomal DNA after exposure to UVC at both 3 and 8 hours as seen in the panels of Figure 33. This distinct region of protected DNA is apparent in all relative protection plots in Figure 33. Our results do not illustrate an apparent effect of radiation on the protection from enzymatic digestion at this specific region of DNA. We also observed that the remainder of amplicons analyzed in this region may also be protected from digestion due to their relative protection values falling higher than one or right around a value of one (Figures 33-34). However, the other amplicons did not appear to show the increase in variance of fold enrichment that was exhibited at 124,894,666-124,894,818. The amount of variance

appears to increase with the mean relative protection value, which can be visualized by comparing all five biological replicates in Figure 34. As the relative protection values were lower and closer to 1, the amount of variance between biological replicates appeared to decrease (Figure 34). Overall, this region appears to exhibit protection from digestion by nucleosome association. The region we analyzed was around 500 bp, which theoretically could contain three nucleosomes.

The DNase digestion allowed us to evaluate regions of DNA protected by either histones or non-histone proteins. This enzyme will digest regions of DNA that are not bound to protein, but regions of DNA that are bound to any protein will be protected. Our analysis allows us to map out these regions based on the remaining amplicons in our digested samples. As discussed in Chapter 2, the DNase digestion does necessarily exhibit fold enrichment of the DNA at protected regions, but rather a relative protection value very close or equal to 1. The "No Exposure" samples showed that the region containing D8 that was analyzed was consistently associated with proteins in all five individuals, as seen in Figure 35. The relative protection values for the no exposure samples ranged from 0.7 to slightly over 1, but were consistently in the range of 0.8-1 for the five individuals at all amplicons analyzed (Figure 35). However, after exposure to UVC for 3 and 8 hours, the relative protection values seemed to decrease slightly, with fractional values around 0.2-0.6, but a similar pattern of protection (Figure 35). In some cases, after 8 hours of exposure, the relative protection value dropped below 0.2 (Figure 35). This trend can also be visualized by the analysis of variance plots in Figure 36 as we see the data points for the no exposure samples (black) seem to be clustered slightly higher than the data points for the 3 hour (blue) and 8 hour (green) exposure data points.

There is still some overlap in the data points from different exposures, which warrants further investigation into this trend. When comparing the five biological replicates, we did not see the heightened variance in relative protection values that resulted in the MNase digestion, as seen by a smaller range of relative protection values in Figure 36. Further analysis may help us to understand if these values are due to expected variance between samples or if the fractional relative values obtained are significantly different in our no exposure samples versus samples that were exposed to radiation.

D13S317 Results

The web-based tools, NuScore and NXSensor, predicted the region containing the STR D13S317 to contain a stiff nucleosome exclusion sequence, which makes it less accessible to associate with histones to form a nucleosome. Additionally, the region containing D13 did not have many potential positions (0-2) for a nucleosome to be located, which was solely based on sequence motif preferences. Based on these results, the region containing D13 was grouped with a low likelihood to contain a nucleosome by a previous research group (156). In this study, our experimental results indicated strong nucleosomal positioning covering amplicons 5 and 6, located on chromosome 13 from 82,118,348-82,118,480 (Figure 37). The fold enrichment of mononucleosomal DNA at this specific region can be visualized in Figures 37 and 38. This region of heightened relative protection values was distinct in all five individuals and regardless of exposure to either 3 or 8 hours of UVC radiation (Figure 37). As we looked into variance among our biological replicates, we again see a pattern that the amount of variance appears to increase with the mean relative protection value, as indicated in Figure 38. At this particular region, the relative protection values appear to range from 2 to 15, but all

values indicate that this region is protected from digestion by MNase. The variance we are seeing across biological replicates at this particular amplicon is not as apparent at the other amplicons in this region. The additional regions analyzed are also suggested to contain potential nucleosomes due to their protection from digestion, but once again, the remainder of the region analyzed did not show as high of fold enrichment, as seen in Figures 37 and 38. The relative protection values at the additional regions of DNA, 82,118,048-82,118,348 and 82,118,480-82,118,576, seem to be clustered around relative protection values in the range of one to two (Figure 38). The positioning pattern observed as this region did not appear to show any variation that can be attributed to radiation exposure.

Similar to the observation made with D8, we saw the relative protection values for the DNase digestion to exhibit consistent protection by proteins in this region containing D13 as seen in Figures 39 and 40. The "No Exposure" samples produced relative protection values that ranged from 0.6 to over 1, but were consistently in the range of 0.8-1 for the five individuals at all amplicons analyzed (Figure 39). Again, we saw a decrease in the relative protection values for some of the amplicons in the samples that were exposed to UVC radiation (Figure 39). At the 3 hour UVC exposure time point, the relative protection values shifted to an average around 0.2-0.6 and at 8 hours, the relative protection values were consistently in the range of 0.2-0.6 as well (Figure 39). The analysis of variance also appears to illustrate this trend, as seen in Figure 40. When comparing the five biological replicates, there was some indication of variance between samples, but the relative protection values were contained within a smaller range, mainly clustered around a relative protection value of 1 (Figure 40). In order to draw any

conclusions regarding this pattern, we must look into the possibility that the patterns we are seeing are due to expected variance or if they are significantly different in our no exposure and radiation-exposed samples. This may require a method of statistical analysis.

D21S11 Results

Differentiating from the web-tools-based prediction for D8 and D13, the region containing D21S11 ranked as the highest likelihood to contain nucleosomes of all STR regions analyzed, according to another research group (156). This was due to a higher number of potential positions where the DNA sequence was favorable to associate with histones as a nucleosome (6-8 potential locations) (156). Although 6-8 potential locations were identified based on the sequence preferences, due to the size of the region analyzed, it would only be spatially possible for three nucleosomes to be located within a 500 bp region of DNA. Again, we must recognize the limitation of software predictions and the fact that only sequence features are considered when making nucleosome positioning predictions. In the experiments that were a part of our study, we observed a distinct protection pattern for the region containing D21 that was analyzed. This pattern is visualized in Figure 41 and additionally in Figure 42. For the analysis of D21, in all samples, there was a distinct region from 19,181,958-19,182,129 that lacked protection by nucleosomes and was at very low fractional relative protection values, averaging around 0.2 (Figure 41). This pattern was observed in all five individuals as well as those samples exposed to 3 and 8 hours of UVC alike as visualized by comparing the relative protection plots in Figure 41. All relative protection values for the biological replicates and exposures were in a very close proximity, with minimal variation (Figure 42). The

proximal regions that bordered the nucleosome-free region, 19,181,820-19,181,958 and

19,182,120-19,182,360 showed heightened relative protection values (Figures 41-42).

The relative protection values at the amplicons outside of the nucleosome-free region

ranged from 1 to 5. As seen in Figure 42, there appears to be more variance across the

biological replicates as we see an increase in the fold enrichment of mononucleosomal

DNA. Based on our experimental results, there did not appear to be any effect of

radiation on the pattern of protection. The relative protection values did seem to vary

between individuals and exposures, but the patterns of protection generated were in

consensus to show a distinct unprotected region that was directly in between two

protected regions. The pattern may suggest three nucleosomes positioned within this 534

bp region.

We also analyzed this particular region of DNA that contained the STR D21 for

samples that had been digested with the enzyme DNase. Again, this enzyme will allow us

to look at regions of DNA that are bound by either a histone or non-histone protein and

thus protected from enzymatic digestion. Our results indicated that this region of DNA

contained consistent protection due to its association with proteins. In the control samples

that had not been exposed to UVC, we saw that the relative protection values range from

0.5-1.5 for all five individuals as seen in Figure 43. The relative protection values for the

samples that were exposed to UVC for 3 or 8 hours, showed relative protection values in

the range of 0.3-1 (Figure 43). There was some variance between the biological

replicates, but it was within a range of about 0.7 as seen by the clustering of data points in

Figure 44. Similar to the DNase digestion results for D8 and D13, we observed that the

relative protection value range decreased slightly for the UVC-exposed samples when

compared to our no exposure control samples. We also saw fractional relative protection

values that were slightly lower than the other amplicons at the region that was

characterized by the MNase digestion as nucleosome-free. However, this region was not

as distinguishable as it was in the MNase digestion. This result may propose that the

nucleosome-free region is protected by another DNA-binding protein.

STR Profiling

In forensic science, DNA analysis culminates with the generation of a DNA

profile, as seen in Figure 32. This is accomplished by the amplification of STRs, which

are distinct regions of non-coding DNA. Analysis of a multiplex of STRs gives a profile

high discriminatory power. CODIS requires laboratories to attempt to amplify 13 loci, but

10 loci must have results to submit a profile to the CODIS database. Our multiplex

amplification in this study amplifies 15 STRs and 1 indel according to PowerPlex 16

(Promega Corporation) (108). Post-amplification, samples were analyzed using capillary

electrophoresis on the 3130 Genetic Analyzer (Applied Biosystems). The fluorescence of

each tagged DNA amplicon is translated into a peak by the computer software and is

visualized as an electropherogram of alleles in GeneMapper (Applied Biosystems). When

the DNA is not compromised or degraded, successful amplification is visualized by

balanced peaks at all 16 loci. In this study, we obtained full, 16-loci profiles from 1 ng of

DNA that had not been exposed to UVC (No Exposure) from all five individuals. On

average, the RFU for peaks was around 1,800. This can be viewed in the first

electropherogram of Individual 3 in Figure 32. This result confirms the success of

amplification techniques and also indicates that there wasn't additional damage induced

in the samples during preparation and analysis that would inhibit this downstream

analysis. We can confirm that there was no damage inflicted on the samples during the protocols of this study and this gives us a baseline to compare the effects of UVC exposure on STR profiling back to.

DNA degradation is visualized in STR profiles by both a decrease in RFU and in some cases a complete drop-out of alleles (157). From our preliminary experiments, we found that increased exposure to UVC caused DNA samples to experience both of these results as detailed in Table 9. In this study, we found that 3 hours of UVC exposure caused an overall decrease in RFU of the peaks from approximately 1,800 RFU to around 400-1,000 RFU on average, but in some cases, the RFU was even lower. Furthermore, we saw the drop out of PENTA D, PENTA E, and FGA alleles in some individuals. This is expected as these STRs are the largest in size, around 400 bp. After 8 hours of UVC exposure, similar results were exhibited with a decrease in the peak height of majority of alleles to below 400 RFU and again, the complete dropout of some alleles. For example, in Individual #3, we saw that D18, PENTA E, D7, D16, CSF, PENTA D, and FGA all dropped out after 8 hours of UVC exposure (Figure 32). It is important to note that our laboratory used a threshold of 150 RFU for calling alleles. This result can be visualized in the 3 Hour UVC and 8 Hour UVC electropherograms in Figure 32. The degradation caused by UVC exposure is apparent when compared back to the control sample. In Figure 32, all three electropherograms have the same scale on the y axis, which is 4,200 RFU. The visual comparison of these electropherograms illustrates the overall decrease in peak height as radiation exposure was increased.

The STRs that we analyzed in this study, D8, D13, and D21 were present at normal RFU in all of the control samples that were not exposed to radiation at a range of

1,200-4,400 RFU, with variance in RFUs depending on the individual. At 3 hours exposure to UVC, the RFU of these three alleles decreased to 200-900 RFU and at 8 hours exposure to UVC the RFU were also lowered to a range of 200-700 RFU. Although it appears that the ranges of RFUs overlap for the different exposures, a consistent pattern of decrease in RFU was consistently exhibited from 0 to 3 hours and from 3 hours to 8 hours in all five individuals. This downward trend of peak height is indicative of the DNA damage caused by increasing exposure to UVC. Although other STRs dropped out or saw a more severe decrease in RFU, the STRs we examined for nucleosome and protein positioning were present in all samples analyzed. We found that the regions of DNA analyzed containing D8, D13, and D21 all appeared to be protected by the association of DNA with histones and potentially other DNA-binding proteins. Additional experiments are necessary to determine if the successful amplification of these STRs may be attributed to protein coverage in addition to the size of the amplicon. All three STRs (D8, D13, and D21) were around 200 bp in size, which suggests that they would be more likely to be retained in degraded samples due to their smaller size. We need to analyze additional STRs in an attempt to separate these variables and fully investigate the relationship between protein coverage and successful STR analysis.

Discussion

In this experiment, we applied the protocols that were optimized in yeast (*Saccharomyces cerevisiae*) to analyze human white blood cells for nucleosome and protein positioning at three forensically important STR loci, D8S1179, D13S317, and D21S11. We also sought to evaluate if exposure to UVC irradiation had an effect on the positioning of histones and non-histone proteins. The results of the work discussed in this

chapter indicate that the techniques and protocols we optimized in yeast can be applied to analyze human cells. It was necessary to vary the protocols used to isolate the cells, but the major steps involved in enzymatic treatment, DNA purification, and qPCR analysis were extremely similar and permitted the successful application. We consider the ability for our laboratory work to be translated from working in yeast to working in humans as an illustration of the usefulness of yeast as a model organism (95). There were many steps and reaction conditions in the protocols that had to be optimized, but this optimization was much more feasible to perform in yeast cells rather than human cells. With yeast, there is no limitation in sample size and a culture stock can be continuously maintained. As we continue to expand on our laboratory experiments, it is reassuring to know that we can use yeast cells in preliminary work and then apply these protocols to analyze human cells.

Similar to the conclusions discussed in Chapters 2 and 3, the results of this study again suggest that exposure to UVC radiation did not appear to have an obvious effect on the positioning of histones and other non-histone proteins at the three STR loci that we examined, D8S1179, D13S317, and D21S11. Overall, we saw that all three STR loci DNA regions were consistently protected from enzymatic digestion by association with histones to form nucleosomes (Figures 33, 37, and 41). This result makes biological sense given the nature of STRs. STRs are contained within regions of DNA that either do not get transcribed into RNA or alternatively, regions that are not translated, intergenic regions and introns respectively (1). Thus, the cell will not have a need to regulate processes, such as transcription, at these particular regions of DNA. Without the necessity of recruiting transcriptional machinery and associated DNA-binding proteins,

the DNA does not necessarily need to be accessible. Further, the DNA that is part of an

STR has the ability to be tightly associated with histones to form a nucleosome.

As we look at the STRs individually, we can start to evaluate the patterns of

protection exhibited at each region of DNA that was analyzed. For D8S1179, we

analyzed a region of DNA on chromosome 8, with a genomic location from 124,894,666

through 124,895,213, which is 547 bp in size (Figure 33). Our mapping results indicated

heightened relative protection values in the region from 124,894,666-124,894,818 as well

as consistent protection in the remaining portion of the region analyzed (Figures 33-34).

Looking at the relative protection maps in Figure 33, we see that this region of DNA has

a higher GC content (above 50%) within its sequence. We know that particular sequence

features, including the motif GG/CC and overall GC content is favorable for nucleosome

formation, so this result is logical (21). Additionally, in the regions excluding

124,894,666-124,894,818, our results did not indicate as much fold enrichment in

mononucleosomal and the relative protection values were not as high. This pattern was

consistent across all five biological replicates (Figures 33-34). Our results do not seem to

illustrate an apparent effect of radiation on the protection from enzymatic digestion at this

region of DNA, as the pattern of protection remained consistent (Figure 33-34). Given

that we analyzed a ~500 bp region of DNA containing each STR, we must also take into

consideration the specific location of the STR analyzed for DNA profiling. The genomic

location of the amplicon generated for forensic STR profiling is at 124,894,821-

124,895,047 and it is 227 bp in length (152). This particular region of DNA was

protected from enzymatic digestion. We also saw that the regions protected from MNase

digestion were also protected from DNase digestion indicated by relative protection

values right around one (Figures 35-36). Again, we expect the values of the MNase digested DNA to be different from the DNase digested DNA due to the fact that the mononucleosomal DNA is excised from a gel and further purified. At this region of DNA, we saw that the MNase and DNase results aligned.

Our analysis of D13S317 included the genomic region from 82,118,048-82,118,576 on chromosome 13, which is 528 bp in length. Based on the relative protection values obtained, we saw high fold enrichment of mononucleosomal DNA at the region from 82,118,348-82,118,480 (Figures 37-38). This region of heightened relative protection values was distinct in all five individuals and regardless of exposure to either 3 or 8 hours of UVC radiation. The remainder of the region analyzed was also protected, but did not show as high of fold enrichment, as seen in Figures 37 and 38, but rather was clustered around relative protection values of one to two. Similar to our analysis of D8S1179, we saw that the region exhibiting heightened relative protection values also has a higher percentage of GC content (Figure 37). This potentially illustrates the importance of sequence features in determining nucleosome positioning. The specific location of the STR analyzed for forensic DNA profiling is from 82,118,154-82,118,346 and it is 192 bp in length. The region was protected from enzymatic digestion based on our analysis. Further, we saw consistent patterns of protection in both the MNase and DNase digested samples (Figure 39). The enzymatic digestions had similar results, with the only difference being in the relative protection values, as there was fold enrichment in the purified mononucleosomal DNA and relative protection values around 1 in the whole, DNase digested sample. Further, according to our results, there was no apparent effect of UVC exposure on the positioning pattern of proteins at this particular region of DNA.

To investigate the STR D21S11, we analyzed the region from 19,181,832 to 19,182,366 on chromosome 21, which is 534 bp in length (Figure 41). Our results at this particular region of DNA revealed an interesting feature that we did not see in D8S1179 or D13S317. In this region of DNA, we saw a distinct region that appeared to be nucleosome-free, bordered by a consistent pattern of nucleosome protection. The region that appears to be nucleosome-free was not protected from enzymatic digestion by MNase and thus resulted in very low relative protection values (less than 0.2) as seen in Figure 41. This particular region was from 19,181,958-19,182,129 and we see that in our chromosomal map, it is characterized by a lower GC content, at a percentage distinctly below 50%. Just as we saw the regions with high relative protection values to have a higher GC content in D8S1179 and D13S317, we see a supporting negative preference at D21S11; a low GC content correlating with a lack of nucleosome association. This illustrates the role that sequence may play in determining nucleosome positioning and its ability to instill both negative and positive preferences for nucleosome formation. The proximal regions that bordered the nucleosome-free region, 19,181,820-19,181,948 and 19,182,120-19,182,360 showed heightened relative protection values in accordance with protection by nucleosomes (Figures 41-42). The location of the STR used for forensic DNA analysis according PowerPlex 16 is from 19,181,941-19,182,163 and is 222 bp in length (152). Contrary to the other two STRs that we looked at, D21S11 appears to be located within a region that is only partially protected from digestion by nucleosomes. Majority of this STR, 171/222 bp, falls within the distinct unprotected region. This is an interesting result and may suggest the importance of proximal nucleosomes to protect regions of DNA. Additionally, we saw that this region was protected according to our

DNase digestion results (Figures 43-44). This result may suggest that there is another DNA-binding protein that is capable of binding to this region and thus protecting it from digestion by DNase. Investigation into the identity of the protein might also help us to understand why it does not appear to associate with nucleosomes. We hope to look into this region in more detail to fully understand what, in addition to GC content and sequence features, may be playing a role in the negative preference for nucleosome association or potentially a positive preference for another DNA-binding protein.

Overall, looking at the results of all three STR loci, we saw a trend that the amount of variance in relative protection values among our biological replicates appears to increase with the mean relative protection value (Figures 34, 38, and 42). As the relative protection values were lower and closer to 1, the amount of variance between biological replicates appeared to decrease. This trend was also suggested in the study we conducted in yeast, as discussed in Chapter 3. We hope to investigate this observation further by eliminating the possibility that the variance is attributed to any experimental variations. We have to ensure that steps such as crosslinking the DNA and protein are complete, which was mentioned in Chapter 2. If we are able to evaluate each step of our protocol and ensure that there is not experimental variation, we can begin to speculate what the variance in relative protection values that we are seeing might mean. This may be related to the strength of nucleosome positioning and given that we are analyzing a population of cells, a heightened and variable relative protection value may indicate that majority of cells have this particular nucleosome configuration. Based on previous literature, it is possible to analyze individual cells for nucleosome positioning. This

technique may provide us with a better idea of what specific nucleosome configurations exist and how that correlates with the results of our multiple cell study (139).

Another interesting trend that we hope to explore appeared at all three STR loci, but in the samples that were digested with DNase (Figures 35, 39, and 43). Looking at analysis of variance plots, we are able to get an idea of the variance across biological replicates as well as the comparison among radiation exposures (0, 3, and 8 hours). Although we did see variance among our biological replicates, there appears to be a pattern that the relative protection values decrease as we increase our UVC exposure from 0 to 3 and 8 hours of exposure (Figures 36, 40, and 44). This pattern would need to be analyzed further to evaluate whether or not the variation in mean relative protection values according to radiation exposure was significant. We hope to use a statistical method to assess if this trend is valid and if the variance in relative protection values is significant. There is the possibility that the variance we are seeing is expected as natural variation and can't be attributed to the exposure to radiation.

In this study, we experimentally evaluated the positioning of nucleosomes and other proteins in three different STR loci, D8S1179, D13S317. This work is beneficial to forensic scientists because it provides a better understanding of the intrinsic properties of DNA at STRS, which are the primary regions of DNA that are analyzed in this field. In this study, we have illustrated that the positioning of nucleosomes and proteins is conserved at three forensically important STR loci after UVC radiation exposure at time points of 3 and 8 hours. This conservation of positioning may suggest the important role that nucleosomes play in protecting particular regions of DNA from damage. We understand that nucleosome positioning is complex and advocate that positioning be

determined experimentally in order to take into account all factors that may influence such positioning. In our experiments, we found that all three STRs analyzed exhibited evidence of nucleosome protection.

To expand on the scope of this project, we believe that it would be beneficial to look at the positioning of nucleosomes and other proteins in physiological stains. Dried stains of biological fluids (blood, saliva, and semen) are a common type of evidence encountered at a crime scene, making them forensically-relevant. It would be interesting to analyze the positioning of nucleosomes in dried physiological stains and compare to the results obtained from living cells, such as those from our experiments. It has been suggested that histones may be removed in forensic stains due to the process of necrosis and lysosomal proteases (157). This experimental comparison could provide further insight to the factors that may affect nucleosome positioning. Because although our experiments suggested that radiation did not appear to affect the positioning of nucleosomes in samples of white blood cells, the process of necrosis may have an effect on such positioning. This experiment would also provide the opportunity to evaluate real-world and case-like samples. A study such as this would give the forensic science community a better of idea of the intrinsic properties of DNA that play a role in the samples that they typically encounter when performing DNA analysis. It might also be beneficial to analyze additional STRs for histone and non-histone protein positioning. For example, we saw that the larger STRs, PENTA E, PENTA D, and FGA, dropped out in some of our 3 hour and 8 hour UVC-exposure samples. This is characteristically due to their larger size, but it may be interesting to analyze the positioning of nucleosomes and

other proteins in these regions to evaluate if the drop out may be correlated with a lack of protection or is solely due to their larger size.

Our future research endeavors center around comprehensively investigating the relationship between the features of the genomic environment and the incidence of DNA damage. Specifically, we would like to focus on DNA sequence and DNA structure and how they may work together to influence sites of DNA damage. The studies we have presented in Chapters 2, 3, and 4 have evaluated an important feature of the genomic environment, which is the association of DNA with proteins. Our results suggest that exposure to radiation does not appear to affect the positioning of nucleosomes and other proteins in the loci evaluated. We look forward to using the methods discussed in these chapters to analyze other regions of DNA and also to correlate these results with an evaluation of DNA sequence and the incidence of DNA damage.

Table 8. Calibration of UV Crosslinker Lamp Intensity.
The Stratalinker 1800 UV Crosslinker (Stratagene, San Diego, CA) was calibrated prior to experimentation. The calibration must be performed every two weeks to ensure accuracy of the instrument. By experimentally measuring the length of time required to deliver a set dosage of 1.0 J/cm^2, the rate of energy delivery of the crosslinker can be calculated. For each time exposure, the UV dosage was then calculated.

Length of time required to deliver dosage of 1.0 J/cm^2 (Experimentally Measured):	6 minutes and 34 seconds
Calculated time in decimal minutes:	6.572 minutes
Rate of Energy Delivery:	0.1522 J/cm^2/minute
0 Hours (0 minutes) Exposure:	0 J/cm^2
3 Hours (180 minutes) Exposure:	27.396 J/cm^2
8 Hours (480 minutes) Exposure:	73.056 J/cm^2

Table 9. Evaluation of STR Profiles.

This table displays the results from the STR profiling of samples of white blood cells that were exposed to various amounts of UVC light (0-16 hours). After UVC exposure, DNA was extracted and purified from the samples. The 16 STR loci of PowerPlex 16 were amplified using fluorescently-tagged primers and end-point PCR. The amplified product was then run on the ABI 3130 Genetic Analyzer and the generated electropherogram was evaluated. The alleles were either classified as normal (white), low RFU/ less than 150 RFU (grey), or a dropped out allele is indicated by a black **X.**

Locus	D3	THO1	D21	D18	PENTAE	D5	D13	D7	D16	CSF	PENTAD	AMEL	VWA	D8	TPOX	FGA
0 Hr.	17, 18	9.3, 9.3	21, 28	12, 14	11, 13	9, 11	11, 11	12, 14	9, 10	11, 12	9, 12	X, X	17, 17	13, 13	8, 8	21, 23
1 Hr.	17, 18	9.3, 9.3	21, 28	12, 14	11, 13	9, 11	11, 11	12, 14	9, 10	11, 12	9, 12	X, X	17, 17	13, 13	8, 8	21, 23
2 Hr.	17, 18	9.3, 9.3	21, 28	12, 14	11, 13	9, 11	11, 11	12, 14	9, 10	11, 12	9, 12	X, X	17, 17	13, 13	8, 8	21, 23
3 Hr.	17, 18	9.3, 9.3	21, 28	12, 14	11, 13	9, 11	11, 11	12, 14	9, 10	11, 12	9, 12	X, X	17, 17	13, 13	8, 8	21, 23
4 Hr.	17, 18	9.3, 9.3	21, 28	12, 14	11, 13	9, 11	11, 11	X	9, 10	11, 12	X	X, X	17, 17	13, 13	8, 8	X
5 Hr.	17, 18	9.3, 9.3	21, 28	12, 14	11, 13	9, 11	11, 11	12, 14	9, 10	11, 12	X	X, X	17, 17	13, 13	8, 8	X
6 Hr.	17, 18	9.3, 9.3	21, 28	12, 14	X	9, 11	11, 11	X	9, 10	11, 12	X	X, X	17, 17	13, 13	8, 8	X
7 Hr.	17, 18	9.3, 9.3	21, 28	X	X	9, 11	11, 11	X	9, 10	X	X	X, X	17, 17	13, 13	8, 8	X
8 Hr.	17, 18	9.3, 9.3	21, 28	X	X	X	11, 11	X	X	X	X	X, X	17, 17	X	X	X
16 Hr.	17, 18	9.3, 9.3	21, 28	X	X	X	11, 11	X	X	X	X	X, X	17, 17	X	X	X

Table 10. D8 Primer Sequences.

These primers were designed using Primer3 in order to analyze a ~500 basepair region of DNA encompassing the CODIS STR, D8S1179 (GenBank: AF216671). The primers were obtained from Sigma Aldrich (St. Louis, MO) as lyophilized oligos. Note: the final primer sequences are included in this table; D8_3I and D8_9Z were due to re-designing as described in the Materials and Methods section of Chapter 4.

Forward Primer Name	Sequence	Reverse Primer Name	Sequence
D8_1F	GCATCAAGGTAGTTAGGTAAAGCTG	D8_1R	GCCACTGGCTACAGAGGTTT
D8_2F	CTTGGGGTGTCGCTTTTCT	D8_2R	TATAAGTTGCCAGGCCGTGT
D8_3IF	GCCTTTGCCTGAGTTTTGCT	D8_3IR	ATACATATAAGTTGCCAGGCCGT
D8_4F	GGCCTGGCAACTTATATGTATTT	D8_4R	GATTATTTTCACTGTGGGGAATAGA
D8_5F	ATCTATCTATCTATTCCCCACAGTGAA	D8_5R	TCACTGTATCGTATCCCATTGC
D8_6F	TCACGCAATGGGATACGATA	D8_6R	TTGTTTCCAGTTTCTTTTACCAAAT
D8_7F	CACAATTTGGTAAAAGAAACTGGA	D8_7R	GAAACCCTGTGCATTGTTGT
D8_8F	ATACATACGGTTTTTGACAGC	D8_8R	TCCTTTCACAGCTATTATCAAA
D8_9ZF	AACAATGCACAGGGTTTCAG	D8_9ZR	GCCCGGCCCAAGTTTTTA

Table 11. D13 Primer Sequences.

These primers were designed using Primer3 in order to analyze a ~500 basepair region of DNA encompassing the CODIS STR, D13S317 (GenBank: AL353628.7) The primers were obtained from Sigma Aldrich (St. Louis, MO) as lyophilized DNA oligos.

Forward Primer Name	Sequence	Reverse Primer Name	Sequence
D13_1F	TTTTCACTCACCAGTTTTA	D13_1R	CAGTGGTAGGAAGACTTTTA
D13_2F	AATGTTAAAAGAGCTGTAAAT	D13_2R	GATAGATAGATAGACAAATATTCC
D13_3F	TTAATTCATAGGAATATTTGTC	D13_3R	AGGCCTTGAAAAGTAGATAG
D13_4F	TTTTCAAGGCCTTATTTATGCAG	D13_4R	AGAACGAGGTTCCGTCTCAT
D13_5F	TTATGAGACGGAACCTCGTT	D13_5R	GAAGGAGAATGGCTTTAACTTG
D13_6F	TTATGAGACGGAACCTCGTT	D13_6R	GGAGAATGGCTTTAACTTGG
D13_7F	GCACGACCTTGGCTCACT	D13_7R	CGGGCGCCTCTAATTCTA
D13_8F	ACTCAAGATATTGGGGGAGTTG	D13_8R	TGCAGCTGAAAAATACACTGAG
D13_9F	TTTGAGTGCTCTCAGTGTATTTTTC	D13_9R	TTGGGCAGGGTTCATTATTC

Table 12. D21 Primer Sequences.
These primers were designed using Primer3 in order to analyze a ~500 base pair region of DNA encompassing the CODIS STR, D21S11 (GenBank AP000433). The primers were obtained from Sigma Aldrich (St. Louis, MO) and in the form of lyophilized DNA oligos.

Forward Primer Name	Sequence	Reverse Primer Name	Sequence
D21_1F	TCAGCTTCCGTTGTTCTAAGG	D21_1R	GAGAAAAGTCCCATAACAGACCA
D21_2F	TCAGACTTGGACAGCCACAC	D21_2R	CACTTGGGGAATTGACTCACA
D21_3F	CCATAAATATGTGAGTCAATTCC	D21_3R	TAGATAGATAGACAGACAGACAGACAG
D21_4F	CAAGTGAATTGCCTTCTA	D21_4R	GACTGGATAGATAGACGATAG
D21_5F	CCAAGTGAATTGCCTTCTA	D21_5R	AGGAGGTAGATAGACTGGATAG
D21_6F	TCCAGTCTATCTACCTCCTATTAGTC	D21_6R	TGATATAACTTGAAATTAAACTGTGAT
D21_7F	CTCCTATTAGTCTGTCTCTGG	D21_7R	TTATATAATGTATGAAGTGGTATGA
D21_8F	GTTTAATTTCAAGTTATATCATACCA	D21_8R	TGTCTGGCACCCAGTAAAAA
D21_9F	ACCTTACAGTGTTTCTCCCTTC	D21_9R	TTCACCACTTAGCAAAATAAAAA
D21_10F	TGGGTGCCAGACACTAATTTT	D21_10R	AACTTTACCCAGATCAACACTCA

Figure 28. Alkaline Gel Electrophoresis of UVC Exposure Range.

Alkaline gel electrophoresis image of the DNA extracted from the white blood cell samples exposed to UVC light at time points ranging from 0-16 hours. The gel was run at 90V for 2 hours. The gel was subsequently stained in SYBR Gold for 1 hour and further stained overnight (12-18 hours). This image indicates the increasing presence of single strand breaks as the UVC exposure was increased.
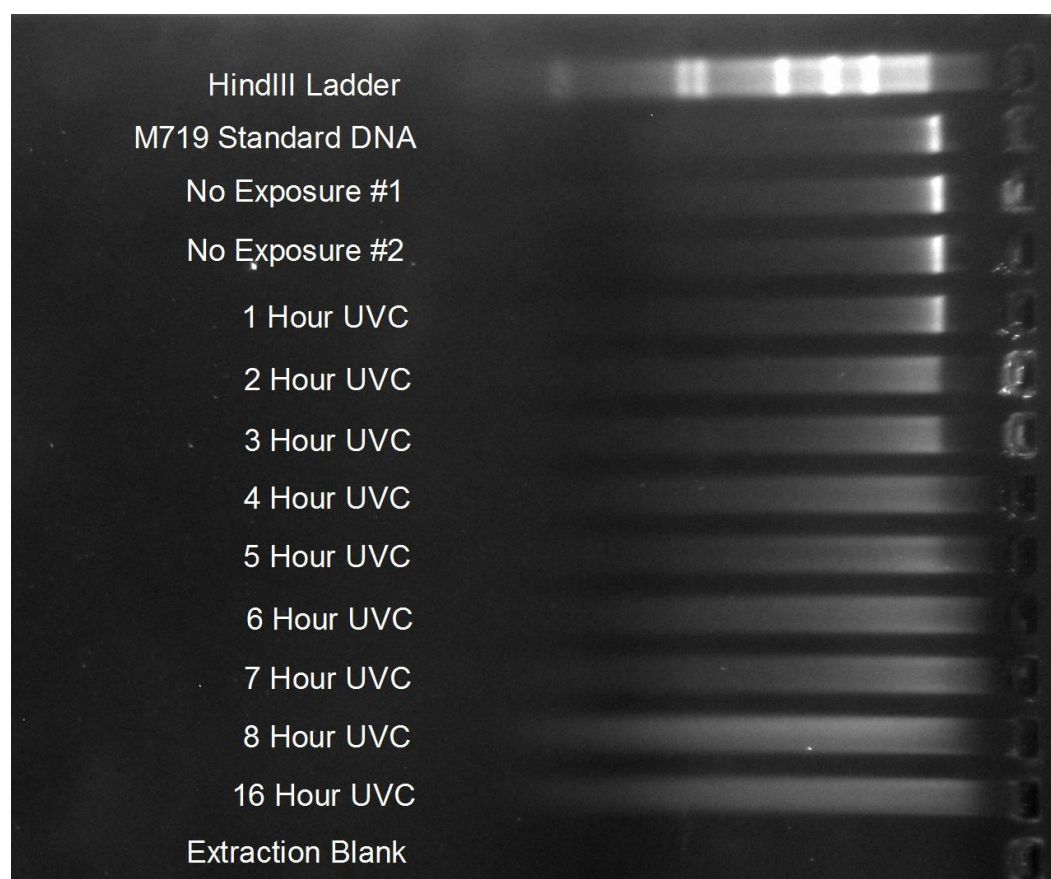
Figure 29. Gel Electrophoresis of Enzymatic Digestions

Native gel electrophoresis was used to confirm the enzymatic digestions for all samples. These images are from Individual #4 and are representative of the results for all five individuals. A λ DNA-HindIII Digest and 100 BP ladder was also run for size comparison purposes. The gel to analyze the MNase digestion (A) was prepared with 1X TBE, EtBr, and agarose and was run for 50V at 3 hours. The gel to analyze the DNase digestion (B) was prepared with 1X TAE, EtBr, and agarose at was run at 100V for 1 hour.

A)

B)
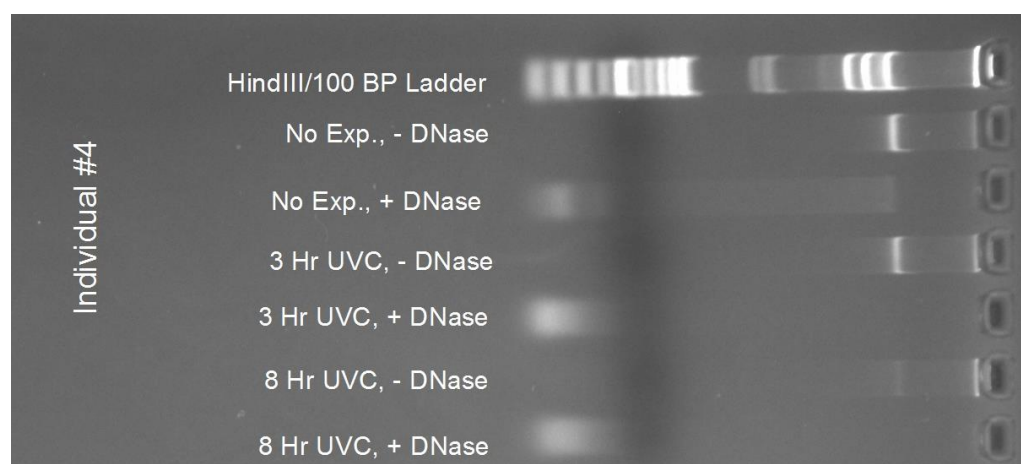
Figure 30. Temperature Gradient for Primer Optimization

The primers to analyze all loci were optimized using a temperature gradient and traditional PCR. After amplification, 5 µl of the PCR product combined with 1 µl of 6X loading dye was analyzed on a native agarose gel. The gel was run at 100 V for 60 minutes. The size of the desired amplicon is around 100 bp. In the first lane, a 100 bp ladder was run alongside the samples to determine sizing. The numbers below the lanes indicate the annealing temperature in degrees Celsius used from the temperature gradient PCR. This analysis indicated non-specific binding at lower temperatures by the presence of multiple bands. This specific gel was from a primer re-design for primer set D8_9 and illustrates the failure of D8_9Y and the success of D8_9Z by the presence of single band and PCR product at an annealing temperature of 60 °C.
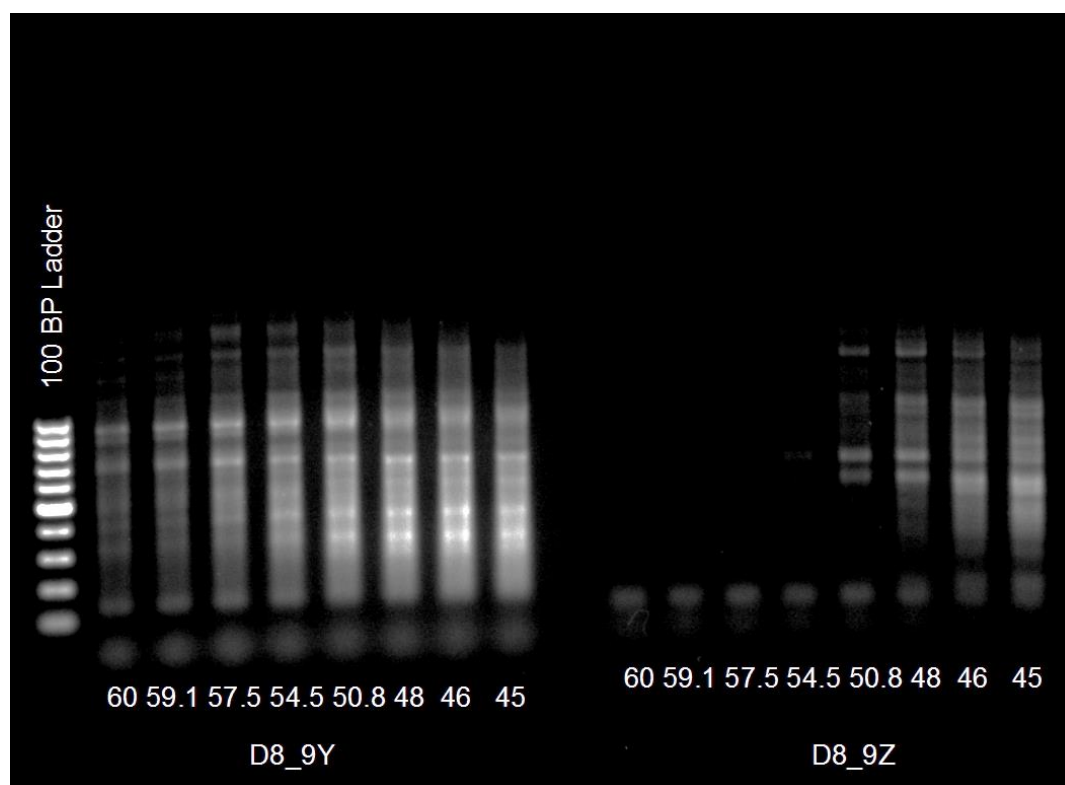
Figure 31. Human Loci qPCR Plots from CFX Software.

 A representation of the plots obtained from the CFX software. This is from amplification with primer set D21_10. These plots are generated from the RFU detected after each PCR cycle (A), then using the standards to generate a standard curve of Cq versus the log of the starting quantity (B) and the unknown samples are plotted on the curve as x's. Lastly, a melt curve is generated by heating the samples from 65 to 95 °C and ensuring a single product is obtained by the presence of a single peak (C).

A)
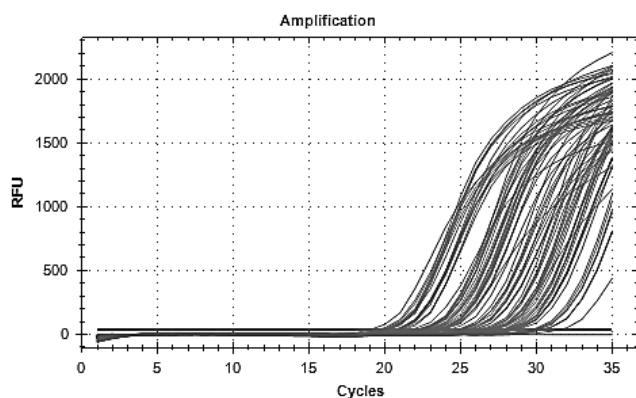
B)
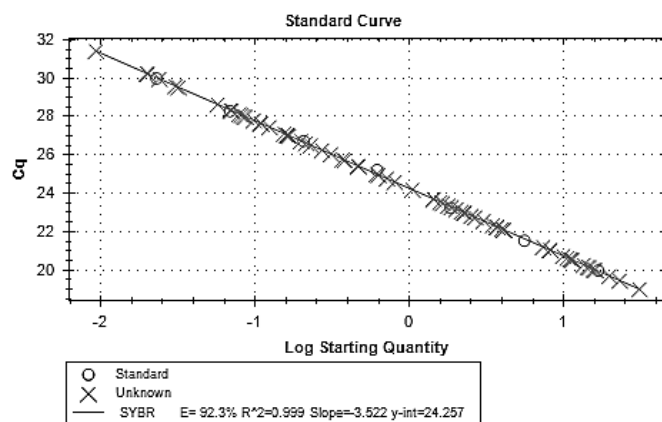
C)
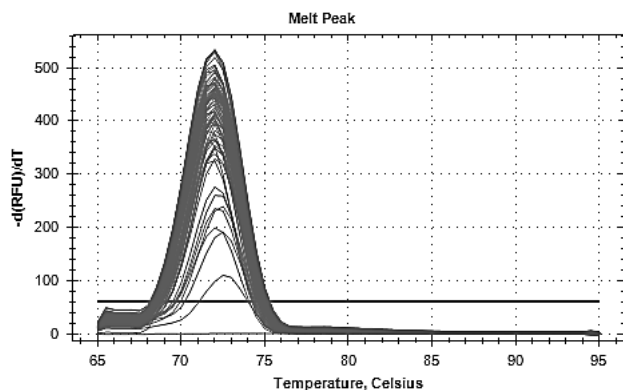
Figure 32. STR Profiles of 0, 3, and 8 hour UVC Exposure.

Electropherograms were generated by the GeneMapper software from analysis of samples on the 3130 Genetic Analyzer (Applied Biosystems). The PowerPlex 16 loci (Promega) were amplified as discussed in Chapter 3, from 1 ng of DNA from the same donor (Individual #3) and show the effect of 0, 3, and 8 hours of UVC exposure on STR profiling. The y axis (RFU) is the same for all three images, 0-4,500 RFU. STRs in brackets ( ), indicate a site of allele drop out. Alleles were called based on a threshold of 150 RFU.

No Exposure:
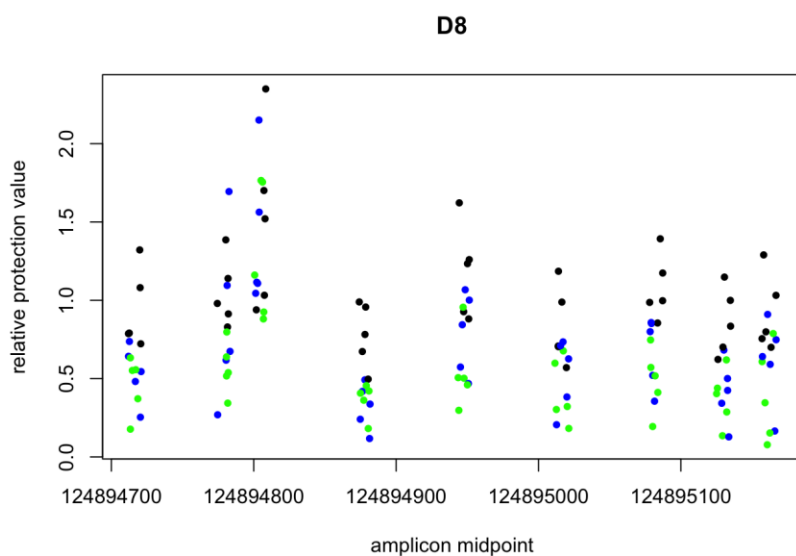
3 Hour UVC:

8 Hour UVC:

Figure 33. Relative Protection Plots of D8S1179 (MNase Digestion).

The relative protection value was calculated by dividing the digested value by the no digest value for each amplicon. These values were mapped along the chromosomal location, on chromosome 8, in Ensembl (137). This shows the five individuals (1-5, top to bottom in each panel) and different UVC exposures- 0, 3, and 8 hours.

No Exposure:

3 Hour UVC:

8 Hour UVC:

Figure 34. Analysis of Variance at D8S1179 (MNase Digestion).

Visualization of relative protection values at all amplicons analyzed at D8S1179. All five biological replicates are mapped for each exposure. The control, 0 hour exposure sample, is colored black, the 3 hour exposure is blue, and 8 hour exposure is green. Amplicons were plotted as bars (A) and a scatter plot as dots at the center of the amplicon (B).
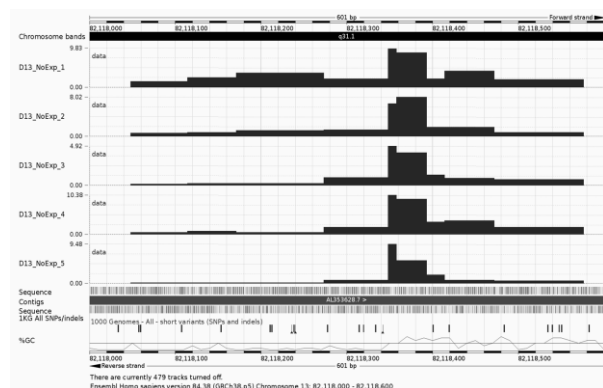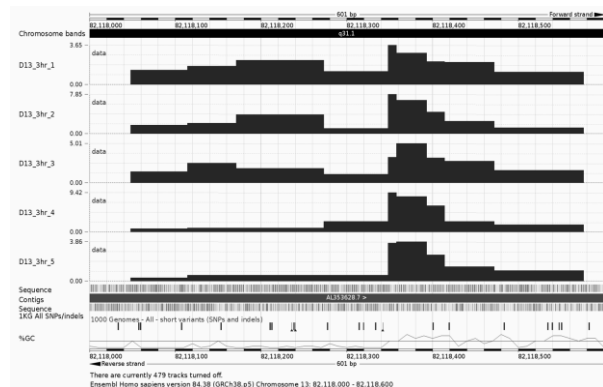
A)
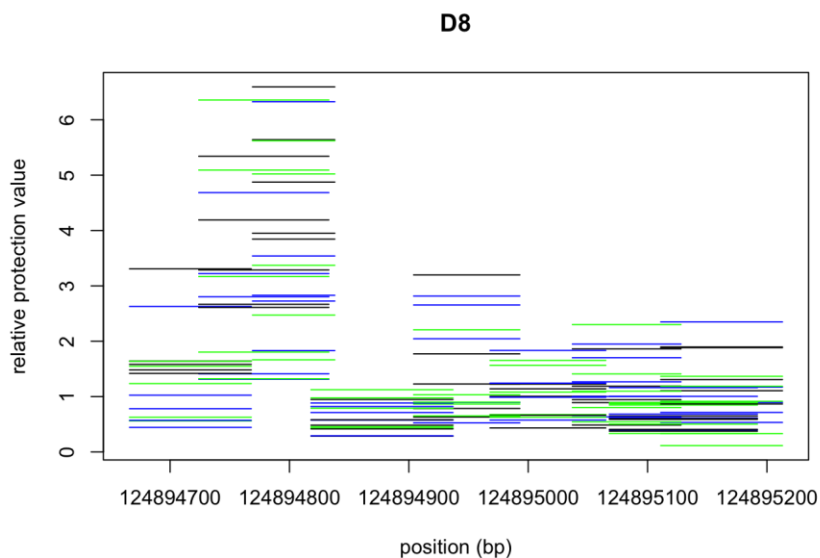
B)
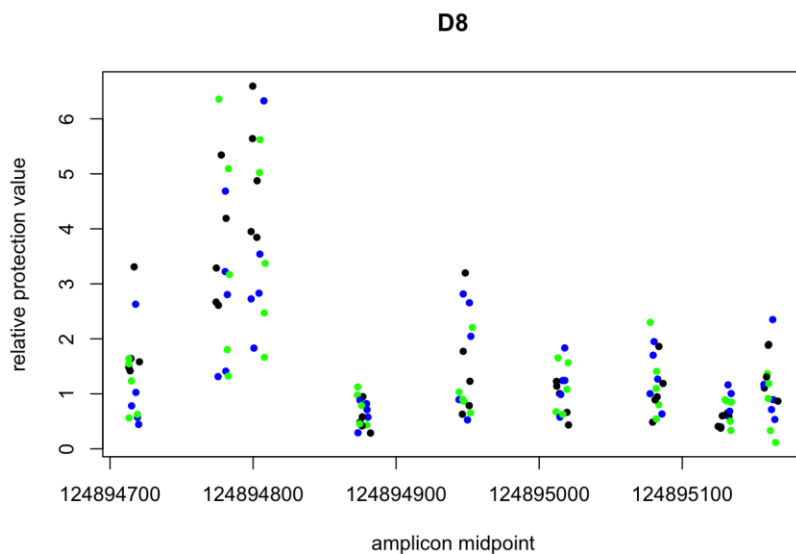
Figure 35. Relative Protection Plots of D8S1179 (DNase Digestion).

The relative protection value was calculated by dividing the digested value by the no digest value for each amplicon. These values were mapped along the chromosomal location, along chromosome 8, in Ensembl (137). This shows the five individuals (1-5, top to bottom in each panel) and different UVC exposures- 0, 3, and 8 hours.
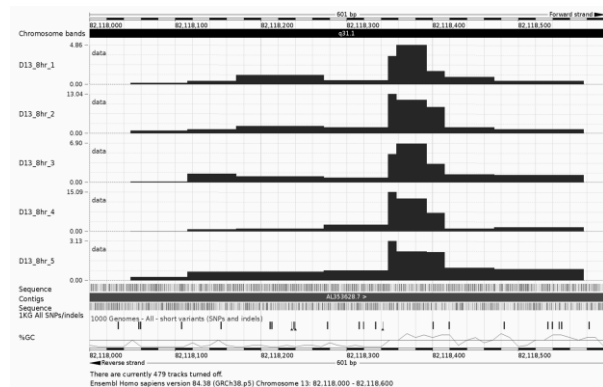
No Exposure:
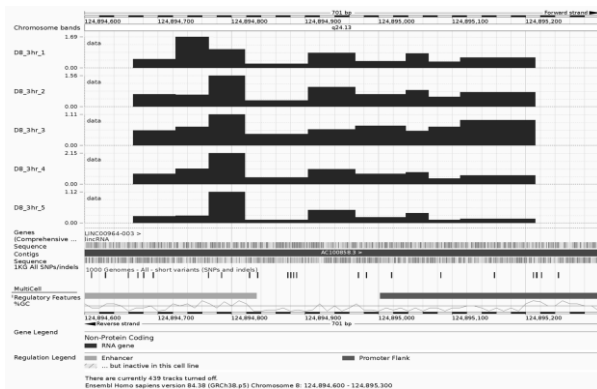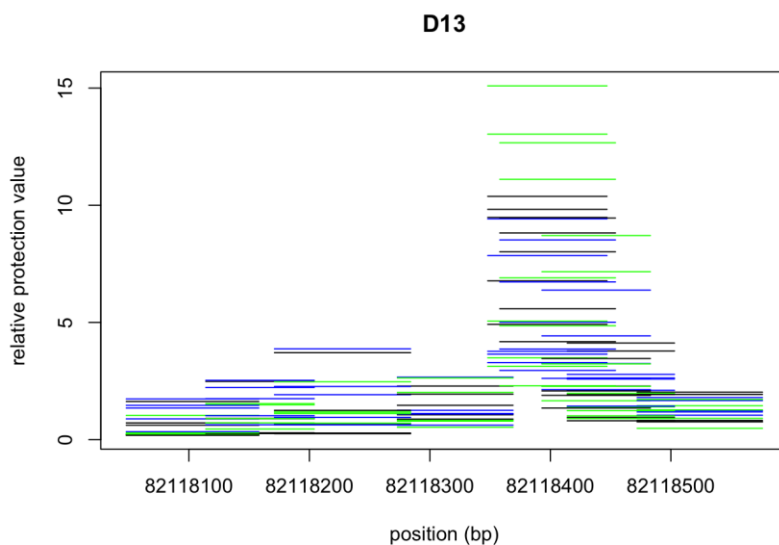

3 Hour UVC:

8 Hour UVC:
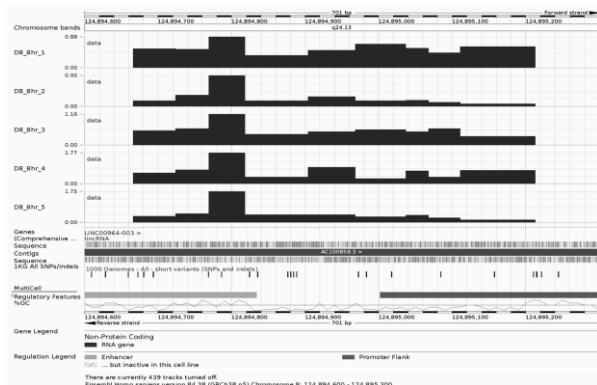
Figure 36. Analysis of Variance at D8S1179 (DNase Digestion).

Visualization of relative protection values at all amplicons analyzed at D8S1179. All five
biological replicates are mapped for each exposure. The control, 0 hour exposure sample,
is colored black, the 3 hour exposure is blue, and 8 hour exposure is green. Amplicons
were plotted as bars (A) and a scatter plot as dots at the center of the amplicon (B).
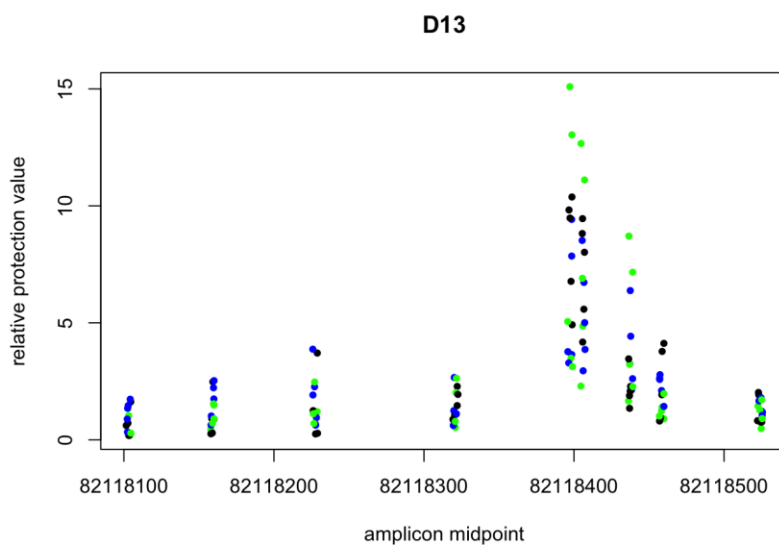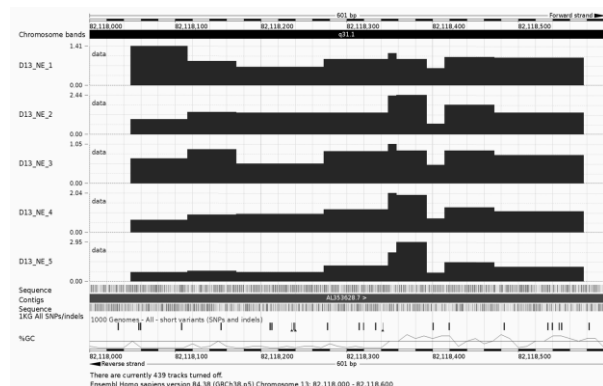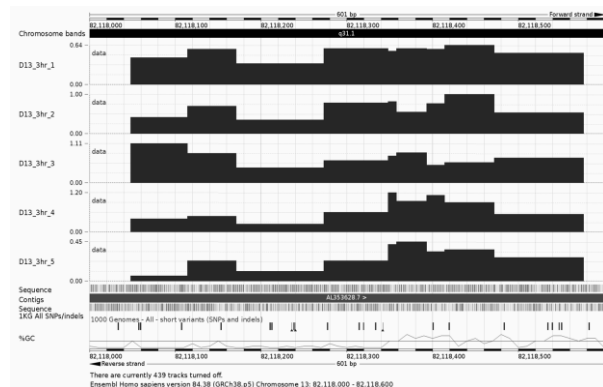
A)
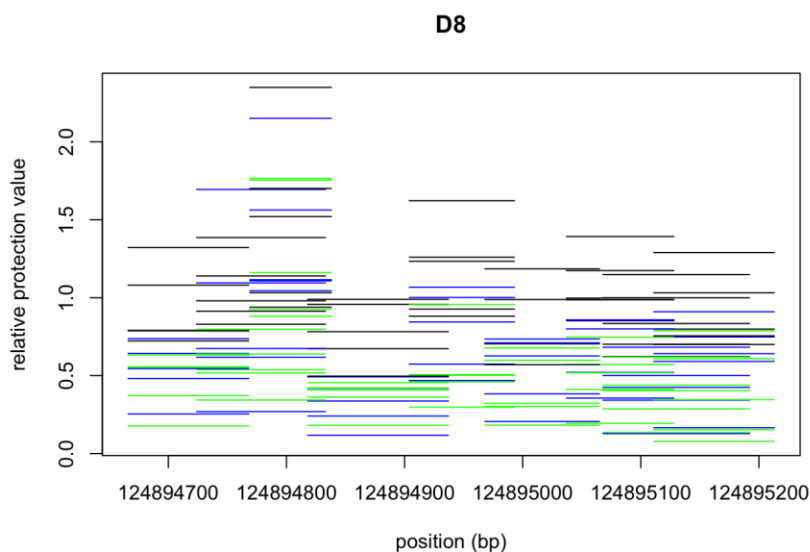
B)

Figure 37. Relative Protection Plots of D13S317 (MNase Digestion).

The relative protection value was calculated by dividing the digested value by the no digest value for each amplicon. These values were then mapped along the chromosomal location on chromosome 13 in Ensembl (137). This shows the five individuals (1-5, top to bottom in each panel) and different UVC exposures- 0, 3, and 8 hours.

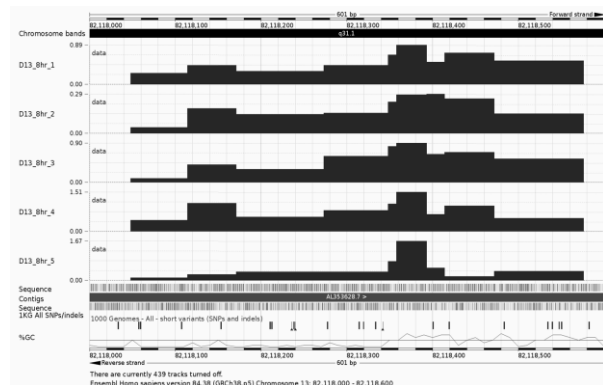No Exposure:

3 Hour UVC:

8 Hour UVC:

Figure 38. Analysis of Variance at D13S317 (MNase Digestion).

Visualization of relative protection values at all amplicons analyzed at D13S317. All five biological replicates are mapped for each exposure. The control, 0 hour exposure sample, is colored black, the 3 hour exposure is blue, and 8 hour exposure is green. Amplicons were plotted as bars (A) and a scatter plot as dots at the center of the amplicon (B).

A)

B)

Figure 39. Relative Protection Plots of D13S317 (DNase Digestion).

The relative protection value was calculated by dividing the digested value by the no digest value for each amplicon. These values were then mapped along the chromosomal location on chromosome 13 in Ensembl (137). This shows the five individuals (1-5, top to bottom in each panel) and different UVC exposures- 0, 3, and 8 hours.
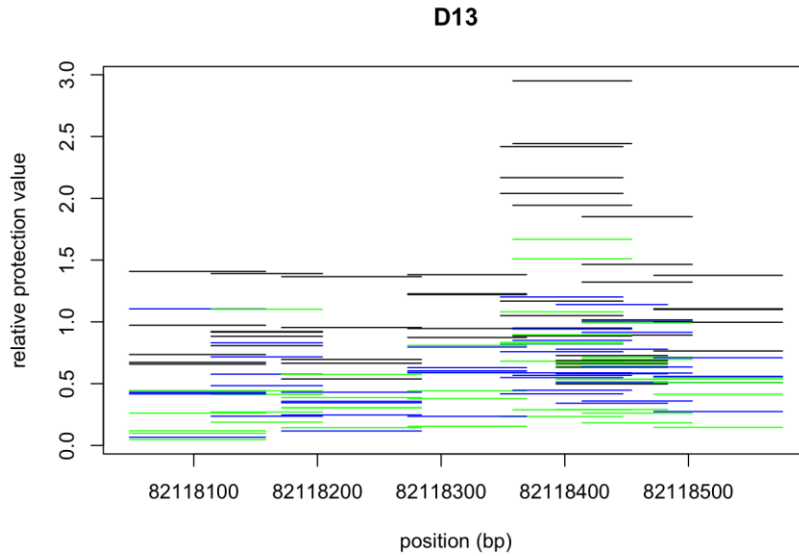
No Exposure:

3 Hour UVC:

8 Hour UVC:

Figure 40. Analysis of Variance at D13S317 (DNase Digestion).

Visualization of relative protection values at all amplicons analyzed at D13S317. All five biological replicates are mapped for each exposure. The control, 0 hour exposure sample, is colored black, the 3 hour exposure is blue, and 8 hour exposure is green. Amplicons were plotted as bars (A) and a scatter plot as dots at the center of the amplicon (B).
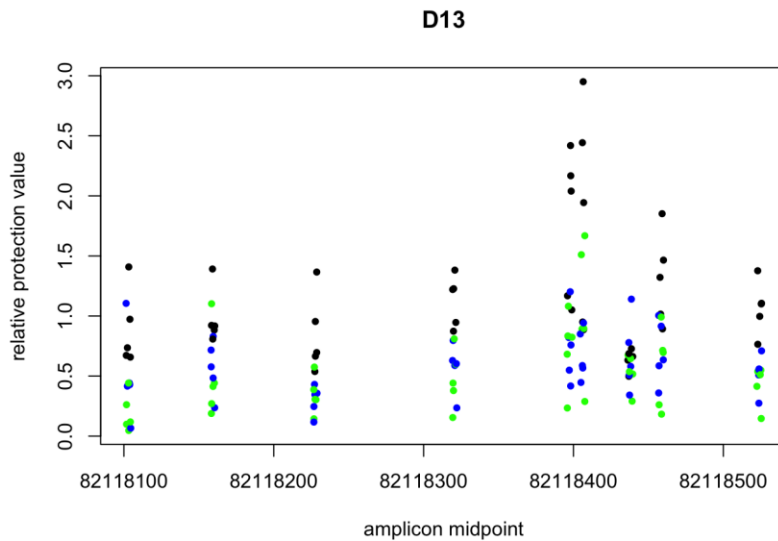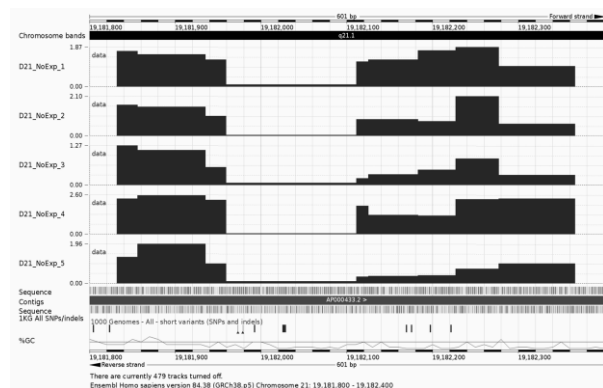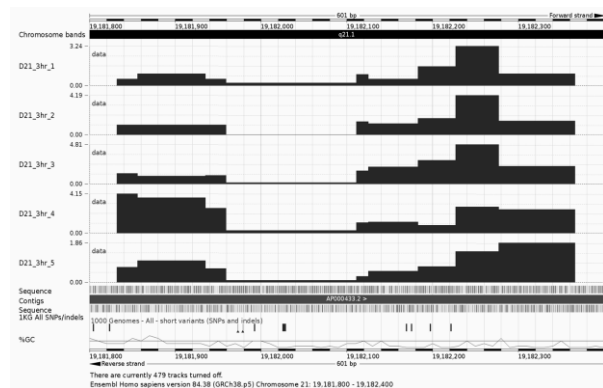
A)

B)

Figure 41. Relative Protection Plots of D21S11 (MNase Digestion).

The relative protection value was calculated by dividing the digested value by the no digest value for each amplicon. These values were then mapped along the chromosomal location on chromosome 21 in Ensembl (137). This shows the five individuals (1-5, top to bottom in each panel) and different UVC exposures- 0, 3, and 8 hours.

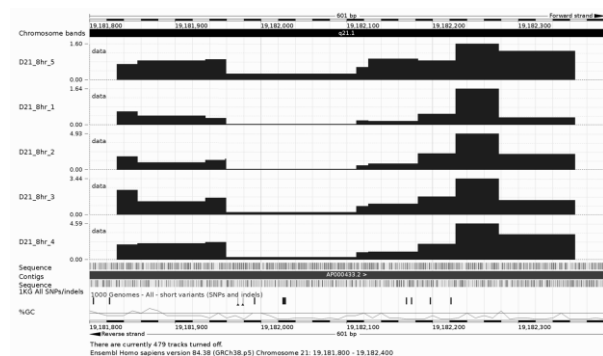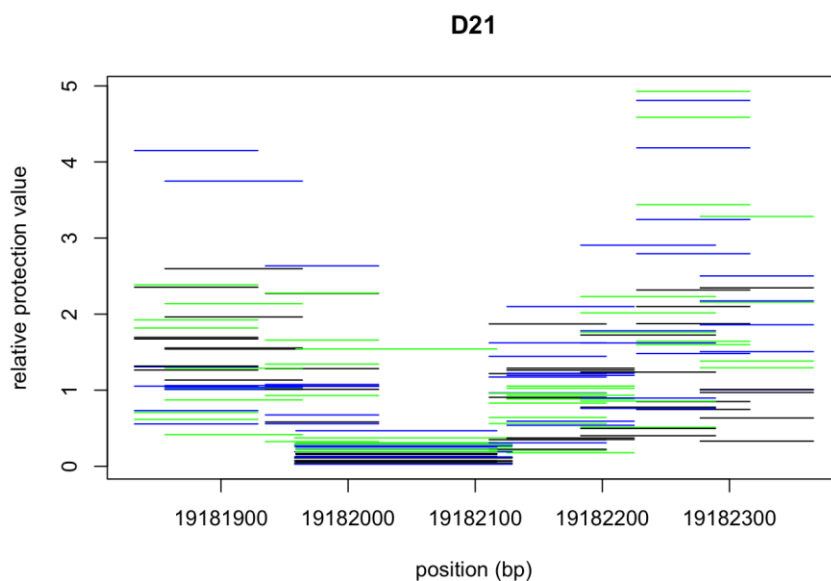No Exposure:

3 Hour UVC:

8 Hour UVC:

Figure 42. Analysis of Variance at D21S11 (MNase Digestion).

Visualization of relative protection values at all amplicons analyzed at D21S11. All five
biological replicates are mapped for each exposure. The control, 0 hour exposure sample,
is colored black, the 3 hour exposure is blue, and 8 hour exposure is green. Amplicons
were plotted as bars (A) and a scatter plot as dots at the center of the amplicon (B).

A)

B)
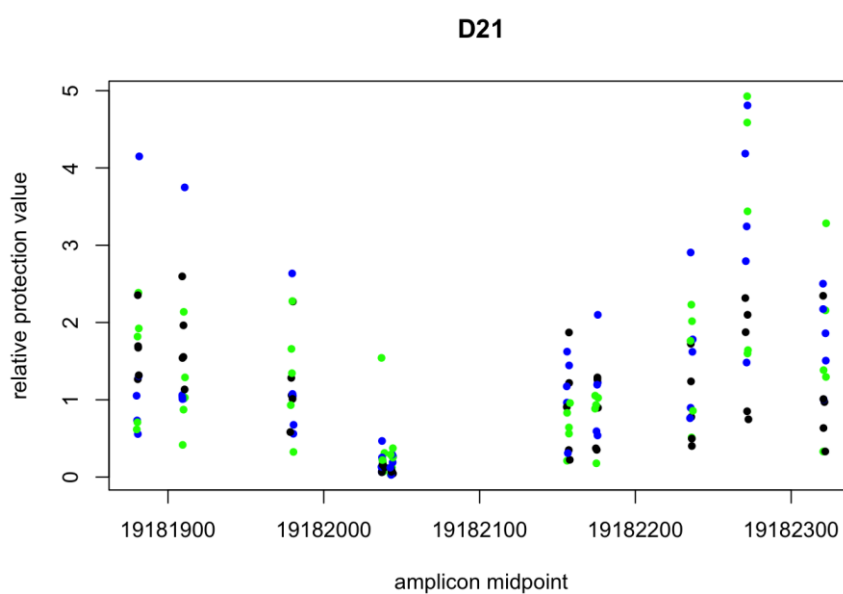
Figure 43. Relative Protection Plots of D21S11 (DNase Digestion).

The relative protection value was calculated by dividing the digested value by the no digest value for each amplicon. These values were then mapped along the chromosomal location on chromosome 21 in Ensembl (137). This shows the five individuals (1-5, top to bottom in each panel) and different UVC exposures- 0, 3, and 8 hours.

No Exposure:

3 Hour UVC:

8 Hour UVC:

Figure 44. Analysis of Variance at D21S11 (DNase Digestion).

Visualization of relative protection values at all amplicons analyzed at D21S11. All five biological replicates are mapped for each exposure. The control, 0 hour exposure sample, is colored black, the 3 hour exposure is blue, and 8 hour exposure is green. Amplicons were plotted as bars (A) and a scatter plot as dots at the center of the amplicon (B).
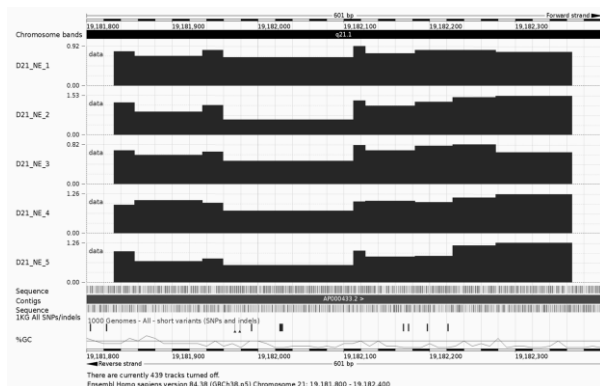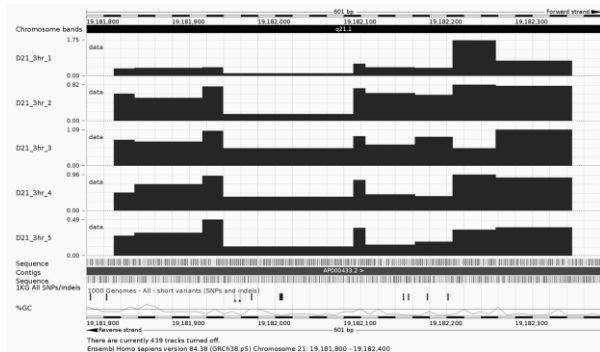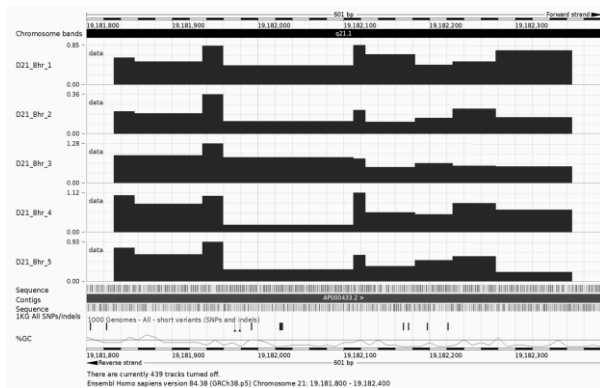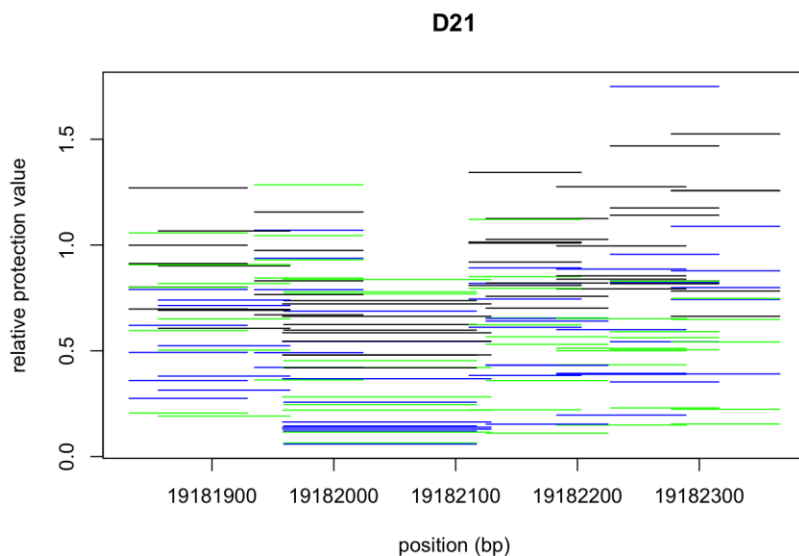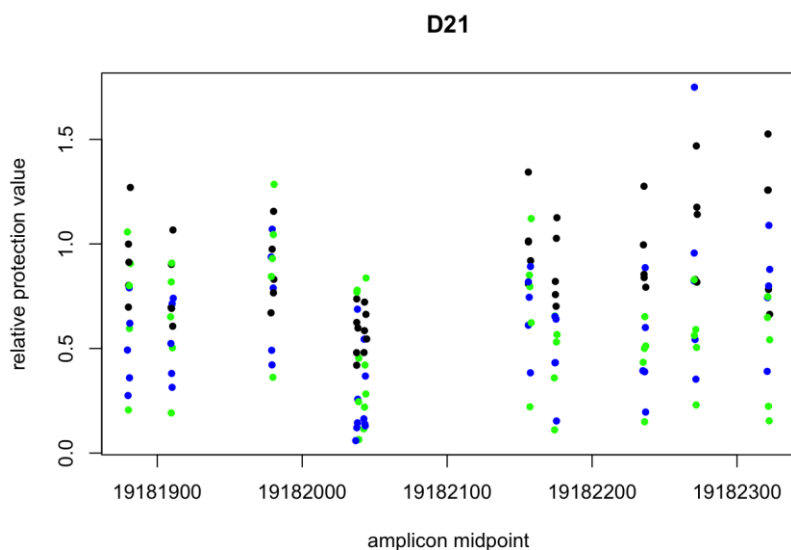
A)

B)

LITERATURE CITED

1. Dong C, *et al.* (2015) Evaluation of the protective capabilities of nucleosome STRs obtained by large-scale sequencing. *Electrophoresis*.

2. Sinden RR (1994) *DNA structure and function* (Academic Press, San Diego) pp xxiii, 398 p.

3. Li G & Reinberg D (2011) Chromatin higher-order structures and gene regulation. *Current Opinion in Genetics & Development* 21(2):175-186.

4. Elmroth K & Stenerlow B (2007) Influence of Chromatin Structure on Induction of Double-Strand Breaks in Mammalian Cells Irradiated with DNA-Incorporated 125I. *Radiation Research* 168(2):175-182.

5. Donohue J & Trueblood KN (1960) Base pairing in DNA. *Journal of Molecular Biology* 2(6):363-371.

6. Butzow JJ & Eichhorn GL (1975) Different susceptibility of DNA and RNA to cleavage by metal ions.

7. Nelson DL, Nelson DL, Lehninger AL, & Cox MM (2008) *Lehninger principles of biochemistry* (W.H. Freeman, New York).

8. Watson JD & Crick FH (1953) Molecular structure of nucleic acids. *Nature* 171(4356):737-738.

9. Packer MJ & Hunter CA (1998) Sequence-dependent DNA structure: the role of the sugar-phosphate backbone 1. *Journal of Molecular Biology* 280(3):407-420.

10. Herbert A & Rich A (1996) The biology of left-handed Z-DNA. *J Biol Chem* 271(20):11595-11598.

11. Kornberg RD (1974) Chromatin structure: a repeating unit of histones and DNA. *Science* 184(4139):868-871.

12. Bradbury EM (1989) K. E. Van Holde. Chromatin. Series in molecular biology. Springer-Verlag, New York. 1988. 530 pp. $98.00. *Journal of Molecular Recognition* 2(3):i-i.

13. Alva V, Ammelburg M, Söding J, & Lupas AN (2007) On the origin of the histone fold. *BMC Structural Biology* 7:17-17.

14. Mersfelder EL & Parthun MR (2006) The tale beyond the tail: histone core domain modifications and the regulation of chromatin structure. *Nucleic Acids Research* 34(9):2653-2662.

15. Mariño-Ramírez L, Kann MG, Shoemaker BA, & Landsman D (2005) Histone structure and nucleosome stability. *Expert review of proteomics* 2(5):719-729.

16. Wal M & Pugh BF (2012) Genome-wide mapping of nucleosome positions in yeast using high-resolution MNase ChIP-Seq. *Methods Enzymol* 513:233-250.

17. Thomas JO (1999) Histone H1: location and role. *Current opinion in cell biology* 11(3):312-317.

18. Wang JP*, et al.* (2008) Preferentially quantized linker DNA lengths in Saccharomyces cerevisiae. *PLoS Comput Biol* 4(9):e1000175.

19. Kornberg RD & Lorch Y (1999) Twenty-Five Years of the Nucleosome, Fundamental Particle of the Eukaryote Chromosome. *Cell* 98(3):285-294.

20. Lowary P & Widom J (1998) New DNA sequence rules for high affinity binding to histone octamer and sequence-directed nucleosome positioning. *Journal of molecular biology* 276(1):19-42.

21. Segal E & Widom J (2009) What controls nucleosome positions? *Trends Genet* 25(8):335-343.

22. Thåström A, Bingham L, & Widom J (2004) Nucleosomal locations of dominant DNA sequence motifs for histone–DNA interactions and nucleosome positioning. *Journal of molecular biology* 338(4):695-709.

23. Widom J (2001) Role of DNA sequence in nucleosome stability and dynamics. *Quarterly reviews of biophysics* 34(03):269-324.

24. Travers AA (2004) The structural basis of DNA flexibility. *Philos Trans A Math Phys Eng Sci* 362(1820):1423-1438.

25. Field Y*, et al.* (2008) Distinct modes of regulation by chromatin encoded through nucleosome positioning signals. *PLoS Comput Biol* 4(11):e1000216.

26. Mavrich TN*, et al.* (2008) A barrier nucleosome model for statistical positioning of nucleosomes throughout the yeast genome. *Genome research* 18(7):1073-1083.

27. Segal E & Widom J (2009) Poly (dA: dT) tracts: major determinants of nucleosome organization. *Current opinion in structural biology* 19(1):65-71.

28. Bird AP (1985) CpG-rich islands and the function of DNA methylation. *Nature* 321(6067):209-213.

29. Nathan D & Crothers DM (2002) Bending and flexibility of methylated and unmethylated EcoRI DNA. *Journal of molecular biology* 316(1):7-17.

30. Ausió J, Abbott DW, Wang X, & Moore SC (2001) Histone variants and histone modifications: a structural perspective. *Biochemistry and cell biology* 79(6):693-708.

31. Guillemette B*, et al.* (2005) Variant histone H2A. Z is globally localized to the promoters of inactive yeast genes and regulates nucleosome positioning. *PLoS Biol* 3(12):e384.

32. Ausió J (2006) Histone variants—the structure behind the function. *Briefings in Functional Genomics & Proteomics* 5(3):228-243.

33. Rogakou EP, Pilch DR, Orr AH, Ivanova VS, & Bonner WM (1998) DNA double-stranded breaks induce histone H2AX phosphorylation on serine 139. *J Biol Chem* 273(10):5858-5868.

34. Fan JY, Gordon F, Luger K, Hansen JC, & Tremethick DJ (2002) The essential histone variant H2A. Z regulates the equilibrium between different chromatin conformational states. *Nature Structural & Molecular Biology* 9(3):172-176.

35. Wolffe AP (1994) Nucleosome positioning and modification: chromatin structures that potentiate transcription. *Trends in biochemical sciences* 19(6):240-244.

36. Vidali G, Gershey EL, & Allfrey VG (1968) Chemical studies of histone acetylation. The distribution of epsilon-N-acetyllysine in calf thymus histones. *J Biol Chem* 243(24):6361-6366.

37. Rossetto D, Avvakumov N, & Côté J (2012) Histone phosphorylation: A chromatin modification involved in diverse nuclear events. *Epigenetics* 7(10):1098-1108.

38. Yun M, Wu J, Workman JL, & Li B (2011) Readers of histone modifications. *Cell Research* 21(4):564-578.

39. Polach K & Widom J (1995) Mechanism of protein access to specific DNA sequences in chromatin: a dynamic equilibrium model for gene regulation. *Journal of molecular biology* 254(2):130-149.

40. Lee C-K, Shibata Y, Rao B, Strahl BD, & Lieb JD (2004) Evidence for nucleosome depletion at active regulatory regions genome-wide. *Nature genetics* 36(8):900-905.

41. Tang L, Nogales E, & Ciferri C (2010) Structure and Function of SWI/SNF Chromatin Remodeling Complexes and Mechanistic Implications for Transcription. *Progress in biophysics and molecular biology* 102(2-3):122-128.

42. Narlikar GJ, Fan H-Y, & Kingston RE (2002) Cooperation between Complexes that Regulate Chromatin Structure and Transcription. *Cell* 108(4):475-487.

43. Engeholm M, *et al.* (2009) Nucleosomes can invade DNA territories occupied by their neighbors. *Nature structural & molecular biology* 16(2):151-158.

44. Cui Y & Bustamante C (2000) Pulling a single chromatin fiber reveals the forces that maintain its higher-order structure. *Proceedings of the National Academy of Sciences* 97(1):127-132.

45. Hoek M & Stillman B (2003) Chromatin assembly factor 1 is essential and couples chromatin assembly to DNA replication in vivo. *Proceedings of the National Academy of Sciences* 100(21):12183-12188.

46. Pazin MJ, Bhargava P, Geiduschek EP, & Kadonaga JT (1997) Nucleosome mobility and the maintenance of nucleosome positioning. *Science* 276(5313):809-812.

47. Roth SY, Shimizu M, Johnson L, Grunstein M, & Simpson RT (1992) Stable nucleosome positioning and complete repression by the yeast alpha 2 repressor are disrupted by amino-terminal mutations in histone H4. *Genes & Development* 6(3):411-425.

48. Cairns BR (2009) The logic of chromatin architecture and remodelling at promoters. *Nature* 461(7261):193-198.

49. Brogaard KR, Xi L, Wang JP, & Widom J (2012) A chemical approach to mapping nucleosomes at base pair resolution in yeast. *Methods Enzymol* 513:315-334.

50. Pusarla R-H & Bhargava P (2005) Histones in functional diversification. *FEBS Journal* 272(20):5149-5168.

51. Fickett JW & Hatzigeorgiou AG (1997) Eukaryotic promoter recognition. *Genome research* 7(9):861-878.

52. Zlatanova J, Seebart C, & Tomschik M (2008) The linker-protein network: control of nucleosomal DNA accessibility. *Trends in Biochemical Sciences* 33(6):247-253.

53. Dixon LA*, et al.* (2006) Analysis of artificially degraded DNA using STRs and SNPs--results of a collaborative European (EDNAP) exercise. *Forensic Sci Int* 164(1):33-44.

54. Takata H*, et al.* (2013) Chromatin compaction protects genomic DNA from radiation damage. *PLoS One* 8(10):e75622.

55. Ljungman M, Nyberg S, Nygren J, Eriksson M, & Ahnstrom G (1991) DNA-bound proteins contribute much more than soluble intracellular compounds to the intrinsic protection against radiation-induced DNA strand breaks in human cells. *Radiat Res* 127(2):171-176.

56. Bednar J*, et al.* (1998) Nucleosomes, linker DNA, and linker histone form a unique structural motif that directs the higher-order folding and compaction of chromatin. *Proceedings of the National Academy of Sciences* 95(24):14173-14178.

57. Ren B*, et al.* (2000) Genome-wide location and function of DNA binding proteins. *Science* 290(5500):2306-2309.

58. Sarai A & Kono H (2005) Protein-DNA recognition patterns and predictions. *Annu. Rev. Biophys. Biomol. Struct.* 34:379-398.

59. Lee TI & Young RA (2000) Transcription of eukaryotic protein-coding genes. *Annual review of genetics* 34(1):77-137.

60. Thomas JO (2001) HMG1 and 2: architectural DNA-binding proteins. *Biochem Soc Trans* 29(Pt 4):395-401.

61. Alaeddini R, Walsh SJ, & Abbas A (2010) Forensic implications of genetic analyses from degraded DNA—A review. *Forensic Science International: Genetics* 4(3):148-157.

62. De Bont R & van Larebeke N (2004) Endogenous DNA damage in humans: a review of quantitative data. *Mutagenesis* 19(3):169-185.

63. Ward JF (1988) DNA Damage Produced by Ionizing Radiation in Mammalian Cells: Identities, Mechanisms of Formation, and Reparability. *Progress in Nucleic Acid Research and Molecular Biology*, eds Waldo EC & Kivie M (Academic Press), Vol Volume 35, pp 95-125.

64. Ciccia A & Elledge SJ (2010) The DNA Damage Response: Making It Safe to Play with Knives. *Molecular Cell* 40(2):179-204.

65. Sutherland BM, Bennett PV, Sidorkina O, & Laval J (2000) Clustered DNA damages induced in isolated DNA and in human cells by low doses of ionizing radiation. *Proc Natl Acad Sci U S A* 97(1):103-108.

66. Ambers A, Turnbough M, Benjamin R, King J, & Budowle B (2014) Assessment of the role of DNA repair in damaged forensic samples. *Int J Legal Med* 128(6):913-921.

67. Gates KS (2009) An overview of chemical processes that damage cellular DNA: spontaneous hydrolysis, alkylation, and reactions with radicals. *Chemical research in toxicology* 22(11):1747-1760.

68. Lindahl T & Nyberg B (1972) Rate of depurination of native deoxyribonucleic acid. *Biochemistry* 11(19):3610-3618.

69. Kim YJ & Wilson DM, 3rd (2012) Overview of base excision repair biochemistry. *Curr Mol Pharmacol* 5(1):3-13.

70. Douki T & Cadet J (1999) Modification of DNA bases by photosensitized one-electron oxidation. *Int J Radiat Biol* 75(5):571-581.

71. Lindahl T (1993) Instability and decay of the primary structure of DNA. *Nature* 362(6422):709-715.

72. Friedl AA, Kiechle M, Fellerhoff B, & Eckardt-Schupp F (1998) Radiation-induced chromosome aberrations in Saccharomyces cerevisiae: influence of DNA repair pathways. *Genetics* 148(3):975-988.

73. Yoon JH, Lee CS, O'Connor TR, Yasui A, & Pfeifer GP (2000) The DNA damage spectrum produced by simulated sunlight. *J Mol Biol* 299(3):681-693.

74. Sinha RP & Hader DP (2002) UV-induced DNA damage and repair: a review. *Photochem Photobiol Sci* 1(4):225-236.

75. Hall A & Ballantyne J (2004) Characterization of UVC-induced DNA damage in bloodstains: forensic implications. *Anal Bioanal Chem* 380(1):72-83.

76. Chandrasekhar D & Van Houten B (2000) In vivo formation and repair of cyclobutane pyrimidine dimers and 6-4 photoproducts measured at the gene and nucleotide level in Escherichia coli. *Mutat Res* 450(1-2):19-40.

77. Hall A, Sims LM, & Ballantyne J (2014) Assessment of DNA damage induced by terrestrial UV irradiation of dried bloodstains: Forensic implications. *Forensic Science International: Genetics* 8(1):24-32.

78. Cadet J & Douki T (2011) Oxidatively generated damage to DNA by UVA radiation in cells and human skin. *J Invest Dermatol* 131(5):1005-1007.

79. Cadet J, Sage E, & Douki T (2005) Ultraviolet radiation-mediated damage to cellular DNA. *Mutat Res* 571(1-2):3-17.

80. Courdavault S, *et al.* (2005) Repair of the three main types of bipyrimidine DNA photoproducts in human keratinocytes exposed to UVB and UVA radiations. *DNA Repair (Amst)* 4(7):836-844.

81. Wehner J & Horneck G (1995) Effects of vacuum UV and UVC radiation on dry Escherichia coli plasmid pUC19. II. Mutational specificity at the lacZ gene. *J Photochem Photobiol B* 30(2-3):171-177.

82. Moscariello M & Sutherland B (2010) Saccharomyces cerevisiae-based system for studying clustered DNA damages. *Radiat Environ Biophys* 49(3):447-456.

83. Crosetto N, *et al.* (2013) Nucleotide-resolution DNA double-strand break mapping by next-generation sequencing. *Nat Methods* 10(4):361-365.

84. Lander ES, *et al.* (2001) Initial sequencing and analysis of the human genome. *Nature* 409(6822):860-921.

85. Lindahl T & Wood RD (1999) Quality control by DNA repair. *Science* 286(5446):1897-1905.

86. Fortini P & Dogliotti E (2007) Base damage and single-strand break repair: mechanisms and functional significance of short- and long-patch repair subpathways. *DNA Repair (Amst)* 6(4):398-409.

87. Petruseva IO, Evdokimov AN, & Lavrik OI (2014) Molecular Mechanism of Global Genome Nucleotide Excision Repair. *Acta Naturae* 6(1):23-34.

88. Soltys DT, Pereira CPM, Ishibe GN, & de Souza-Pinto NC (Effects of post mortem interval and gender in DNA base excision repair activities in rat brains. *Mutation Research/Fundamental and Molecular Mechanisms of Mutagenesis* (0).

89. Fousteri M & Mullenders LH (2008) Transcription-coupled nucleotide excision repair in mammalian cells: molecular mechanisms and biological effects. *Cell Res* 18(1):73-84.

90. Friedberg EC WG, Siede W (1995) *DNA Repair and Mutagenesis* (ASM Press, Washington D.C.).

91. Engel SR, *et al.* (2014) The reference genome sequence of Saccharomyces cerevisiae: then and now. *G3 (Bethesda)* 4(3):389-398.

92. Lindegren CC & Lindegren G (1949) Unusual Gene-Controlled Combinations of Carbohydrate Fermentations in Yeast Hybrids. *Proceedings of the National Academy of Sciences of the United States of America* 35(1):23-27.

93. Goffeau A, *et al.* (1996) Life with 6000 genes. *Science* 274(5287):546, 563-547.

94. Mortimer RK & Johnston JR (1986) Genealogy of principal strains of the yeast genetic stock center. *Genetics* 113(1):35-43.

95. Botstein D, Chervitz SA, & Cherry JM (1997) Yeast as a Model Organism. *Science (New York, N.Y.)* 277(5330):1259-1260.

96. Botstein D & Fink GR (1988) Yeast: an experimental organism for modern biology. *Science* 240(4858):1439-1443.

97. Lehle L, Strahl S, & Tanner W (2006) Protein glycosylation, conserved from yeast to man: a model organism helps elucidate congenital human diseases. *Angewandte Chemie International Edition* 45(41):6802-6818.

98. Venter JC, *et al.* (2001) The sequence of the human genome. *Science* 291(5507):1304-1351.

99. Consortium EP (2012) An integrated encyclopedia of DNA elements in the human genome. *Nature* 489(7414):57-74.

100. Birney E, *et al.* (2007) Identification and analysis of functional elements in 1% of the human genome by the ENCODE pilot project. *Nature* 447(7146):799-816.

101. Jobling MA & Gill P (2004) Encoded evidence: DNA in forensic analysis. *Nature Reviews Genetics* 5(10):739-751.

102. Jeffreys AJ, Wilson V, & Thein SL (1985) Hypervariable 'minisatellite' regions in human DNA. *Nature* 314(6006):67-73.

103. Roewer L (2013) DNA fingerprinting in forensics: past, present, future. *Investigative Genetics* 4:22-22.

104. Koreth J, O'Leary JJ, & J ODM (1996) Microsatellites and PCR genomic analysis. *J Pathol* 178(3):239-248.

105. Vinogradov AE (2005) Noncoding DNA, isochores and gene expression: nucleosome formation potential. *Nucleic Acids Research* 33(2):559-563.

106. Plohl M, Luchetti A, Meštrović N, & Mantovani B (2008) Satellite DNAs between selfishness and functionality: Structure, genomics and evolution of tandem repeats in centromeric (hetero)chromatin. *Gene* 409(1–2):72-82.

107. Butler JM (2006) Genetics and genomics of core short tandem repeat loci used in human identity testing. *Journal of forensic sciences* 51(2):253-265.

108. Krenke BE*, et al.* (2002) Validation of a 16-locus fluorescent multiplex system. *J Forensic Sci* 47(4):773-785.

109. Moretti TR*, et al.* (2001) Validation of short tandem repeats (STRs) for forensic usage: performance testing of fluorescent multiplex STR systems and analysis of authentic and simulated forensic samples. *J Forensic Sci* 46(3):647-660.

110. Butler JM, Buel E, Crivellente F, & McCord BR (2004) Forensic DNA typing by capillary electrophoresis using the ABI Prism 310 and 3100 genetic analyzers for STR analysis. *Electrophoresis* 25(10-11):1397-1412.

111. Butler JM (2005) *Forensic DNA Typing: Biology, Technology, and Genetics of STR Markers* (Elsevier Science).

112. Lazaruk K*, et al.* (1998) Genotyping of forensic short tandem repeat (STR) systems based on sizing precision in a capillary electrophoresis instrument. *ELECTROPHORESIS* 19(1):86-93.

113. Puch-Solis R*, et al.* (2013) Evaluating forensic DNA profiles using peak heights, allowing for multiple donors, allelic dropout and stutters. *Forensic Sci Int Genet* 7(5):555-563.

114. Buckleton JS, Krawczak M, & Weir BS (2011) The interpretation of lineage markers in forensic DNA testing. *Forensic Science International: Genetics* 5(2):78-83.

115. Ayres KL & Overall ADJ (1999) Allowing for within-subpopulation inbreeding in forensic match probabilities. *Forensic Science International* 103(3):207-216.

116. Ham S-K*, et al.* (2014) Optimization of STR locus enrichment for STR profiling of fragmented DNA. *ELECTROPHORESIS* 35(21-22):3158-3164.

117. Butler JM (2015) The future of forensic DNA analysis. *Philosophical Transactions of the Royal Society of London B: Biological Sciences* 370(1674).

118. Budowle B, Moretti TR, Niezgoda SJ, & Brown BL (1998) CODIS and PCR-based short tandem repeat loci: law enforcement tools. *Second European Symposium on Human Identification*, (Promega Corporation, Madison, Wisconsin), pp 73-88.

119. Weir BS (2007) THE RARITY OF DNA PROFILES. *The annals of applied statistics* 1(2):358-370.

120. Weir BS (2004) Matching and partially-matching DNA profiles. *J Forensic Sci* 49(5):1009-1014.

121. Bieber FR (2006) Turning Base Hits into Earned Runs: Improving the Effectiveness of Forensic DNA Data Bank Programs. *The Journal of Law, Medicine & Ethics* 34(2):222-233.

122. Weir BS & Zheng X (2015) SNPs and SNVs in forensic science. *Forensic Science International: Genetics Supplement Series* 5:e267-e268.

123. Yuan GC*, et al.* (2005) Genome-scale identification of nucleosome positions in S. cerevisiae. *Science* 309(5734):626-630.

124. Orlando V (2000) Mapping chromosomal proteins in vivo by formaldehyde-crosslinked-chromatin immunoprecipitation. *Trends in Biochemical Sciences* 25(3):99-104.

125. Infante JJ, Law GL, & Young ET (2012) Analysis of nucleosome positioning using a nucleosome-scanning assay. *Methods Mol Biol* 833:63-87.

126. Brenowitz M, Senear DF, & Kingston RE (2001) DNase I footprint analysis of protein-DNA binding. *Curr Protoc Mol Biol* Chapter 12:Unit 12 14.

127. Staynov DZ & Proykova YG (1998) Quantitative analysis of DNase I digestion patterns of oligo- and polynucleosomes1. *Journal of Molecular Biology* 279(1):59-71.

128. Amberg DC, Burke DJ, & Strathern JN (2005) Methods in Yeast Genetics: A Cold Spring Harbor Laboratory Course Manual, 2005 Edition (Cold Spring).

129. Knorr D, Shetty K, & Kinsella J (1979) Enzymatic lysis of yeast cell walls. *Biotechnology and Bioengineering* 21(11):2011-2021.

130. Sambrook J & Russell DW (2006) Purification of Nucleic Acids by Extraction with Phenol:Chloroform. *Cold Spring Harbor Protocols* 2006(1):pdb.prot4455.

131. Zeugin JA & Hartley JL (1985) Ethanol precipitation of DNA. *Focus* 7(4):1-2.

132. Huibregtse JM & Engelke DR (1991) [49] Direct sequence and footprint analysis of yeast DNA by primer extension. *Methods in Enzymology*, (Academic Press), Vol Volume 194, pp 550-562.

133. Singer VL, Jones LJ, Yue ST, & Haugland RP (1997) Characterization of PicoGreen reagent and development of a fluorescence-based solution assay for double-stranded DNA quantitation. *Anal Biochem* 249(2):228-238.

134. Nicklas JA & Buel E (2003) Quantification of DNA in forensic samples. *Anal Bioanal Chem* 376(8):1160-1167.

135. Bustin SA*, et al.* (2009) The MIQE guidelines: minimum information for publication of quantitative real-time PCR experiments. *Clin Chem* 55(4):611-622.

136. Thomson JM*, et al.* (2005) Resurrecting ancestral alcohol dehydrogenases from yeast. *Nature genetics* 37(6):630-635.

137. Herrero J*, et al.* (2016) Ensembl comparative genomics resources. *Database* 2016.

138. Ono B*, et al.* (1992) Cloning and characterization of the CYS3 (CYI1) gene of Saccharomyces cerevisiae. *J Bacteriol* 174(10):3339-3347.

139. Small EC, Xi L, Wang J-P, Widom J, & Licht JD (2014) Single-cell nucleosome mapping reveals the molecular basis of gene expression heterogeneity. *Proceedings of the National Academy of Sciences* 111(24):E2462-E2471.

140. Senissar M*, et al.* (2014) The DEAD-box helicase Ded1 from yeast is an mRNP cap-associated protein that shuttles between the cytoplasm and nucleus. *Nucleic acids research* 42(15):10005-10022.

141. Sekinger EA, Moqtaderi Z, & Struhl K (2005) Intrinsic histone-DNA interactions and low nucleosome density are important for preferential accessibility of promoter regions in yeast. *Mol Cell* 18(6):735-748.

142. Bornaes C, Ignjatovic MW, Schjerling P, Kielland-Brandt MC, & Holmberg S (1993) A regulatory element in the CHA1 promoter which confers inducibility by serine and threonine on Saccharomyces cerevisiae genes. *Mol Cell Biol* 13(12):7604-7611.

143. Kubota S*, et al.* (2004) Effect of Ethanol on Cell Growth of Budding Yeast: Genes That Are Important for Cell Growth in the Presence of Ethanol. *Bioscience, Biotechnology, and Biochemistry* 68(4):968-972.

144. Klis FM, Boorsma A, & De Groot PWJ (2006) Cell wall construction in Saccharomyces cerevisiae. *Yeast* 23(3):185-202.

145. Morozova O & Marra MA (2008) Applications of next-generation sequencing technologies in functional genomics. *Genomics* 92(5):255-264.

146. Gasch AP*, et al.* (2000) Genomic expression programs in the response of yeast cells to environmental changes. *Molecular Biology of the Cell* 11(12):4241-4257.

147. Teste M-A, Duquenne M, François JM, & Parrou J-L (2009) Validation of reference genes for quantitative expression analysis by real-time RT-PCR in Saccharomyces cerevisiae. *BMC Molecular Biology* 10:99-99.

148. Hennequin C*, et al.* (2001) Microsatellite typing as a new tool for identification of Saccharomyces cerevisiae strains. *J Clin Microbiol* 39(2):551-559.

149. Nowrousian M (2010) Next-Generation Sequencing Techniques for Eukaryotic Microorganisms: Sequencing-Based Solutions to Biological Problems. *Eukaryotic Cell* 9(9):1300-1310.

150. Beutler E, West C, & Blume K (1976) The removal of leukocytes and platelets from whole blood. *J Lab Clin Med* 88(2):328-333.

151. Freeman SE*, et al.* (1986) Quantitation of radiation-, chemical-, or enzyme-induced single strand breaks in nonradioactive DNA by alkaline gel electrophoresis: Application to pyrimidine dimers. *Analytical Biochemistry* 158(1):119-129.

152. Ruitberg CM, Reeder DJ, & Butler JM (2001) STRBase: a short tandem repeat DNA database for the human identity testing community. *Nucleic Acids Research* 29(1):320-322.

153. Dieffenbach C, Lowe T, & Dveksler G (1993) General concepts for PCR primer design. *PCR Methods Appl* 3(3):S30-S37.

154. Koressaar T & Remm M (2007) Enhancements and modifications of primer design program Primer3. *Bioinformatics* 23(10):1289-1291.

155. Saiki RK (1989) The design and optimization of the PCR. *PCR technology*, (Springer), pp 7-16.

156. Thanakiatkrai P & Welch L (2011) Evaluation of nucleosome forming potentials (NFPs) of forensically important STRs. *Forensic Sci Int Genet* 5(4):285-290.

157. Alaeddini R, Walsh SJ, & Abbas A (2010) Forensic implications of genetic analyses from degraded DNA--a review. *Forensic Sci Int Genet* 4(3):148-157.